Calibration of TLD700:LiF for Clinical Radiotherapy Beam Modalities & Verification of a High Dose Rate Brachytherapy Treatment Planning System

James D Rijken

Thesis submitted for the degree of

Master of Philosophy (Science)

in the School of Chemistry and Physics
The University of Adelaide

Supervisors:
Dr Wendy Harriss-Phillips
Mr John Lawson
Dr Judith Pollard

February 2014

TABLE OF CONTENTS

List of Tables

List of Figures

Abbreviations

AAPM	American Association of Medical Physicists in Medicine
ARPANSA	Australian Radiation Protection and Nuclear Safety Agency
CI	Confidence Interval
d_{max}	Depth of maximum dose
DVH	Dose volume histogram
EBRT	External Beam Radiotherapy
EC	Electron Capture
FSD	Focus to Surface Distance
HDR	High Dose Rate
HVL	Half Value Layer
IC	Ionisation Chamber
ISL	Inverse Square Law
kVp	peak kilovolts (superficial x ray tube)
LDR	Low Dose Rate
LiF	Lithium Fluoride
Linac	Linear Accelerator
MC	Monte Carlo
MU	Monitor Units
OAR	Organs at Risk
OCP	Oncentra Prostate
PDD	Percentage Depth Dose
PTV	Planned Target Volume
RAH	Royal Adelaide Hospital
SD	Standard Deviation
SSD	Source to Surface Distance
SXR	Superficial X Ray
TCS	Treatment Control System
TG	Task Group
TL	Thermoluminescent
TLD	Thermoluminescent Dosimeter
TPS	Treatment Planning System
US	Ultrasound

I. ABSTRACT

When heated, lithium fluoride (LiF) crystals that have been exposed to ionising radiation emit light proportional to their absorbed dose, in a phenomenon known as thermoluminescence. This phenomenon has applications in dose measurement for radiation research, clinical cancer treatment and personal safety dose monitoring.

LiF thermoluminescent dosimeters (TLDs) have a response that is dependent on the energy spectrum of the incoming radiation. Therefore, TLDs need to be calibrated for each spectrum they are exposed to, in order to be used as accurate dosimeters.

The TLD energy response was investigated specifically for a set of TLD700:LiF(Mg,Ti) chips for a range of clinical radiation beams used for Radiation Oncology treatments, including Linear Accelerator electron and x ray beams, superficial x rays and an ^{192}Ir brachytherapy source. Once calibrated, the TLD chips were used to verify the accuracy of the high dose rate (HDR) brachytherapy treatment planning system, Oncentra Prostate.

To carry out this investigation, the TLD700:LiF chips were exposed to known doses of radiation from nominal 6 MV and 18 MV photon beams as well as nominal 6 MeV, 9 MeV, 12 MeV, 16 MeV and 20 MeV electron beams from a Linear Accelerator. The TLDs were read and the response from each beam was normalised to that from the 6 MV beam. The TLDs were also exposed to a series of known doses from a superficial x ray machine with peak energies of 30 kVp, 40 kVp, 50 kVp, 80 kVp, 100 kVp, 120 kVp and 150 kVp. The response to these was similarly compared to the response from the 6 MV beam with equivalent dose.

The TLDs were then calibrated for exposure to an iridium-192 source, used for HDR brachytherapy. The delivered dose was determined by Monte Carlo simulation of the experimental setup using the package GEANT4. The TLDs were exposed to the source in air and at varying depths in water. The response for each of these scenarios was compared to the response from the 6 MV beam.

Finally, the calibrated TLDs were used to verify the Oncentra Prostate treatment planning system by exposing them within a water phantom. A realistic prostate treatment plan was created on a reconstructed ultrasound image data set of the phantom. The treatment plan was delivered to the phantom with the TLD chips at known locations. The dose to the TLDs was compared to the simulated doses at corresponding points in the phantom within Oncentra Prostate.

Results show that, relative from the response to the 6 MV beam, TLDs under-respond by approximately 4% for electron beams and by approximately 3% for the 18 MV photon beam. An over-response of up to 54% was observed for SXR beams with peak energies between 40 and 150 kV. The TLD700 chips over-respond by approximately 11% when exposed to the gamma spectrum of ^{192}Ir in air and were shown to have a depth dependent response in water.

The TLDs used to verify Oncentra Prostate produced a dose ratio of D_{TLD}/D_{OCP} that was not statistically different from the expected value of 1.0 at the 5% significance level. With confidence level 95%, the true value of D_{TLD}/D_{OCP} was shown to lie in the confidence interval 1.023±0.041. Therefore, Oncentra Prostate was considered verified for the full prostate treatment. When compared directly with Monte Carlo predictions, the dose ratio values of D_{MC}/D_{OCP} were also found not to be statistically different to 1.0 at the 5% significance level for a single dwell treatment plan. With confidence level 95%, the true value of D_{MC}/D_{OCP} was shown to lie in the confidence interval 1.029±0.064, so Oncentra Prostate was also considered verified for the single source dwell treatment plan.

II. DECLARATION

I certify that this work contains no material which has been accepted for the award of any other degree or diploma in any university or other tertiary institution and, to the best of my knowledge and belief, contains no material previously published or written by another person, except where due reference has been made in the text. In addition, I certify that no part of this work will, in the future, be used in a submission for any other degree or diploma in any university or other tertiary institution without the prior approval of the University of Adelaide and where applicable, any partner institution responsible for the joint-award of this degree. I give consent to this copy of my thesis, when deposited in the University Library, being made available for loan and photocopying, subject to the provisions of the Copyright Act 1968. I also give permission for the digital version of my thesis to be made available on the web, via the University's digital research repository, the Library catalogue and also through web search engines, unless permission has been granted by the University to restrict access for a period of time.

Signature: ……..

Date: ……..

III. ACKNOWLEDGEMENTS

I would firstly like to acknowledge and thank my supervisors. Many thanks to Dr Wendy Harriss-Phillips for her driving force in this research project. She did a fantastic job in her first research project supervision and I wish her all the best for many more projects to come. Thanks go to Mr John Lawson for his careful and thoughtful guidance through the experimental and thesis writing phases. His considered input has been greatly helpful and appreciated. Thanks to Dr Judith Pollard for her administrative direction throughout this entire process and for her valued input into the thesis revision.

I would also like to thank and acknowledge the University of Adelaide for accepting me into the Master of Philosophy program, for funding me and providing me with a stipend for the first year of study. Thanks to all the office people at the School of Chemistry and Physics for helping me to sort out all my forms and papers.

I would also like to acknowledge all the extra people at the Royal Adelaide Hospital that contributed to this project. Thanks to Mr John Schneider for constructing ancillary equipment like the templates and phantoms. Thanks to Mr Johan Asp for teaching me how to use the TLD equipment. Thanks to Dr Scott Penfold for answering my persistent questions regarding GEANT4 and C++. Many thanks to Associate Professor Eva Bezak for allowing me to use the Royal Adelaide Hospital's linacs, x ray machines and brachytherapy suite.

I would like to thank the people at home that also made this whole project possible. Thanks to Mum and Dad for fostering in me a love for learning and science. I would like to give many thanks to Anna, my wife, for her love and support during this process. She has also helped me greatly by proof reading, providing general opinions on the thesis and providing invaluable knowledge on statistics - on which the results of the project are completely reliant. I would finally like to acknowledge the LORD for the intelligibility, mathematical order and fine-tuning of the universe which makes such endeavours as these even possible.

1. INTRODUCTION

Thermoluminescent dosimeters (TLDs) are useful in the hospital environment because they are physically very small relative to other dose measuring devices and are approximately tissue equivalent. Consequently, they provide a simple and convenient method of dose measurement at external/surface locations during patient irradiation and within phantoms during quality assurance procedures. For example, TLDs can be attached to a patient's face during a radiotherapy treatment fraction to provide the doctor and physicist information on the surface dosimetry in the eye, nose etc. compared to the initial treatment plan.

TLDs can only provide relative dosimetry data and there are many different varieties of TLD, each with their own properties. Since each type of TLD will respond differently when exposed to various energies of ionising radiation, they need to be calibrated for each beam energy spectrum to which they are exposed.

The TLDs investigated for this work had a greater ^{7}Li content compared to other more common TLDs, and have previously not had their energy dependence comprehensively determined. A thorough literature review and relevant background knowledge is provided in Section 2.

The first part of this project involved the determination of calibration factors for a specific set of sensitive TLD chips for a number of different beam energies used clinically for Radiation Oncology procedures. Section 3 explores the energy response of the TLDs for all the beam modalities available from a modern linear accelerator (linac), which includes both high energy photons (6 - 18 MV) and high energy electrons (6 - 20 MeV). The energy dependence of the TLDs for superficial x ray (SXR) machine was also explored and included numerous spectra with peak energies in the range of 30 - 150 kVp.

Before the TLDs were calibrated for exposure from the gamma ray spectrum of an ^{192}Ir source used for brachytherapy, a dose formalism had to be established. This has been explored in Section 4, where a Monte Carlo program was written in GEANT4 to simulate the brachytherapy source in both a water and air medium. Once the dose deposition in water and air had been determined for an ^{192}Ir source, the energy dependence of the TLDs could be explored for the gamma spectrum of ^{192}Ir in air and at varying depths in water, as presented in Section 5.

After the TLDs were calibrated for ^{192}Ir irradiation, the aim was to use them for dosimetric verification of the treatment planning system, i.e. Oncentra Prostate (OCP) (Nucletron Pty. Ltd., an Elekta company, Stockholm, Sweden), used for the

treatment of high risk prostate cancer at the Royal Adelaide Hospital (RAH). Oncentra Prostate is a popular brachytherapy treatment planning system used world-wide. However, a literature search has found no evidence that it has been independently verified experimentally through the use of TLDs for a full prostate plan scenario. Section 6 compares the treatment planning system's dose predictions to the measurements made with TLDs, within a water phantom and catheter system that mimics the prostate treatment setup.

This work enabled a thorough energy response comparison of the TLD chips over a large clinical energy range, which will be useful for the RAH in the future, and provided an independent verification of a brachytherapy treatment planning system.

2. BACKGROUND AND LITERATURE REVIEW

2.1 Theory of Thermoluminescence

Thermoluminescent dosimeter (TLD) chips are made of a crystalline material that, when irradiated with ionising radiation, absorbs and stores a small fraction of the energy in the crystal lattice. This energy can be recovered later as light when the crystal is heated. Impurities in the crystalline structure, such as magnesium and titanium, create allowed energy levels between the conduction and valence bands (forbidden region) in the crystal's subatomic structure, known as electron traps. When radiation is incident on a TLD material, there may be sufficient energy to promote a fraction of the electrons from the valence band into the conduction band. An excited electron may then decay to the electron trap in the forbidden region forming a metastable state. The number of trapped electrons is proportional to the dose delivered to the crystal. Electrons remain in the metastable state until they are excited back into the conduction band and decay to the valence band (Figure 1). During this process (phosphorescence), light is emitted. Since the process is very slow at room temperature, TLD measurements require additional heating of the crystal to enhance the phosphorescence process - this is called thermoluminescence.

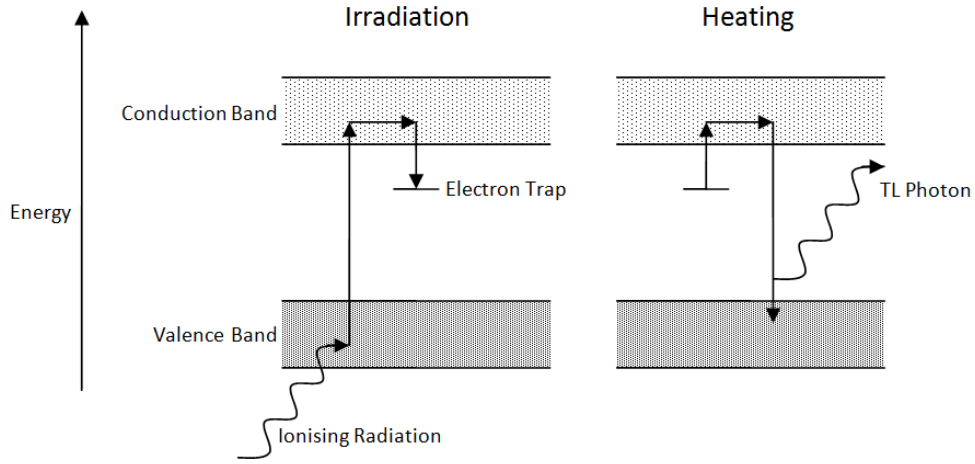

Figure 1. Energy band diagram of TLDs.

A glow curve (Figure 2) is a plot of the thermoluminescence signal intensity versus temperature. As the temperature of the TLD is increased, the probability of releasing trapped electrons increases. Since the TLDs contain many metastable states at various energies in the forbidden region, the glow curve consists of a

number of different peaks corresponding to these energy levels. After heating the TLD, one can convert the light intensity detected, as a measure of charge, to absorbed dose. Since TLDs can only provide relative dose, the TLD batch needs to be calibrated by exposing a subset of TLDs to a known dose of radiation. These chips are read and the response serves as a reference for the dose given. The TLDs are left to settle for 24 hours before being read to give more reproducible results.

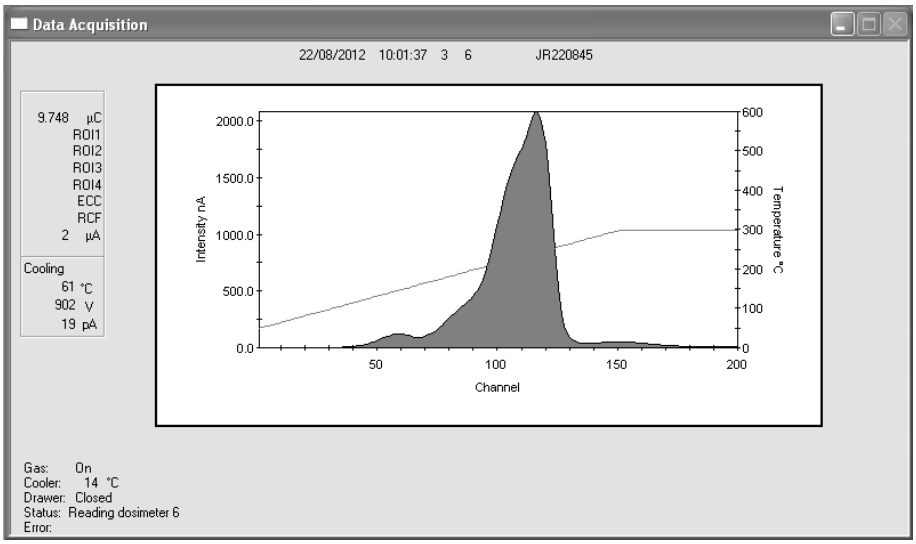

Figure 2. Glow curve. Screenshot of software package WinREMS, version PL-26732.8.1.0.0, Saint-Gobain Crystals and Detectors, Copyright 1999-2002.

The use of lithium fluoride (LiF) TLDs for radiation dosimetry is relatively common because their linear attenuation coefficients and stopping powers are comparable to that of water. This is because of their similar atomic weight and electron density properties, affecting the type of interaction occurring at kilovoltage to megavoltage beam energies, predominately the photoelectric, Compton scattering and pair production effects. LiF, with the current standard doping of Mg, Ti, has good sensitivity and is approximately water equivalent. Water equivalence is crucial because the TLD chips will attenuate radiation by approximately the same amount as the human body and, hence, will not alter the primary or secondary scatter component of the beam.

TLDs are particularly suitable for *in vivo* dosimetry due to the convenient small size of the available chips. Their small size also provides more accurate dosimetry in high dose gradient regions. TLDs are reusable after exposure but must be annealed to remove the remaining electrons residing in electron traps. The annealing process involves heating the TLD material to 400°C for one hour, followed by flash cooling and then heating at 100°C for another three hours.

2.2 Thermoluminescent Dosimeter (TLD) Materials and Calibration

There are several TL phosphor materials available such as LiF, Li_2B_{407}:Mn, CaF_2:Mn, CaF_2:nat and $CaSO_4$:Mn (Cameron, Suntharalingham & Kenney 1968). This study has used the TL phosphor LiF. The different thermoluminescent grades of LiF produced by Harshaw (Harshaw Chemicals Company, Solon, Ohio, USA) include TLD100, TLD110, TLD600 and TLD700. They differ in their relative abundance of the isotopes ^{6}Li and ^{7}Li. This study has utilised the properties of TLD700 grade LiF, the purest (and most expensive) of the four listed. TLD700 has 99.99% ^{7}Li and 0.01% ^{6}Li (Cameron, Suntharalingham & Kenney 1968). A higher percentage of ^{7}Li accounts for the increased accuracy of TLD700:LiF because ^{7}Li is not as susceptible as ^{6}Li to neutron reactions. The most common doping is LiF(Mg,Ti) (Pradhan & Quast 2000). Another variant is also available in the form of LiF(Mg,Cu,P) (Bilski 2002). The most apparent difference between LiF(Mg,Ti) and LiF(Mg,Cu,P) is the sensitivity to gamma radiation, with Mg,Cu,P doping consistently reported to be thirty times more sensitive than the Mg,Ti doping. There are also differences between the two doping types in the supralinearity of the dose response for given energies, however the majority of TLD reports in the literature are concerned with energy and dose response of the LiF(Mg,Ti) doping type of TLD.

The underlying solid state physical principles concerning the TLD response with increasing energy are not fully understood, however several studies have suggested that the energy response trend may follow that of the changing probabilities of physical interactions occurring between the incoming radiation and the TLD material. These physical processes include the photoelectric effect, incoherent and coherent scattering and pair production. The study by Mobit et al. (1998) showed that the energy response of TLD100 is roughly uniform to within ±3% over an energy range from approximately 300 kVp (approximately 0.5 mm Cu Half Value Layer (HVL)) to 25 MV x rays. Their data showed that at lower energies, the dose to LiF:water ratio response roughly followed the ratio of mass energy attenuation coefficients for LiF and water. Above 5 MeV, the dose to LiF:water ratio response tended toward the mass collision stopping power ratio for LiF:water. TLD energy response may be related to mass attenuation factors, which are themselves derived from the varying probabilities of different physical processes (photoelectric, Compton and pair production) occurring. Consequently, it is important to calibrate

the response of TLDs for the specific energy or energy spectrum of the beam used to give an energy response curve.

Energy response curves for TLDs may be based on values calculated from available absorption coefficients for the various photon energies, or be experimentally determined for various sources (Cluchet & Joffre 1967). Experimentally measured values are more appropriate when correcting for the energy responses in specific clinical beams. In a recent paper, Kron et al. (1998) devised a simple model to describe the variation of TLD100 response with energy. This was based on the assumption that the response at low energies reduces exponentially and that it varies at medium energies with the energy dependence of the photoelectric effect. The curve fitting formula produced by Kron et al. assumes the use of monoenergetic x rays beams (e.g. synchrotron radiation), which was not considered as the most accurate method for the current project which requires exposure from energy spectra from all beam modalities utilised.

An ideal TLD phosphor has a dose response curve that is linear over a large dose range to simplify calibration procedures. Some TLD phosphors do not respond linearly and require calibration for the limited dose range of interest. Researchers have written several papers on the dose response of different types of TLDs. Generally, the dose response of TLD100:LiF is linear from approximately 1 Gy up to 10 Gy; beyond this it becomes supralinear, exhibiting a plateau region at around 5×10^3 Gy before decreasing (Cameron, Zimmerman & Bland 1967). TLD700 response follows this general trend, however it has been shown to display a supralinear response at around 2 Gy, and the supralinearity is greater than that of TLD100 chips (Almond, Wright & Lontz 1967). This response shown by Almond, Wright and Lontz is contrary to the manufacturer's data and general consensus for all LiF TLDs which is a linear dose range of 1 -10 Gy.

2.3 Superficial X Ray (30 - 150 kVp) Beam TLD Response

There is little in the literature regarding the energy response of the TLD700:LiF(Mg,Ti) for superficial x ray energies, however, studies of the energy response of TLD100:LiF may provide an indication of their response. There have been conflicting published results for the energy response of TLD100:LiF(Mg,Ti) to superficial x ray beams (Das, Perera & Williamson 1996) (Davis et al. 2003). Both Das et al. and Davis et al. used Monte Carlo methods to calculate the dose to TLD chips for different energy photon beams to determine whether the measured TLD

response was directly proportional to the energy deposited in the TLD. The energies tested were filtered x ray spectra in the superficial energy range of 20–250 kVp. Das concluded that the TLD response was constant with changing photon energy, while Davis found an energy dependent change in TLD response.

In a more recent paper by Muhogora et al. (2002), the differences in energy response of TLD100:LiF, TLD110:LiF and TLD700:LiF to a range of diagnostic x ray beams were investigated. The researchers sourced diagnostic energy x rays from two different Siemens machines and one Phillips machine. The study found that TLD700 exhibited the smallest maximum to minimum response ratio of 1.4, followed by TLD100 (1.51) and TLD110 (1.56). The relative mean TLD energy response for Siemens Vertix B x rays for radiation qualities of 55 kVp (1.45 mm HVL Al), 70 kVp (2.35 mm HVL Al), 80 kVp (2.4 mm HVL Al), 90 kVp (2.45 mm HVL Al) and 125 kVp (2.48 mm HVL Al) showed an over response at the 90 kVp spectrum and a tapering off for higher energies. The relative mean TLD energy response for the Siemens 8463168X1706 machine x rays for radiation qualities 70 kVp (2.8 mm HVL Al), 81 kVp (3.2 mm HVL Al) and 90 kVp (3.4 mm HVL Al) showed an approximately constant over-response. The relative mean TLD energy response for Phillips MRS for radiation qualities 90 kVp (4.5 mm HVL Al), 100 kVp (4.7 mm HVL Al) and 120 kVp (4.9 mm HVL Al) showed a steady decrease in response up to 100 kVp where it started to rise again slowly. The study showed that while there were similarities in the response of the different types of LiF TLD, there were many differences in the energy responses to different energy x ray spectra.

The low energy x ray responses of TLD LiF(Mg,Cu,P) and TLD LiF(Mg,Ti) were compared by Edwards et al. (2005). Measurements of the response per unit air kerma strength of LiF(Mg,Cu,P) and LiF(Mg,Ti) irradiated with nine quasi-monoenergetic x ray beams with mean energies ranging from 12 keV to 208 keV were made. Edwards et al. normalised each measurement to the value produced by 6 MV x rays. The research found that LiF(Mg,Cu,P) under-responded to most of the beams, whereas LiF(Mg,Ti) over-responded. The lowest energy beam produced their smallest relative measured response, and the maximum measured relative response of 1.21 for LiF(Mg,Ti), occurred for 33 keV. For the region of 30-120 keV, the TLD response decreased with increasing energy, however, this paper was concerned with quasi-monoenergetic x ray beams, not clinically used spectra, so the results in this project are not expected to be exactly the same.

In a recent study by Duggan et al. (2004), the energy response of LiF TLDs doped with Mg,Cu,P was compared with those doped with Mg,Ti. The TLDs used

came from the GR series (China) (not from Harshaw) and the study found that the energy response of TLD materials may depend on the manufacturer. While the energy response of Mg,Cu,P was close to unity for low energy x rays, TLDs with Mg,Ti doping had an over-response of up to 50%. This supported claims made by Kron (1994) and Kron et al. (1996) that LiF:Mg,Ti TLDs over-respond by approximately 40% for low energy x rays, which he displayed with Harshaw TLD100s.

2.4 Megavoltage (6 - 18 MV) Photon Beam TLD Response

A literature search has found no published results on the energy response of TLD700:LiF(Mg,Ti) for high-energy linac photon beams (6 – 18 MV), however similar work has been performed by Crosby, Almond & Shalek (1966), Mobit, Nahum & Mayles (1998) and Almond & McCray (1970) regarding TLD100. In addition, approximate interpolation in this region has been performed with the model developed by Kron et al. (1998). This model indicates that the response at high photon beam energies for TLD100 is approximately uniform, so a similar result is to be expected for this study with TLD700.

2.5 Megavoltage (6 – 20 MeV) Electron Beam TLD Response

Past research has investigated the energy response of TLD700:LiF(Mg,Ti) to high-energy electrons (Holt, Edelstein & Clark 1975). Holt et al. noted that the energy dependence for high-energy electron beams might also have a dependence on the size of the TLD cavity in the solid phantom. Holt et al. measured the absorbed dose in water with an absolute cavity consisting of a parallel plane, cylindrical ionization chamber (pancake chamber) and compared this to the TLD response. The TLD700:LiF dose response in water was investigated for various electron beam energies from both linac and betatron sources. Although the ratio of the mass collision stopping powers between LiF and water is nearly constant over all energies, the TLD response dropped sharply for electron beam energies below 5 MeV.

At beam energies greater than 5 MeV, there was little variation in the response of TLD700:LiF compared to water. The experimental results matched the theory developed in the paper, where Holt et al. included a cavity perturbation correction factor. This factor accounted for the loss of sensitivity for the lower energy electrons (< 5 MeV).

The cavity theory developed by Holt et al. replaced the previous theory developed by Almond et al. (1967). However, Almond's paper was only concerned with the dose response and did not deal with the energy response for high-energy electron beams. Cavity theory corrections were deemed negligible for such small TLDs and were not considered in calculations.

The energy dependence of TLDs for high-energy electron beams shown by Holt et al. agrees with the results of Suntharalingham et al. (1969), who did not find any energy dependence in the response of TLD700:LiF and TLD100:LiF to electron beam energies 6 to 33 MeV. The results of Crosby et al. (1966) also showed an energy dependence consistent with Holt's results.

2.6 Iridium-192 brachytherapy Source TLD Response

There is little in the literature regarding the energy response of TLD700:LiF(Mg,Ti) after irradiation with a ^{192}Ir brachytherapy source, compared with the response from 6 MV linac x rays. The main limitation for ^{192}Ir dosimetry is the difficulty in obtaining a traceable radiation dose calculation because many standards laboratories (including the Australian Radiation Protection and Nuclear Safety Agency (ARPANSA)) do not currently offer an iridium dose standard. Dosimetry standards laboratories often calibrate ionisation chambers at an effective energy of 164 keV and with ^{137}Cs and assume that most significant photons from ^{192}Ir lie between those two energies (Duggan et al. 2004).

Almond et al. (1967) showed that TLD100:LiF(Mg,Ti) had similar effects to the TLD700:LiF(Mg,Ti), but there has been no further research. ^{192}Ir emits a wide spectrum of low to medium photon energies, mostly in the range of 201–884 keV and has a relatively high atomic number (Z = 77) (Anderson, Nath & Weaver 1990), (Chang 2013). Several studies performed by Haworth et al. (2012) (2013) have considered the average energy of the ^{192}Ir spectrum and derived an energy response factor for TLD100 of 1% by interpolating on a model devised by Kron et al. (1998) for monoenergetic x rays.

In an investigation by Pradhan and Quast (2000), an answer was sought for the prevailing controversy regarding the over-response of LiF to the softened photon spectra of ^{192}Ir source at certain depths in a phantom due to energy dependence. The report only concerned TLD100 but may give an indication of what to expect from TLD700. Pradhan and Quast reported that LiF TLDs over-responded

by 8.5% at depths of 100 mm in a phantom, which meant that they needed depth-dependent correction factors.

Others claimed that no over-responses were observed. Thomason and Higgins (1989) found that, compared to a calibrated farmer type ion chamber having a photon energy-independent response within 2%, the over-response of TLD100:LiF rods was less than 2.5% at a depth of 100 mm in the phantom (reference measurement at a depth of 10 mm). By using equivalent photon beams, they evaluated the photon energy dependence of the dosimeters. For TLD100:LiF rods, the energy response was found to be in close agreement with the ratios of mass energy absorption coefficients of LiF and water for effective photon energies ranging from 26 keV to 1.25 MeV.

A recent study by Haworth et al. (2012) investigated different TLD100:LiF calibration methods for ^{192}Ir dosimetry. The group exposed the TLDs to a range of x ray energies and an energy response factor for ^{192}Ir of 1.03 was derived through interpolation, assuming a mean energy of 258 keV at a depth of 50 mm in water. The model for their energy response formula was derived from the work of Kron et al. (1998) for monoenergetic x rays. They also gave the response, relative to 6 MV x rays, to be 1.01 for a mean energy of 397 keV in air. Haworth et al. assumed a mean gamma energy of ^{192}Ir when interpolating on a plot for monoenergetic x rays and dose calculations were based on corrections to air kerma strength with ratios of mass energy absorption coefficients for water and air, averaged over the ^{192}Ir spectrum. The study utilised average energies in order to use tabulated ratios of mass energy absorption coefficients (Johns & Cunningham 1983).

In another recent study, Duggan et al. (2004) derived an over-response of 12% from the model developed by Kron et al. (1998). The study also experimentally produced an over-response of 7.5% relative to the response of TLD100 from exposure to a 4 MV beam, highlighting possible issues with the assumption of monoenergetic beams.

The current study has aimed to improve on the accuracy of past methods by calibrating the TLDs for exposure to ^{192}Ir through Monte Carlo simulations which takes into account the full ^{192}Ir spectrum and the spectral changes that occur at depth in water.

2.7 Monte Carlo (MC) Modelling of an Iridium-192 Source

This project involves computer modelling of the MicroSelectron v2 HDR Brachytherapy source, supplied by Nucletron, using the popular simulation toolkit, GEANT4. GEANT4 simulates the passage of particles through matter and may be used to model high-energy, nuclear and accelerator physics, as well as studies in medical and space science (GEANT4 Collaboration 2013).

GEANT4 utilises object orientated programming using the C++ programming language and provides a complete set of tools for all areas of detector simulation: geometry, tracking, detector response, run, event and track management, visualization and user interface. The multi-disciplinary nature of the toolkit requires that it supply an abundant set of "Physics Processes" to handle diverse interactions of particles with matter over a wide energy range. For many physics processes a choice of different models is available. A large set of utilities is provided, including a powerful set of random number generators. Other features, including a set of physics units and constants, particle management compliant with the Particle Data Group, interfaces to event generators, and object persistency solutions, complete the toolkit (GEANT4 Collaboration 2013).

The object-oriented design of GEANT4 allows the user to understand, customize or extend the toolkit in all the domains. At the same time, its modular architecture allows the user to load and use only the components needed. GEANT4 software was developed by RD44, a world-wide collaboration of about 100 scientists participating in more than 10 experiments in Europe, Russia, Japan, Canada and the United States. The GEANT4 source code is freely available, accompanied by an Installation Guide and an extensive set of documentation (GEANT4 Collaboration 2013).

Monte Carlo modelling of brachytherapy sources is well researched. It is the basis for most of the data in TG43 (Nath et al. 1995) which concerns the dosimetry of brachytherapy sources. One particular paper provides very precise details on the dosimetry and spectrum of an ^{192}Ir source by using Monte Carlo methods (Borg & Rogers 1991). Detailed measurements of air kerma strength are used in brachytherapy in the Royal Adelaide Hospital to perform source calibration checks in air. The Monte Carlo study in this project was performed to provide absolute calibration of TLD700:LiF chips in water.

2.8 Brachytherapy Treatment Planning System (TPS) Verification

Brachytherapy is a radiotherapy treatment where a radioactive source is used to treat cancer by placing it near or in contact with a tumour. The radioactive sources may be inserted into the body within closed ended catheters which are in direct contact with the malignant tissue so that a very high dose can be delivered to the treatment volume. Brachytherapy offers distinct advantages over external beam radiotherapy (EBRT) because it allows for very localised dose distributions to the planned target volume (PTV) and minimises the dose to normal tissue because of the sharp dose fall-off from the source. The disadvantage of brachytherapy is that it is significantly more invasive than EBRT. It is also delivered with a higher dose rate which may or may not be preferable radiobiologically for the tissues exposed. Traditionally, radium was used for most brachytherapy treatments, but with the advent of nuclear reactors and cyclotrons many new isotopes have been used to replace it. These new isotopes include ^{137}Cs, ^{60}Co, ^{198}Au, ^{192}Ir, ^{125}I, ^{90}Sr and ^{182}Ta.

Prostate cancer at the Royal Adelaide Hospital may be treated using brachytherapy through one of two methods usually. Low dose rate (LDR) brachytherapy is a treatment for low to intermediate risk disease using a monotherapy technique involving the insertion of low activity ^{125}I seeds (0.4 mCi) into the prostate that remain in the patient indefinitely and constantly treat the prostate while they decay. For intermediate to high risk prostate cancer, HDR brachytherapy is used as a boost to image-guided EBRT. In HDR prostate brachytherapy, a high activity ^{192}Ir source is remotely driven out of a shielded unit into the patient's prostate via catheters inserted through the perineum. The source then dwells at a number of locations along the catheter for a short period of time (seconds to minutes) before being retracted and driven into the next catheter. The superposition of all dwell positions and dwell times produces a dose distribution throughout the prostate that maximises the dose to the PTV while minimising dose to organs at risk (OAR). The source dwell locations and dwell times are determined through use of a brachytherapy treatment planning system (TPS).

The HDR procedure involves a Urologist inserting the catheters into the prostate through the perineum, which are visualised using a rectal ultrasound probe. These ultrasound images are transferred to the treatment planning system where a medical physicist reconstructs the catheters in OCP and a Radiation Oncologist contours the PTV which includes the prostate and seminal vesicles, as

well as the OAR. The desired dose to the prostate, as prescribed by the Oncologist (15 Gy in one fraction at the RAH), is entered into OCP and the dwell times for the ^{192}Ir source are calculated to optimise the dose distribution in the prostate and to restrict dose to the urethra and rectum (OAR). OCP then sends the treatment plan to the treatment console system (TCS) computer, which controls the remote after loading machine that drives the ^{192}Ir source in and out of the patient during the procedure.

In this project, the calibrated TLDs were used to verify a commercially available TPS software package currently used at the RAH. The package, developed by Nucletron, is called Oncentra Prostate (OCP) and assists in planning HDR prostate brachytherapy treatments by calculating 3D dose distributions based on dwell times of an ^{192}Ir source within the PTV.

OCP uses well known and formulated dose calculations, based on dose to water, according to the TG43 protocol set out by the American Association of Physicists in Medicine (AAPM) (Nath et al. 1995). This protocol defines the dose rate $\dot{D}(r,\theta)$ at a point in a medium from the centre of a source with air kerma strength S_k by Equation 2.1.

$$\dot{D}(r,\theta) = \Lambda S_k \frac{G(r,\theta)}{G\left(1,\frac{\pi}{2}\right)} F(r,\theta) g(r) \tag{2.1}$$

where Λ is the dose rate constant, defined as the dose rate per unit air kerma strength at 10 mm along the transverse axis:

$$\Lambda = \frac{\dot{D}(1,\pi/2)}{S_k} \tag{2.2}$$

For ^{192}Ir, the AAPM recommends using the values calculated through Monte Carlo simulation by Williamson (1991). $G(r,\theta)$, the geometry factor, accounts for the geometric fall-off of photon fluence with distance from the source and depends on the distribution of the radioactive material. $F(r,\theta)$ is the anisotropy factor (Equation 2.3) normalized at θ = π/2 with the geometry factor removed. It accounts for the angular dependence of the photon absorption and scatter in the source encapsulation material and the radioactive material itself.

$$F(r,\theta) = \frac{\dot{D}(r,\theta) G(r,\pi/2)}{\dot{D}(r,\pi/2) G(r,\theta)} \tag{2.3}$$

Nath et al. (1993) have accurately calculated values for the anisotropy function. The radial dose function, *g(r)*, accounts for the radial dependence of photon absorption and scatter in the medium along the transverse axis, and is given by Equation 2.4.

$$g(r) = \frac{\dot{D}(r,\pi/2)G(1,\pi/2)}{\dot{D}(1,\pi/2)G(r,\pi/2)} \tag{2.4}$$

In AAPM Report TG43, values for the radial dose function are derived from experimental work (Chiu-Tsao & Anderson 1991), (Meigooni, Sabnis S & Nath 1990).

This project involves creating a typical prostate treatment plan in OCP and delivering the plan in a custom made phantom made of PMMA set up inside a water bath. It was assumed that the phantom material did not affect the delivered dose to the TLDs as the percentage of PMMA compared to water in the experimental setup was minimal. TLDs were placed at various locations in the phantom and the dose at these locations was compared to OCP. While the RAH has verified OCP by checking its TG43 compliance and by comparison to another brachytherapy TPS, it has not been verified experimentally for an entire treatment plan. Measurements in the phantom may include the effect of the transit time of the source and air gaps in the surrounding catheters, whereas the TPS does not consider these factors.

Most studies regarding brachytherapy TPSs, including OCP, use the TPS to verify the effectiveness of a new dosimeter technology rather than using a dosimeter of known accuracy to verify the treatment planning process. Nucletron informs the purchaser that OCP accurately delivers the simulated dose, which may often be verified experimentally for a single dwell position plan by the user. However, verification of a full clinical plan using TLDs has not yet been reported in the literature.

Researchers have made previous verifications of other clinical TPSs using ^{192}Ir sources. For example, Schumer et al. (1991) verified a Nucletron TPS called "Brachytherapy Planning System (v. 13.3)". This software is a predecessor to OCP and calculates dwell times of the ^{192}Ir source at each point along a catheter to give the prescribed dose. While this project will used TLDs to measure dose, Schumer et al. used radio-chromatic films, where the change in optical density of the films is proportional to the absorbed dose. The experiment validated the dose distribution calculated by the Nucletron Brachytherapy Planning System (v. 13.3) to within ±4%. Though this is not the exact method used in this project to verify OCP, it provided an indication of factors that needed to be considered. For example, the results of the experiment run by Schumer illustrated the significance of exact geometry in the

experimental setup due to the inverse square law and the small distances involved. The study showed that a non-concentric shift in source position of 0.25 mm caused a ±5% variation in dose at 10 mm. Schumer recommended replication of measurements, although costly and time consuming, to minimise the effect of inherent errors.

A study by Das et al. (2007) verified another brachytherapy treatment planning system called Plato (v 13.5 to 14.1, Nucletron) through the use of TLD100 rods inserted into catheters during prostate treatments. Das et al. found that the average difference in TLD and TPS doses was 0.1 Gy but the error in TLD measurements was 5%, not including the error that is derived from the spatial uncertainty of the source and TLDs. The study calibrated the TLD rods through exposure to 6 MV x rays with no mention of an energy correction factor. The group also showed that the source transit time had no effect on the measurements. The effect of the transit time was most likely within the uncertainty of the TLD measurement. The experimental work of Das et al. was essentially repeated by Toye et al. (2009) who found an average difference between the TPS and TLD dose measurements of 6% with a standard deviation of 18%.

In a recent paper, Haworth et al. (2013) performed a pilot study of a brachytherapy audit with several participating centres across Australia using TLD100 in a water phantom. TLDs were given 1.0 Gy by the TPS from 6 dwell locations of the ^{192}Ir source. The TLD doses were then compared to the TPS predicted values. Dosimetry was calculated through the use of ionisation chambers and calibration factors derived from the model developed by Kron et al. (1998), as discussed previously (Haworth et al. 2012). All TLD results were within 4.5% of their predicted values, supporting the feasibility of such an audit.

The current project sought to incorporate two improvements to methods found in the literature: the TLD700:LiF chips were to be calibrated through Monte Carlo methods (rather than using mass attenuation corrections and interpolation on an energy response model for monoenergetic x rays) and a clinically realistic prostate treatment was simulated.

3. TLD Energy Dependence for Radiotherapy External Radiation Beams

The project began by experimentally determining the energy response of TLD700:LiF chips for a variety of beam modalities used for EBRT at the RAH.

3.1 Linac and SXR TLD Calibration Materials and Method

3.1.1 TLD Equipment and Sensitivity Correction

The Harshaw TLD700:LiF(Mg,Ti) chips used had dimensions of $3 \times 3 \times 0.9$ mm^3. Before the TLD chips could be used to measure the energy responses of the clinical beams, they had to be calibrated for their inter-chip dose responses due to small differences in mass between the chips in the batch and the presence of small crystal fractures.

A template, shown in Figure 3, was created to hold the TLDs for exposure from a linac. This template consisted of a square PMMA block measuring $25 \times 25 \times 1$ cm^3. A 10 by 10 grid of 1 mm deep circular wells were drilled into the PMMA sheet to accommodate the 100 TLD chips. The TLDs irradiated in the work fitted into a 7×7 cm^2 area on the template.

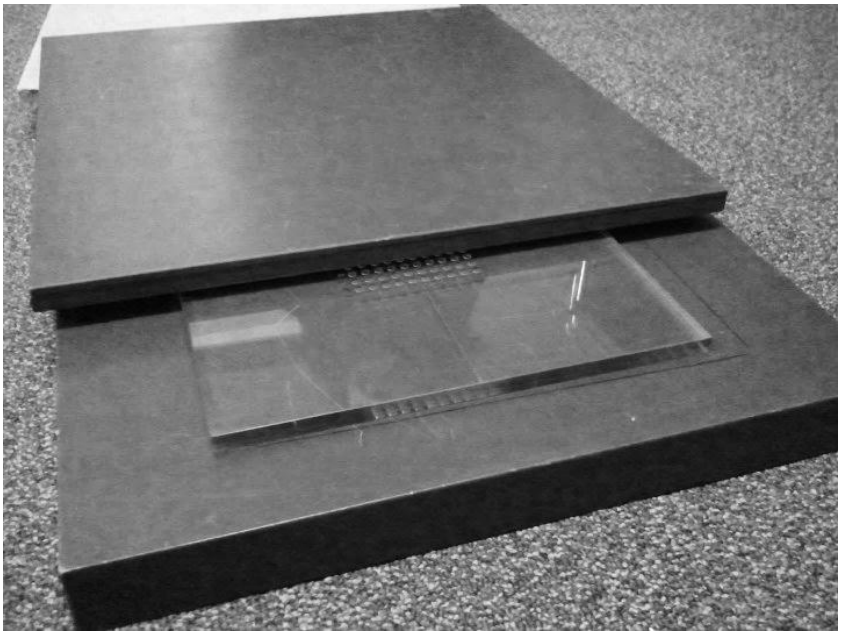

Figure 3. Solid water material (brown) and TLD PMMA template.

The filled template containing the TLDs was exposed to a 6 MV beam from a Varian iX Linear Accelerator (Varian Medical Systems, Inc., Palo Alto, USA), utilising 8 cm of Solid Water build-up to achieve electronic equilibrium. 4 cm of Solid water was placed beneath the template to supply backscatter. A 20 × 20 cm^2 field also was used to ensure a flat beam profile across the TLDs, such that each would receive identical dose within a tolerance of ±1%.

Three separate exposures of 200 monitor units (MUs) were performed and each time the TLDs were read with a Harshaw 3500 TLD reader (Thermo Fisher Scientific Australia Pty Ltd, Victoria, Australia) by heating them to 300°C (TLDs were annealed between exposures). Individual chip-to-chip factors were calculated by normalising the TLD readings to the mean reading of all one hundred chips. In all cases within this project the mean is taken as the arithmetic mean of the sample given by Equation 8.1 in Section 8.2.

After the three exposures and calculation of three sets of chip-to-chip factors, the standard error in the average of the three measurements for each chip was used to select the most consistent fifty chips. These fifty chips were used for the remainder of the project.

3.1.2 Linear Accelerator Exposure TLD Calibration

Before the TLDs were exposed to the linac beams, the relative dose output of the linac was measured. The photon beams that were chosen had nominal energies of 6 MV and 18 MV (6 MV would serve as the reference for all exposures) and the electron beams had nominal energies of 6 MeV, 9 MeV, 12 MeV, 16 MeV and 20 MeV. A calibrated NE 2577 Farmer type field ionisation chamber (IC) was used to measure the dose in gray (Gy) per 100 monitor units (MU) at a depth of d_{max}, with a 100 cm source to surface distance (SSD) and with a 10 × 10 cm^2 field size. This was done immediately prior to TLD irradiation and enabled TLD readings to be normalised for dose. These measurements were traceable to an absolute dose measurement in water using the TRS398 protocol and a secondary standard NE 2611A Farmer type IC (International Atomic Energy Agency 2000). The electrometer used was an Inovision 35040 (Fluke Australia Pty Ltd, Melbourne, Australia). The linacs at the RAH are calibrated such that the dose output is 1 Gy per 100 MUs at the reference conditions detailed above (±1% tested biannually for photons and annually for electron and with a constancy of ±2% tested fortnightly in accordance with the TG142 protocol) (Klein et al. 2009). For the relative dosimetry

checks, the IC was inserted into a specially made poly block phantom that contained the necessary build-up and backscatter dimensions.

The PMMA TLD template was used to expose the TLD700:LiF chips to the linac beams. The template was loaded with 8 TLDs for each beam, arranged in a 2 cm × 2 cm symmetrical pattern at the centre of the template. The template was centred in the beam using the light field and calibrated cross hairs. Dose profiles obtained, which are verified annually, showed less than 1% variation in dose ±1 cm from the central axis. The other conditions used included a 10 × 10 cm^2 field size, a 100 cm SSD and TLD placement the depth d_{max}, where dose is at a maximum (Figure 4). The TLDs were then read and the readings were normalised to the 6 MV linac output readings. After readout, the TLDs were annealed, ready for subsequent exposures.

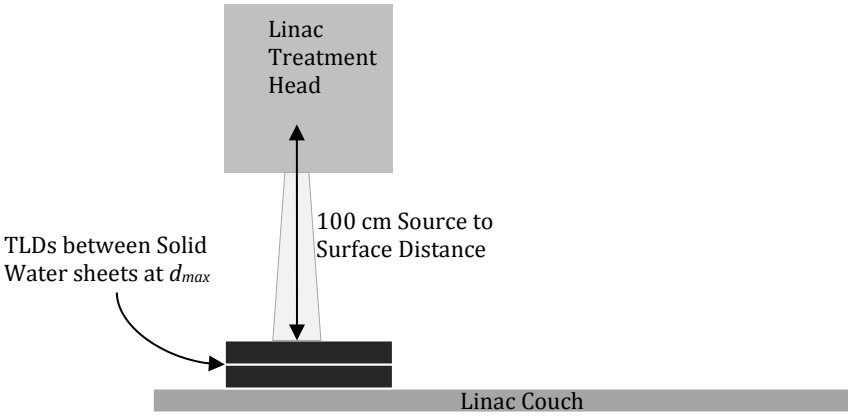

Figure 4. Linac setup for TLD exposure.

3.1.3 Superficial X Ray Exposure TLD Calibration

The TLD700:LiF chips were exposed to the various x ray spectra from the department's Gulmay D3150 (Gulmay Limited, Surrey, United Kingdom) superficial x ray machine. The calibration of output dose rate of each beam was performed in accordance with the IPEMB Code of Practice and its addendum (Aukett et al. 1996) (Aukett et al. 2005). The calibrated dose rate (Gy/min) of the machine for each filter with a 25 cm focus to surface distance (FSD) and a 10 cm diameter applicator cone was determined through the use of calibrated ionisation chambers. A PTW Freiburg 0.02 cc low energy parallel plate (NE2532, Q23342) was used for very low energies (30, 40, 50 kVp) and a NE 2611A Farmer type ionisation chamber was used for low energies (80, 100, 120, 140 and 150 kVp).

The TLDs were exposed without a build-up layer and with at least 10 cm of backscatter material (Solid Water) such that a back scatter factor need not be

applied. The TLDs were exposed to a dose of 2 Gy, where the beam-on time was calculated from the calibrated output dose-rate of each beam. 9 TLDs were placed in a different PMMA template that had holes measuring 3 × 3 × 0.9 mm^3, the exact dimensions of the TLD chips, such that any horizontal scatter contributing to dose was not lost. The TLDs were then read and normalised to the 6 MV linac readings.

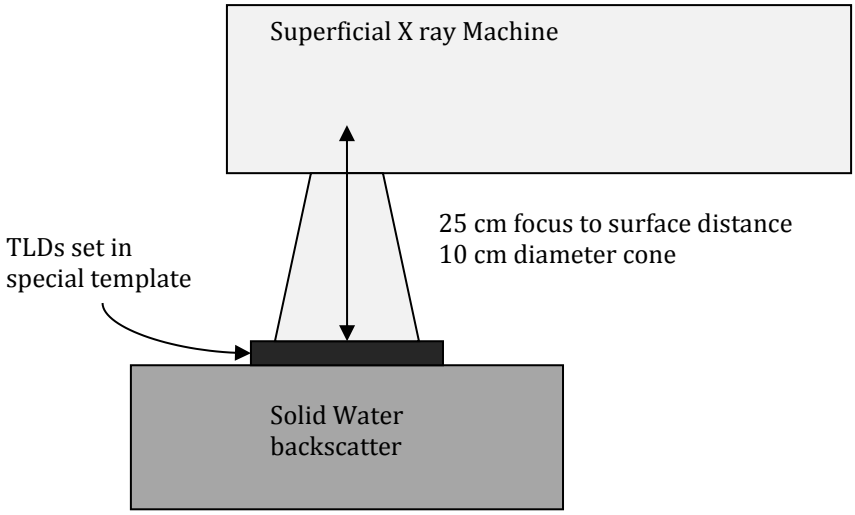

Figure 5. Superficial x ray setup for TLD exposure.

3.2 Linac and SXR Beam TLD Calibration Results

The sensitivity factors of the TLD chips, calculated from TLDs exposed to uniform radiation from a Varian iX linac, ranged from 1.132 to 0.930. Chips that were used had standard errors less than 0.014 where the standard error was the sample standard deviation divided by the square root of the number of values.

The linac output for each beam modality, as determined using a PTW 2577 farmer type ionization chamber, ranged from 0.992±0.005 to 1.005±0.005 cGy/MU. The TLDs received 200 MUs (approximately 2 Gy) of radiation and were placed at a depth of approximately d_{max} under TRS 398 reference conditions. The chips were read and the readings were corrected for linac output (cGy/MU), percentage depth dose (TRS 398) and the chip sensitivity factor such that the final chip reading represented exactly 2 Gy. These readings were then normalised to the reading from the 6 MV beam, such that the energy response from the 6 MV beam was 1.0. The error in the energy response for a particular beam was determined by the quadrature sum of the relative errors in the readings (six TLDs were used per beam) and the experimental error. The absolute error was taken to be the sample standard deviation, which accounted for the uncertainty in the linac output beam profile and

the TLD positioning (< 1%). The energy responses for the different beams are shown in Table 1.

Table 1. Energy response for seven linac beams (6 MV normalised).

Photon Beam	Energy Response
6 MV	1.000±0.017
18 MV	0.972±0.015

Electron Beam	Energy Response
6 MeV	0.967±0.015
9 MeV	0.968±0.015
12 MeV	0.954±0.017
16 MeV	0.968±0.016
20 MeV	0.952±0.016

TLDs were then exposed to the full range of filtered x ray energy spectra from the Gulmay D3150 SXR unit. Five TLD700:LiF chips were used per beam. Calibrated output rates from the SXR unit ranged from 1.362±0.027 Gy/min to 6.379±0.128 Gy/min for surface exposures, a 25 cm focus to surface distance and a 10 cm diameter applicator cone. The TLDs were exposed and their readings corrected for exposure time, the percentage depth dose (PDD) curve across the 0.9 mm depth of the TLD chip (determined in water during commissioning of the SXR unit) and chip sensitivity factors. The uncertainty calculation for the experimental results took into account the error from the calibrated output dose-rates (< 2%), PDD curve and the exposure time (< 0.2%). The total uncertainty in energy response was the relative error in the TLD readings combined with the experimental setup uncertainty. TLD readings were normalised to the 2 Gy reading from the TLDs exposed to the 6 MV linac beam. The energy responses for the nine SXR beams are shown in Table 2.

Table 2. Energy response for nine superficial x ray beams (6 MV normalised).

kVp	HVL	Energy Response
30	0.2 mm Al	0.950±0.039
40	0.5 mm Al	1.327±0.038
50	1 mm Al	1.526±0.059
80	2 mm Al	1.528±0.050
100	3 mm Al	1.529±0.055
120	4 mm Al	1.460±0.043
120	5 mm Al	1.457±0.036
140	8 mm Al	1.371±0.050
150	0.5 mm Cu	1.364±0.065

3.3 Linac and SXR Beam TLD Calibration Discussion

As the energy dependence of LiF is not fully understood, the best avenue for discussion of results is to compare the findings with previously published works.

Compared to the response from the 6 MV beam irradiation, there was a slight under-response of the TLDs to the 18 MV beam and to all electron beams from the linac. Though not completely analogous, a study by Almond et al. (1966) compared the energy response of TLD700s exposed to ^{60}Co gamma rays and 22 MeVp x rays (the nominal energy for ^{60}Co gamma rays is approximately 1.25 MeV). Almond and his team found that TLD700 did indeed have a slight under-response of 0.916±0.012 for the 22 MeVp x ray beam compared to the same dose from the ^{60}Co beam. This is consistent with the result of a slight under response of 0.972±0.015 from the 18 MV beam compared to the 6 MV in the current study.

A similar under response was observed for the electron beams as compared to the response from the 6 MV photon beam. Furthermore, the experimental results did not show a definite trend with changing electron energy, with a total energy response value for all electron beams of 0.961±0.011. These results support claims made by Crosby et al. (1966) and Almond et al. (1967) regarding energy responses for high-energy electrons beams. The present study's findings conflict with assertions made by Suntharalingam and Cameron (1969) that no energy response was found for TLD700:LiF or TLD100:LiF using electron beam energies ranging from 6 to 33 MeV. Almond et al. (1966) found a slight under-response when using the Co-60 beams to compare the energy response of LiF to high-energy electrons. The energy response for 6 MeV electrons was 0.931±0.008 and decreased to 0.886±0.015 for 18 MeV electrons. The slight under-response found in this work is consistent with these results.

Data from a study performed by Mobit et al. (1998) showed that the energy response of TLD100 was flat (±3%) over an energy range of 300 kV to 25 MV. Similarly, the current project's results show that the energy response of TLD700 is relatively flat (within approximately 5%) for the linac beam energies used in the range of 6 MV to 18 MV.

The energy response for SXR energies was much greater than that for the linac photon and electron beams. A large over-response ranging from approximately 33% to 53% was observed. Interestingly, an under response of 5% was observed for the lowest energy x rays (30 kVp 0.2 mm HVL Al). There was greater uncertainty in SXR results when compared to the linac results, because the machine output dose

determination had greater uncertainty. Additionally, the experiment was performed at the surface of the Solid Water block, so the TLDs spanned a greater percentage dose gradient than when they were exposed with the linac beams (13.6% drop in PDD for the first millimetre with the lowest energy SXR beam and 0.2% for highest). Despite this uncertainty, the results from repeated experiments had mean values of energy response that were reproducible to within 0.2%.

The results produced from these experiments contradict conclusions made by Das et al. (1996), who determined, by Monte Carlo methods, that the TLD response was constant with changing photon energy in the range of 20 – 250 kVp. The results found by Das et al. have been disputed a number of times previously, in particular, by Davis et al. (2003) who demonstrated an energy response by Monte Carlo methods. In a study made by Muhogora et al. (2002), it was found that TLD700 exhibited a definite over-response for diagnostic x ray energies between 55 and 120 kVp, demonstrated on a few different Siemens machines. Muhogara et al. showed that the over-response of TLD700:LiF tapers off for higher energies, which is certainly what the current study has shown. An over-response was also shown by Kron (1994) and Duggan et al. (2004) of 40% and 50% respectively for low energy photons.

Muhogora et al. (2002) showed that TLD energy dependence differs among SXR machines but follow the same general trend, therefore this project's results appear reasonable but also unique to the SXR unit used at the RAH. Since the energy dependence of LiF will differ among machines, it is advised that this experiment be repeated in each department where TLD700:LiF will be used clinically for SXR dosimetry.

Data from the study by Mobit et al. (1998) showed that for lower energy x rays, the energy dependence of LiF TLDs varies considerably at kilovoltage energies. Mobit compared the response of LiF to various beams to the response of the LiF exposed to ^{60}Co, through Monte Carlo simulations. Because the study used monoenergetic beams and TLD100:LiF, it can only serve as an indication for the trends to be observed in this project, not a direct comparison. The results from Mobit's study are shown in Table 3.

Table 3. TLD100:LiF(Mg,Cu,P) quality response (Mobit, Nahum & Mayles 1998).

Beam Quality	TLD100:LiF Quality Response
50 kV x rays	1.625±0.010
100 kV x rays	1.502±0.008
150 kV x rays	1.412±0.009
250 kV x rays	1.082±0.010
300 kV x rays	1.061±0.009
^{60}Co γ rays	1.009±0.008
6 MV x rays	1.000±0.008
10 MV x rays	1.001±0.008
25 MV x rays	0.996±0.008

Mobit's data displays the same trends as seen in the current work, in that the TLD energy response is much greater for low energy x rays and tapers off for higher energies, becoming almost constant at MV beam energies. The results from this project have not been compared with equation-based models reported in the literature, due to the complex spectra of the beams utilised.

4. MONTE CARLO MODELLING OF AN IRIDIUM-192 SOURCE

In order for the TLD700 chips to have their energy response determined for exposure from the gamma spectrum of an ^{192}Ir source, the dose to the chips had to be determined so that the response could be properly normalised to that from the 6 MV linac exposure.

4.1 MC Geometry and Physics

Oncentra Prostate's dosimetry algorithm is based on dose to water according to AAPM report TG43 (Nath et al. 1995). However, routine source strength calibration measurements are performed with an ionisation chamber in air, utilising an in-air calibration factor, N_k, to measure the air kerma strength, S_k (ARPANSA). This factor is only available in the low (superficial) energy range and for ^{60}Co irradiation. This means that the dose to water cannot be directly determined using an ionisation chamber for the range of energies applicable to ^{192}Ir irradiation.

Due to the lack of direct dose to water calibration methods of ^{192}Ir, Monte Carlo modelling methods were employed. This was deemed advantageous due to the spatial and dosimetric accuracy of the modelling technique and because it was a direct approach (without using conversions from dose-to-air to dose-to-water). Currently, no direct in-water calibration methods are available in Australia, apart from AAPM report TG43 equations, which could not be used because the TLDs would not be providing an independent verification but rather a self-verification of Oncentra Prostate's TG43 based dosimetry.

Formalism exists for in-air measurements with ionisation chambers for dose to air. However, ratios of mass attenuation coefficients $(\mu/\rho)_{\text{air}}^{\text{water}}$ are not available for converting dose to air into dose to water for an attenuated ^{192}Ir spectrum.

The ^{192}Ir source utilised in this work was the MicroSelectron v2 HDR Brachytherapy source (Nucletron Pty. Ltd. an Elekta AB Company, Stockholm, Sweden). The source arrives 3-monthly to the RAH Department of Medical Physics along with a source certificate (Section 8.10) detailing the apparent activity and air kerma strength of the source on a specific manufacturer calibration date. This apparent activity and air kerma strength were used to calculate daily air kerma

strength values for this study in accordance with the half-life of the source (73.827 days).

For the Monte Carlo program to effectively model the radiation interactions within the brachytherapy source, in the water medium and within the TLD material (if required), the decay characteristics of ^{192}Ir were required. An ^{192}Ir nucleus in the 4^+ ground state has a 95.13% probability of decaying via β^- to ^{192}Pt (Figure 6) and a 4.87% chance of decaying via electron capture to ^{192}Os (Figure 7). The energy levels (in MeV) of the daughter nuclei, which dictate the energies of the emitted gamma rays, are shown in Figures 6 & 7 on the right (Chang 2013).

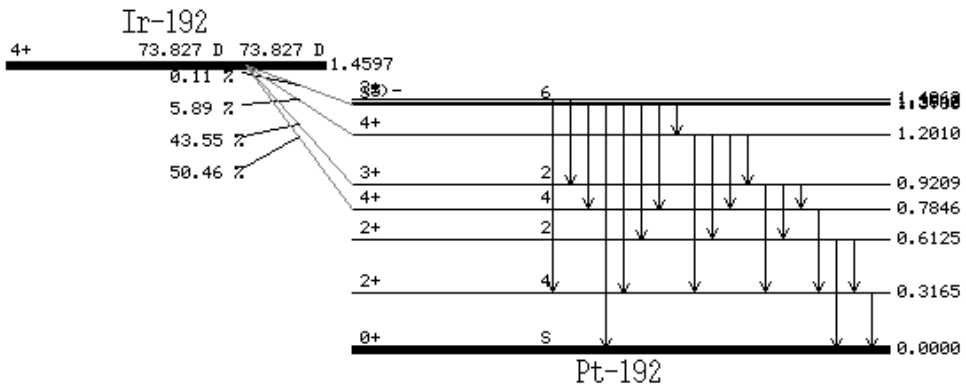

Figure 6. Beta minus decay of ^{192}Ir from the ground state (Chang 2013).

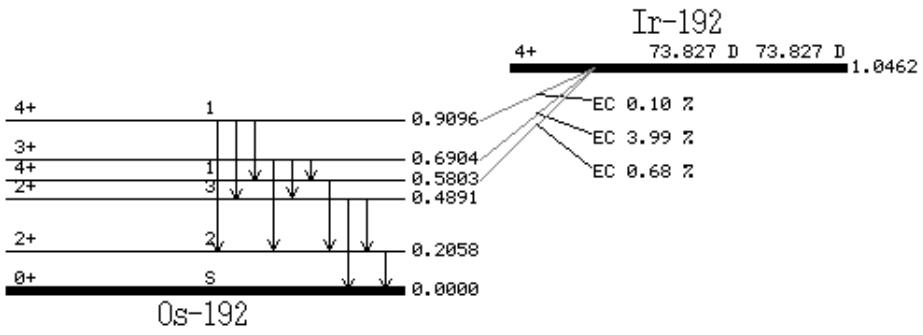

Figure 7. EC decay of ^{192}Ir from the ground state (Chang 2013).

The ^{192}Ir source is encapsulated in stainless steel, which attenuates the β^- particles to insignificant levels. The daughter nuclei emit gamma rays when they decay to their ground states. It is these gamma rays that penetrate the capsule and are utilised for treatment.

To simulate this process, the ^{192}Ir source was constructed in GEANT4 to model the real source and steel cable (laser welded to the source) as closely as possible. A 3.6 mm long cylinder of ^{192}Ir was created with a diameter of 0.7 mm. This was encapsulated in a steel cylinder that had a diameter of 0.9 mm and extended

beyond the end of the iridium source by 0.2 mm as shown in Figure 8. The steel cable, which attaches to the ^{192}Ir source, was constructed to reach the edge of the GEANT4 environment, which had a volume of 1 m^3.

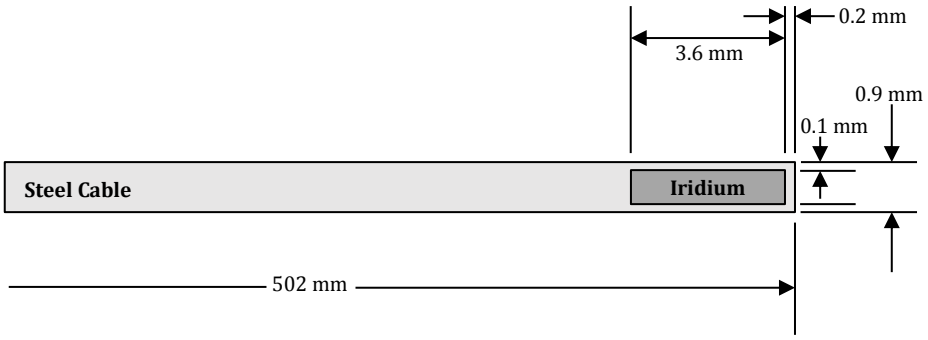

Figure 8. Model of the MicroSelectron v2 HDR source.

The centre of the iridium source was located at the origin of the GEANT4 lab volume. The modelled steel was composed of 68% iron, 19% chromium, 10% nickel, 2% manganese and 1% silicon and was assigned a density of 8.02 g/cm^3 (Borg & Rogers 1991).

For the actual experiment, the real source and its cable were remotely driven through a nylon catheter. This catheter was modelled in GEANT4 as a cylinder with an inner diameter of 1.5 mm and an outer diameter of 2.0 mm. The nylon was made of 63.7% carbon, 14.2% oxygen, 12.4% nitrogen and 9.7% hydrogen (derived from molecular formula $C_{12}H_{22}N_2O_2$) and was given a density of 1.10 g/cm^3 (Palmer 2001). The iridium source was modelled as pure iridium because the true osmium and platinum percentages of the hospital's source at time of manufacturer calibration could not be obtained.

In GEANT4, only the number of ^{192}Ir nuclear decays could be set when running the simulation, not the source's apparent activity or exposure time. This posed some challenges for matching the number of primary particles released in the simulation to the real life situation. However, solving this problem was necessary for converting the known source data into a parameter available for use in the simulation.

The data sheet supplied by Nucletron only detailed the apparent activity of the source and not the contained activity (apparent activity is the activity measured outside the source at 1 m in air, whereas the contained activity is the true number of decays per second of the radioactive isotope before self-attenuation). The number of beta particles per second (apparent activity A_{app}) released from the ^{192}Ir core of the

source before attenuation is related to the number of daughter gamma particles released N_{photon} by Equation 4.1 (Borg & Rogers 1991).

$$N_{photon} = A_{app} \times (2.363 \pm 0.3\%) \tag{4.1}$$

Using this equation, the number of gamma particles passing through a certain area over a particular exposure time could be determined. In the simulation, if the number of gamma particles could be counted passing through the voxel of interest for the duration of the simulation and this number was compared to the number of photons expected in the live experiment, a scale-up factor could be determined for the corresponding dose given in that voxel by the Monte Carlo simulation. For example, if the actual apparent activity of the source is A_{app}, the cross sectional area of the TLD is Ω, the distance from the TLD voxel to the source is r and the exposure time is t, then the number of photons N that pass through the voxel is given by Equation 4.2 (N is some fraction of the total number of photons released N_{photon} according to Ω).

$$N = A_{app} \times 2.363 \times t \times \frac{\Omega}{4\pi r^2} \tag{4.2}$$

If a MC simulation of n primary particles is run which gives a dose D_{MC} to the voxel of interest (which makes up the volume of the TLD) and N_{MC} photons are counted, then the dose D to the detector volume in reality is given by Equation 4.3.

$$D = D_{MC} \times \frac{N}{N_{MC}} \tag{4.3}$$

The energy deposited in each voxel was determined in the GEANT4 simulation by recording the kinetic energy deposited after each interaction of the photon while travelling through the voxel, and summing the results for all photons. The minimum step length is set by the user in the MC program and is recommended to be less than half the width of the voxel. The minimum step length used for this project was chosen to be 0.045 mm because it was much less than half the thickness of the TLD, so every interaction that should have occurred in the voxel was recorded.

GEANT4 then determines the particle's minimum energy before it is programmed to stop and it deposits any remaining energy at that step point. The total dose deposited in each TLD voxel was then a simple calculation of dividing the total energy deposited in the voxel by the mass of the voxel.

To achieve this, the number of photons passing through each detector voxel was determined by creating a counter array that increased an element every time a unique track was made in the voxel. Code was also written to ensure that other particles creating tracks in the voxels, such as electron and neutrinos, were not counted.

4.2 Verification of the MC Model

The Monte Carlo program was verified by calculating the dose to a voxel of air (in-air medium) and comparing it to the analytic calculations for dose using the standard air kerma strength formalism. This method involves an ionisation chamber that measures exposure X in air, which is a product of the measurement result M and the exposure calibration factor N_x. The air kerma rate $\dot{K}_{air}$ can then be calculated by Equation 4.4 (Johns & Cunningham 1983).

$$\dot{K}_{air} = \dot{X}_r \left(\frac{\overline{W}}{e}\right) r^2 \ [\text{cGy m}^2\ \text{h}^{-1}] \tag{4.4}$$

where $\dot{X}_r$ is the exposure rate at a distance r from the source and the factor $(\overline{W}/e)$ is the energy required by the gamma rays to produce an ionisation event. The air kerma rate measured at 1 m is called the air kerma strength S_k. The dose to air at any distance from the iridium source can then be calculated by Equation 4.5.

$$D_{air} = \frac{S_k t}{r^2} \ [\text{cGy}] \tag{4.5}$$

For the chosen reference activity of 224 GBq, the corresponding air kerma strength was calculated from the source data sheet to be 2.695 cGyh^{-1} (different source to that shown in Section 8.10). Equation 4.5 therefore provides a dose to air value at a 60 mm and for an exposure of 300 s to be 0.6238 Gy.

A simulation with 10^7 primary particles released (16 hours) with a dose scoring voxel cylinder at a distance of 60 mm between its inner surface and the origin of the lab volume was made. The voxel details and results are given in Table 4.

Table 4. Simulation results for 10^7 particles, air voxel, air medium, 60 mm.

Inner r (m)	Outer r (m)	Average r (m)	Cross section Ω (m^2)	Fraction of sphere	Volume (m^3)	Mass (kg)
0.0600	0.0609	0.0605	7.540×10^{-4}	0.0167	6.837×10^{-7}	8.375×10^{-7}

Energy (J)	Counts N	Dose D_{MC}	Projected counts N_{MC}	Projected dose D (Gy)	Analytic dose (Gy)
6.64×10^{-14}	329882	7.92×10^{-8}	2.647×10^{12}	0.636	0.624

The physical cross-section of the air voxel was calculated by the inner radius multiplied by $2\pi \times 0.002$ mm since the width of the voxel cylinder was 0.002 m. The mass of the voxel cylinder was calculated using an air density of 1.225 kg/m^3. The "fraction of sphere" term is purely the $\Omega/4\pi r^2$ term seen in Equation 4.2. The energy is the total kinetic energy released inside the detector voxel volume and the counts is the number of unique photons counted losing energy in the same volume. The dose was calculated as the energy divided by the mass; and the number of projected tracks, for the reference conditions of 224 GBq and a 300 s exposure, was calculated using Equation 4.2. The projected dose was then calculated using Equation 4.3.

Since the projected dose was in close agreement with the dose predicted by Equation 4.5 (differed by 2%, see Table 4), the simulation was run three times with additional voxel cylinders with 10, 20, … 100 mm radii. Table 5 details the voxel parameters and the results of the simulation. The projected dose standard deviation was calculated by considering the ratios of each projected dose point and the average dose on the same row. The average ratio was taken to be the relative error in the simulation and the standard deviation was then simply the relative error multiplied by the projected dose. The relative error for the simulations given in Table 5 where dose was recorded in air voxels within an air medium was 6.4%.

Table 5. Simulation results for 10^7 particles, air voxel, air medium, 10 - 100 mm.

Cylinder arc dimensions (m)			Cross section ($\times 10^{-4}$ m^2)	Fraction of sphere	Volume ($\times 10^{-7}$ m^3)	Mass ($\times 10^{-7}$ kg)
Inner *r*	Outer *r*	Mean *r*				
0.01	0.0109	0.01045	1.26	0.1000	1.18	1.45
0.02	0.0209	0.02045	2.51	0.0500	2.31	2.83
0.03	0.0309	0.03045	3.77	0.0333	3.44	4.22
0.04	0.0409	0.04045	5.03	0.0250	4.57	5.60
0.05	0.0509	0.05045	6.28	0.0200	5.71	6.99
0.06	0.0609	0.06045	7.54	0.0167	6.84	8.37
0.07	0.0709	0.07045	8.80	0.0143	7.97	9.76
0.08	0.0809	0.08045	10.1	0.0125	91.0	11.1
0.09	0.0909	0.09045	11.3	0.0111	10.2	12.5
0.1	0.1009	0.10045	12.6	0.0100	11.4	13.9

Energy deposited ($\times 10^{-14}$ J)			Photon counts ($\times 10^5$)			Dose ($\times 10^{-8}$ Gy)		
Run 1	Run 2	Run 3	Run 1	Run 2	Run 3	Run 1	Run 2	Run 3
32.2	28.2	30.2	18.9	18.9	18.9	222	195	209
17.0	17.4	17.3	9.85	9.86	9.86	60.1	61.3	61.0
13.6	11.6	11.7	6.59	6.59	6.59	32.2	27.4	27.8
9.11	8.20	9.34	4.94	4.95	4.95	16.2	14.6	16.7
9.27	7.61	8.97	3.95	3.96	3.96	13.3	10.9	12.8
6.64	6.58	6.80	3.30	3.30	3.30	7.92	7.86	8.11
6.38	6.05	5.38	2.83	2.83	2.83	6.54	6.20	5.51
5.21	5.24	4.20	2.47	2.48	2.47	4.68	4.70	3.77
4.83	4.91	4.27	2.20	2.20	2.20	3.86	3.91	3.40
4.23	4.27	4.63	1.98	1.98	1.98	3.04	3.07	3.33

Projected tracks ($\times 10^{12}$)	Projected dose (Gy)			Mean projected dose (Gy)	Standard Deviation (Gy)	Analytic dose (Gy)
	Run 1	Run 2	Run 3			
15.9	18.7	16.3	17.5	17.5	1.1	20.6
7.94	4.85	4.93	4.91	4.90	0.31	5.37
5.29	2.59	2.20	2.23	2.34	0.15	2.42
3.97	1.31	1.17	1.34	1.27	0.08	1.37
3.18	1.07	0.875	1.03	0.990	0.063	0.882
2.65	0.636	0.630	0.651	0.639	0.041	0.615
2.27	0.524	0.496	0.442	0.488	0.031	0.452
1.98	0.375	0.377	0.303	0.352	0.022	0.347
1.76	0.310	0.314	0.274	0.299	0.019	0.275
1.59	0.244	0.246	0.268	0.252	0.016	0.223

The plot of the analytic dose vs. projected dose for the reference conditions is given by Figure 9.

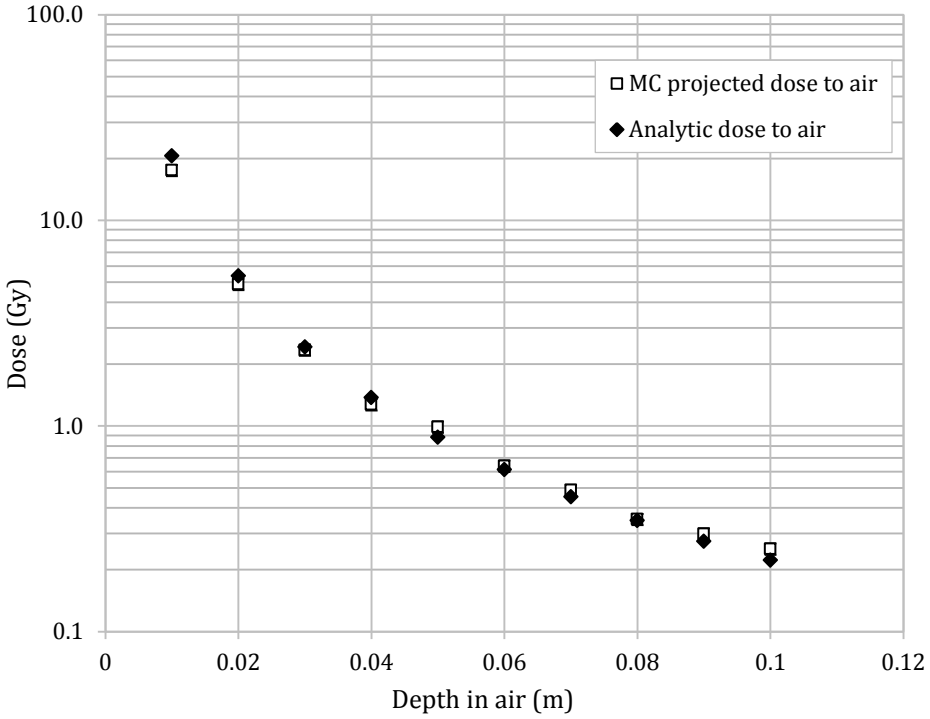

Figure 9. Analytic dose vs. projected dose in air.

The depths plotted in Figure 9 are the midpoints of the TLD volume voxels, not the closest surface. The standard deviation in the simulated doses was very small except for the closest voxel at 10 mm where the dose gradient was the greatest (Table 5). The average ratio of the Monte Carlo simulated dose and that calculated by the analytical equation was 0.995±0.098 (1 SD).

Since there was good agreement between the dose predicted by the independent Monte Carlo simulation of the ^{192}Ir source and the analytically derived dose based on the air kerma strength, it was reasonable to assume that the method of dose calculation and experimental setup in GEANT4 was correct. The method of dose calculation refers to Equation 4.2 and Equation 4.3 where projected dose is derived from the number of photons passing through detector voxels. The experimental setup included the materials and their properties and the spatial distribution and orientation of the materials in the GEANT4 lab volume.

On average, the Monte Carlo derived doses differed from the analytically derived doses by 1.30%. However, for distances less than 50 mm from the centre of the source dwell position, the MC predicted doses were less than the analytical dose. For distances greater than 50 mm, the MC predicted dose was greater than the analytic dose, most likely due to the contribution of scatter. Consequently, the MC

predicted dose did not fall away as quickly as shown by the analytical equation for air kerma strength, which solely relies on the inverse square law for dose drop off.

4.3 MC Simulation Results and Discussion

Once the Monte Carlo program had been verified against Equation 4.5, calculations in a water medium could begin. Both dose to LiF voxels and water voxels were simulated to observe differences in dose deposition. If the differences in mass attenuation coefficients for water and LiF indeed contribute to the energy response of TLDs as suggested by Mobit, Nahum & Mayles (1998), then there would be evidence for a depth dependent response if the ratio of dose to LiF and water was dependent on depth. The simulation results for the dose to water would be used to calibrate the energy response of the TLDs for use in a water medium.

Since a single TLD chip measured 3.0 × 3.0 × 0.9 mm^3, most of the simulated particles did not pass through the TLD voxel and were effectively a waste to simulate. Therefore, instead of simulating a single LiF chip, hollow LiF cylinder arcs concentric with the ^{192}Ir source were used to capture more particles and increase computational efficiency and simulation accuracy. The cylinder arcs had depth 0.9 mm and width 2.0 mm and had an inner radius r the same as the distance from the source to the chip. Cylinder arc voxels were simulated instead of full cylinders so that, for the simulations with LiF, interactions in the detector volumes would have a minimum effect on radiation reaching other voxels. As such, multiple voxels at different depths could be simulated, increasing the efficiency of the simulation (Figure 10).

The dose to the LiF or water cylinder arcs was equal to that of the small chip because dose is normalised to mass by definition. The composition of the simulated TLD700:LiF was derived from the chemical formula and relevant atomic numbers to be 73% fluorine and 27% lithium-7.

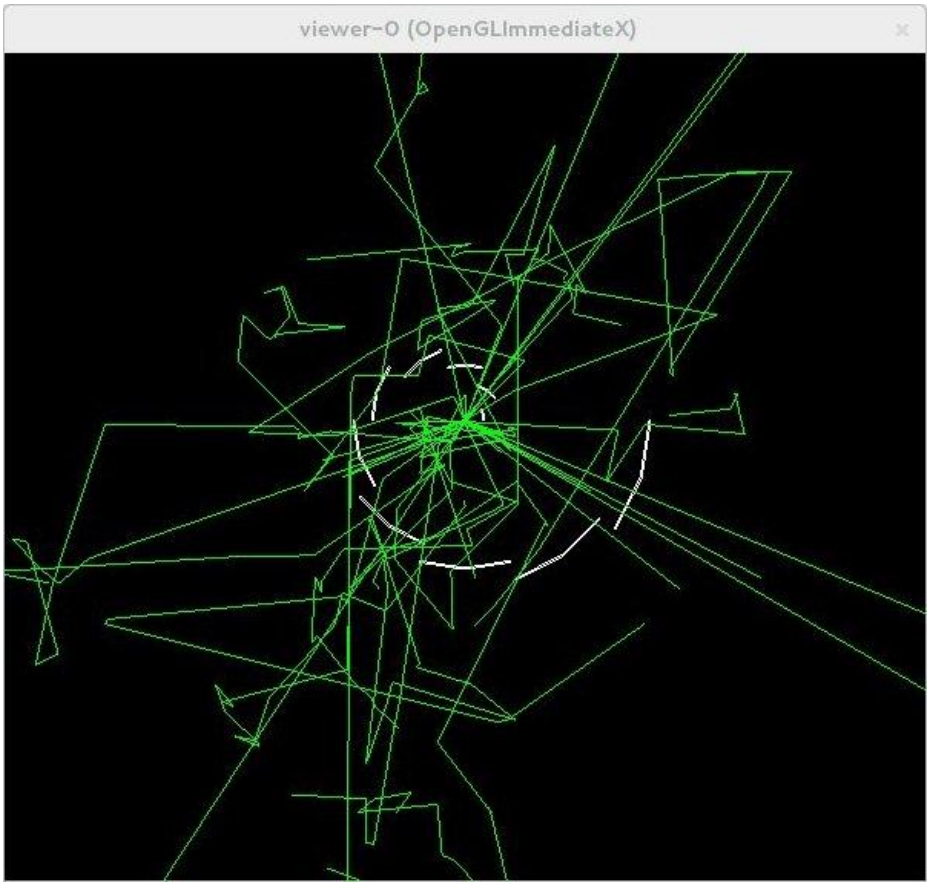

Figure 10. Visualisation of MC simulation with 10 primary particles.
Photon tracks are shown in green, the source is depicted at the centre of the image and the TLD arcs are represented in white.

Figure 10 shows ten TLD arcs at 10 mm, 20 mm, … 100 mm distances from the source each spanning 36 degrees. Simulations of 5×10^6 primary particles were made multiple times and took approximately 8 hours each. Their results were averaged to increase accuracy. The results with LiF voxels at depths from 10 to 100 mm in a water medium are given by Table 6, with the projected dose scaled to the reference conditions (224 GBq apparent activity and a 300 s exposure).

Table 6. Simulation results for 5×10^6 particles, LiF voxel, water medium, 10 - 100 mm.

Cylinder arc dimensions (m)			Cross section ($\times10^{-5}$ m^2)	Fraction of sphere	Volume ($\times10^{-8}$ m^3)	Mass ($\times10^{-5}$ kg)
Inner *r*	Outer *r*	Mean *r*				
0.01	0.0109	0.01045	1.26	0.0100	1.18	3.11
0.02	0.0209	0.02045	2.51	0.0050	2.31	6.09
0.03	0.0309	0.03045	3.77	0.0033	3.44	9.07
0.04	0.0409	0.04045	5.03	0.0025	4.57	12.1
0.05	0.0509	0.05045	6.29	0.0020	5.71	15.0
0.06	0.0609	0.06045	7.54	0.0017	6.84	1.80
0.07	0.0709	0.07045	8.80	0.0014	7.97	21.0
0.08	0.0809	0.08045	10.1	0.0013	9.10	24.0
0.09	0.0909	0.09045	11.3	0.0011	10.2	27.0
0.1	0.1009	0.10045	12.7	0.0010	11.4	29.9

Energy deposited ($\times10^{-12}$ J)			Photon counts ($\times10^4$)			Dose ($\times10^{-8}$ Gy)		
Run 1	Run 2	Run 3	Run 1	Run 2	Run 3	Run 1	Run 2	Run 3
34.4	34.8	34.8	10.5	8.70	8.66	111	112	112
18.7	18.4	18.0	5.74	4.17	4.19	30.7	30.2	29.5
12.3	13.0	12.6	4.16	2.63	2.62	13.6	14.4	13.8
9.83	9.35	9.36	3.28	1.86	1.88	8.15	7.75	7.77
7.57	7.50	7.71	2.78	1.40	1.40	5.03	4.99	5.13
5.42	5.91	6.09	2.44	1.09	1.09	3.01	3.28	3.38
5.13	4.79	4.66	2.15	0.891	8.89	2.44	2.28	2.22
4.63	4.49	4.52	1.92	0.729	0.726	1.93	1.87	1.89
3.96	3.82	3.56	1.75	0.614	61.9	1.47	1.42	1.32
3.35	3.55	3.87	1.58	0.525	52.6	1.12	1.18	1.29

Projected tracks ($\times10^{11}$)	Projected dose (Gy)			Average projected dose (Gy)	Standard deviation (Gy)
	Run 1	Run 2	Run 3		
15.9	17.8	18.0	18.0	18.0	0.6
7.94	4.96	4.87	4.77	4.86	0.16
5.29	2.19	2.32	2.23	2.25	0.08
3.97	1.31	1.25	1.25	1.27	0.04
3.18	0.812	0.804	0.828	0.814	0.028
2.65	0.486	0.529	0.545	0.520	0.018
2.27	0.394	0.368	0.358	0.373	0.013
1.98	0.311	0.302	0.304	0.306	0.010
1.76	0.237	0.228	0.213	0.226	0.008
1.59	0.181	0.191	0.209	0.193	0.007

The relative error for the simulations given in Table 6, where dose was recorded in LiF voxels within a water medium, was 3.39%. The relative error was calculated by considering the sample standard deviation of the ratios of each projected dose value and the average value on the same row.

The LiF voxels were then changed to water and four simulations of 5×10^6 particles were performed. The results for these simulations are given in Table 7.

Table 7. Simulation results for 5×10^6 particles, water voxel, water medium, 10 - 100 mm.

Energy deposited ($\times10^{-12}$ J)				Photon counts ($\times10^4$)				Mass ($\times10^{-5}$ kg)
Run 1	Run 2	Run 3	Run 4	Run 1	Run 2	Run 3	Run 4	
16.1	14.7	15.6	15.3	8.67	8.68	8.68	8.67	1.18
8.15	7.85	8.45	9.52	4.17	4.13	4.14	4.22	2.31
4.91	5.59	5.27	5.18	2.63	2.63	2.64	2.60	3.44
4.00	4.24	4.65	4.36	1.85	1.88	1.87	1.86	4.58
3.55	3.26	3.66	3.78	1.40	1.43	1.43	1.41	5.71
2.62	3.22	3.11	2.51	1.12	1.10	1.10	1.11	6.84
2.43	2.35	2.67	2.35	0.908	0.897	0.888	0.890	7.97
2.18	2.06	1.95	1.99	0.744	0.731	0.743	0.732	9.10
1.74	1.99	1.76	1.69	0.612	0.607	0.619	0.614	10.2
1.70	1.52	1.82	1.65	0.516	0.525	0.510	0.515	11.4

Dose ($\times10^{-8}$ Gy)				Projected tracks ($\times10^{11}$)	Projected Dose (Gy)			
Run 1	Run 2	Run 3	Run 4		Run 1	Run 2	Run 3	Run 4
136	125	132	129	15.9	22.0	20.0	21.3	20.8
35.2	33.9	36.5	41.1	7.94	5.68	5.47	5.89	6.64
14.3	16.2	15.3	15.0	5.29	2.30	2.62	2.47	2.43
8.73	9.27	10.2	9.53	3.97	1.41	1.50	1.640	1.54
6.22	5.71	6.42	6.63	3.18	1.00	0.921	1.035	1.07
3.83	4.70	4.54	3.67	2.65	0.617	0.759	0.733	0.592
3.04	2.95	3.35	2.95	2.27	0.491	0.476	0.541	0.476
2.39	2.27	2.14	2.19	1.98	0.386	0.365	0.345	0.353
1.70	1.94	1.72	1.65	1.76	0.274	0.313	0.277	0.267
1.49	1.34	1.60	1.45	1.59	0.241	0.216	0.259	0.234

Average projected dose (Gy)	Standard deviation (Gy)
21.1	1.3
5.92	0.37
2.45	0.16
1.52	0.19
1.01	0.06
0.675	0.043
0.496	0.031
0.362	0.023
0.283	0.018
0.238	0.015

For the data in Table 7, the voxel details were identical to those seen in Table 6, with only the mass changed. The projected dose was again scaled to the reference conditions (224 GBq apparent activity and a 300 s exposure). The relative error for the simulations given in Table 7 where dose was recorded in water voxels within a water medium was 6.31%. Therefore, changing the voxels from LiF to water approximately doubled the relative error of the simulation.

The plots of the Monte Carlo projected dose to LiF in water and the Monte Carlo projected dose to water in water are given by Figure 11. In each case, the projected dose was calculated in the same fashion as shown in Table 4 for the air voxel at 60 mm from the centre of the source dwell location. The error bars in Figure 11 are given by the sample standard deviation in the results and the points are plotted on a log graph to better show detail in the voxel doses at distances greater than 30 mm.

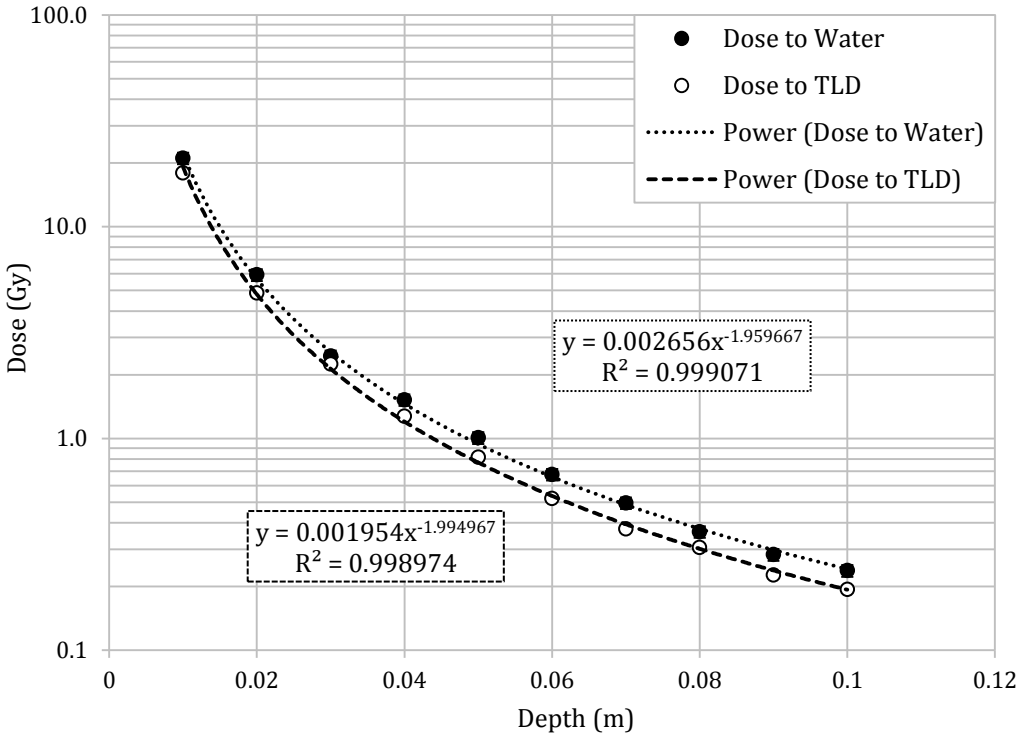

Figure 11. MC projected dose to water and TLDs in a water medium.

The dose to water at increasing depth was fitted to the curve given by Equation 4.6, with an R^2 value of 0.999.

$$D_{water}[\mathrm{Gy}] = (2.66 \times 10^{-3}) \times (r[\mathrm{m}]^{-1.96}) \ (\pm 6.3\%) \qquad (4.6)$$

This equation was useful in quantifying the effect of positional uncertainty on dose and for determining doses at points without linearly interpolating between simulated points. The dose to LiF was also fitted with a curve (Equation 4.7) with the ratios of D_{water} and D_{TLD}, determined through the ratios of Equations 4.6 and 4.7, shown in Figure 12.

$$D_{LiF}[Gy] = (1.95 \times 10^{-3}) \times (r[\mathrm{m}]^{-1.99}) \ (\pm 3.4\%) \qquad (4.7)$$

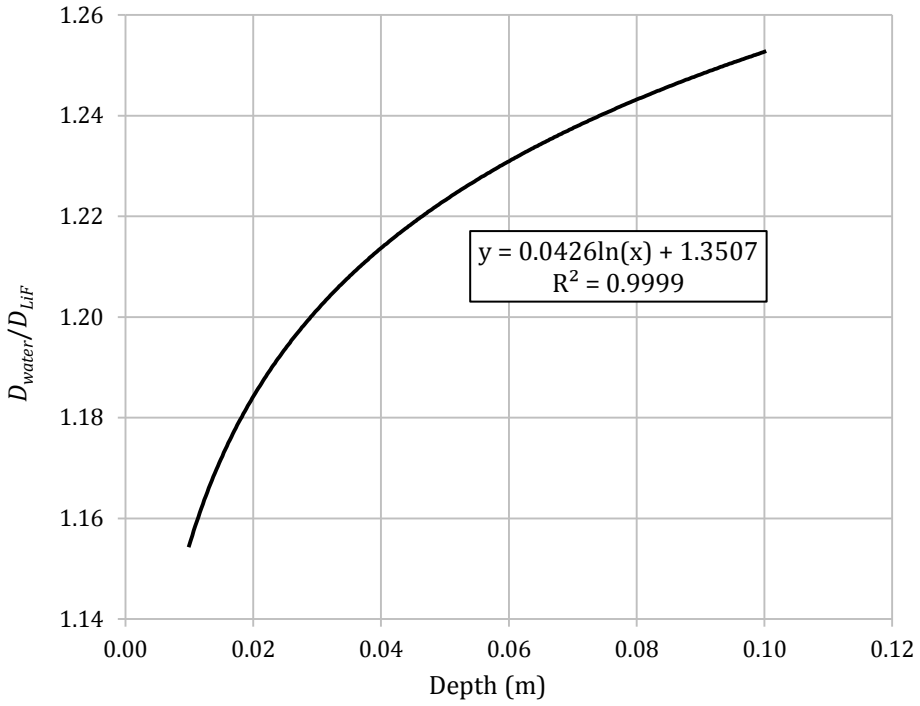

Figure 12. MC simulated differences in dose to water and dose to TLD in a water medium.

The ratio of D_{water} and D_{TLD} was observed to increase at greater depths in water. Therefore, if these differences in D_{water} and D_{TLD} do indeed contribute to the energy response of TLD700:LiF, then a depth dependent response can be expected. In this case, the response of the TLD was expected to be less at greater depths because the TLDs absorb relatively less dose than water (Figure 12).

The effect of attenuation due to the presence of a water medium was explored by plotting the dose to air against the dose to water, shown in Figure 13.

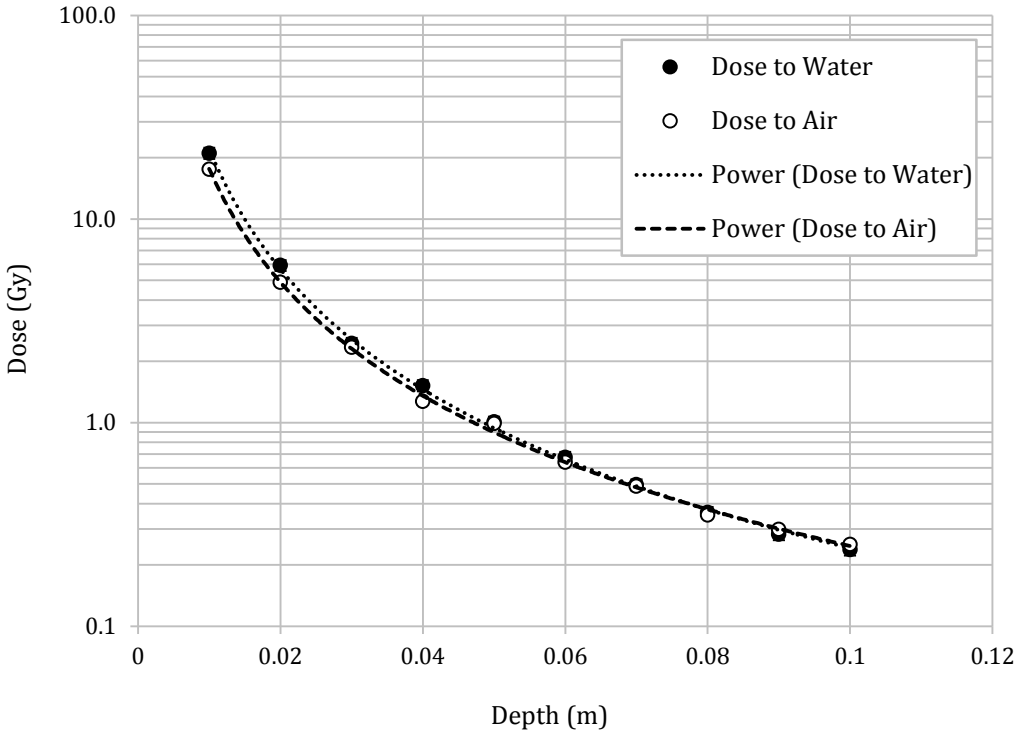

Figure 13. Dose deposition in water compared to air.

Surprisingly, the dose deposition in water did not differ significantly from the dose deposition in air (Figure 13). This indicated that the presence of water had little effect on the dose distribution around the ^{192}Ir source. Either there was very little attenuation of the photons by water or there was enough scattered secondary radiation to compensate for the loss of dose caused by attenuation.

Since the effect of attenuation appeared insignificant, additional Monte Carlo simulations were run to further verify the model and collect more data concerning the MicroSelectron v2 HDR source. The first of these simulations collected data for the gamma spectra at different depths in water, to explore the effect of attenuation on the energy spectrum. This was done by recording the initial kinetic energy of the photon on its first step through the voxel and binning it in an array of 100 elements, each of width 10 keV (the 100 element array could therefore bin photons between zero and 1000 keV).

Each newly simulated photon increased one of the elements in the array by one until a complete gamma spectrum was created by the end of the simulation. This simulation was performed with TLDs at distance of 1, 10, 50 and 100 mm from the centre of the source. The normalised spectra were plotted against each other to qualitatively observe the effect of attenuation (Figure 14 and Figure 15).

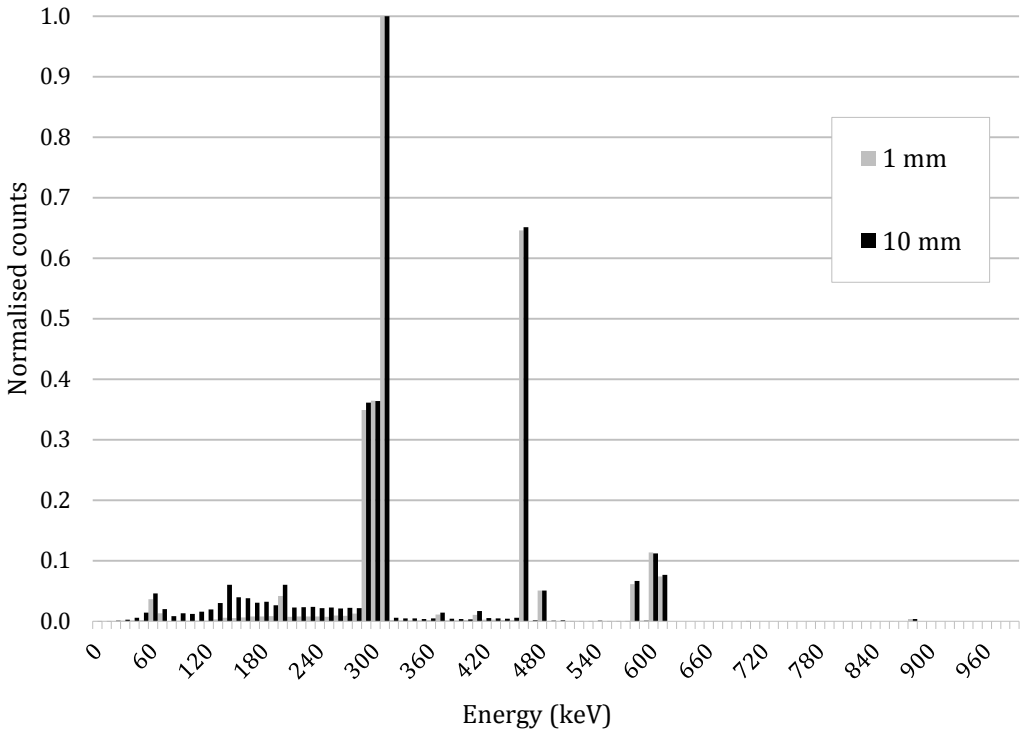

Figure 14. ^{192}Ir normalised γ spectra at 1 and 10 mm depths in water.

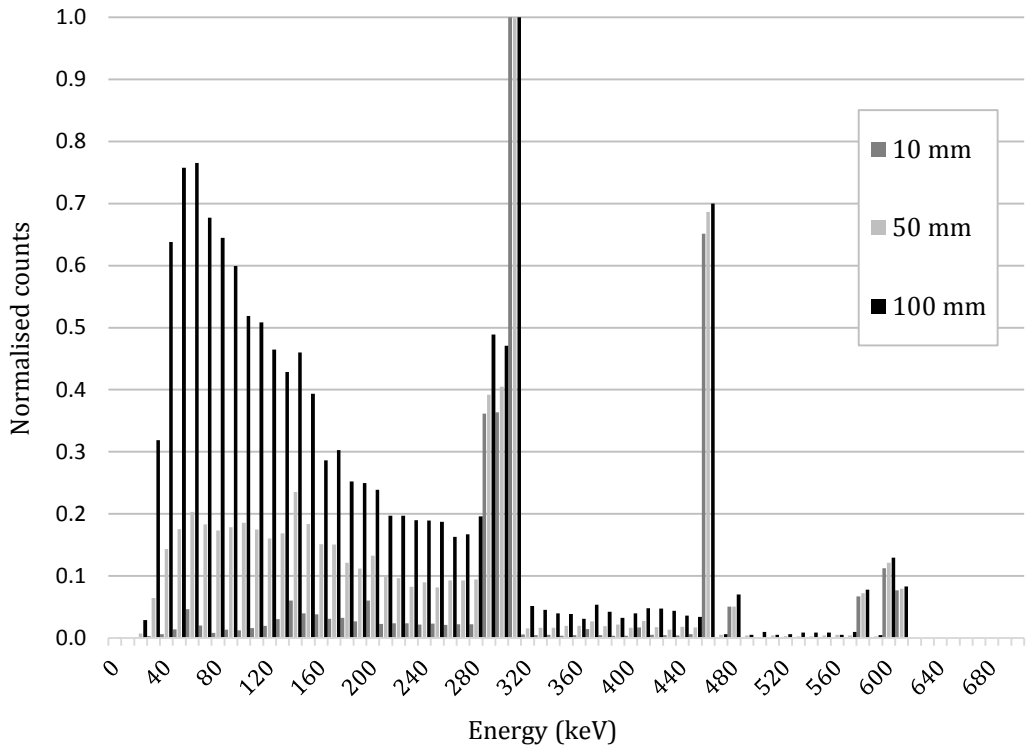

Figure 15. ^{192}Ir normalised γ spectra at 10, 50 and 100 mm depths in water.

Table 8. Average energy of the ^{192}Ir spectra at different depths in water.

Depth (mm)	Mean Energy (keV)
10	335
20	307
30	285
40	264
50	249
100	190
air	*359*

The average energy of 258 keV assumed by Haworth et al. (2012) for a depth of 50 mm in water was very close to the Monte Carlo value of 249 keV derived in this project. The average energy of the gamma spectrum followed Equation 4.8 with close conformity ($R^2 = 0.999$) for depths x from 10 to 100 mm in water.

$$E_{ave} = 0.0113x^2 - 2.29x + 360 \qquad (4.8)$$

It was expected that the gamma spectrum would change in water, even without the effects of scatter, because higher energy photons would not be attenuated as much as lower energy photons due to differences in their corresponding mass attenuation coefficients. This is known as beam hardening. As expected, there were negligible spectral changes within 10 mm of the source (Figure 14). The histogram of photon energies seen in Figure 14 is consistent with ^{192}Ir gamma spectra shown by Borg et al. (1991) and Anderson et al. (1990). This provided confidence that GEANT4 correctly simulates the gamma decays of the ^{192}Ir daughter nuclei ^{192}Os and ^{192}Pt.

In Figure 15, it was shown that considerable spectral changes do indeed occur for larger distances (50 mm – 100 mm) as expected but with considerable beam softening rather than beam hardening. At 50 mm, lower energy photons (< 200 keV) are shown to contribute substantially to the spectrum; and at 100 mm, the lower energy photons dominate the spectrum. These lower energy photons came from the scatter of the original gamma peaks and made up a large proportion of the photon spectra at depth. It was concluded that these lower energy photons contributed a large amount to the dose, so much so that they compensated for the dose lost due to attenuation of the main gamma peaks. The intensity of the low energy scatter at depth is in contrast to MC derived spectral data collected by Karaiskos et al. (1998) who claimed that the attenuated spectrum of ^{192}Ir in water only showed a slight increased proportion of low energy photons at a depth of 100 mm in water.

To verify that GEANT4 was simulating attenuation accurately, further investigations were made on the effect of attenuation by changing the water medium to steel and running several simulations. The simulation was carried out with voxels at distances of 10 – 100 mm from the centre of the source dwell position and for 10^7 primary particles. The resultant PDDs from water and steel media were then normalised for the inverse square law (ISL) and compared (Figure 16).

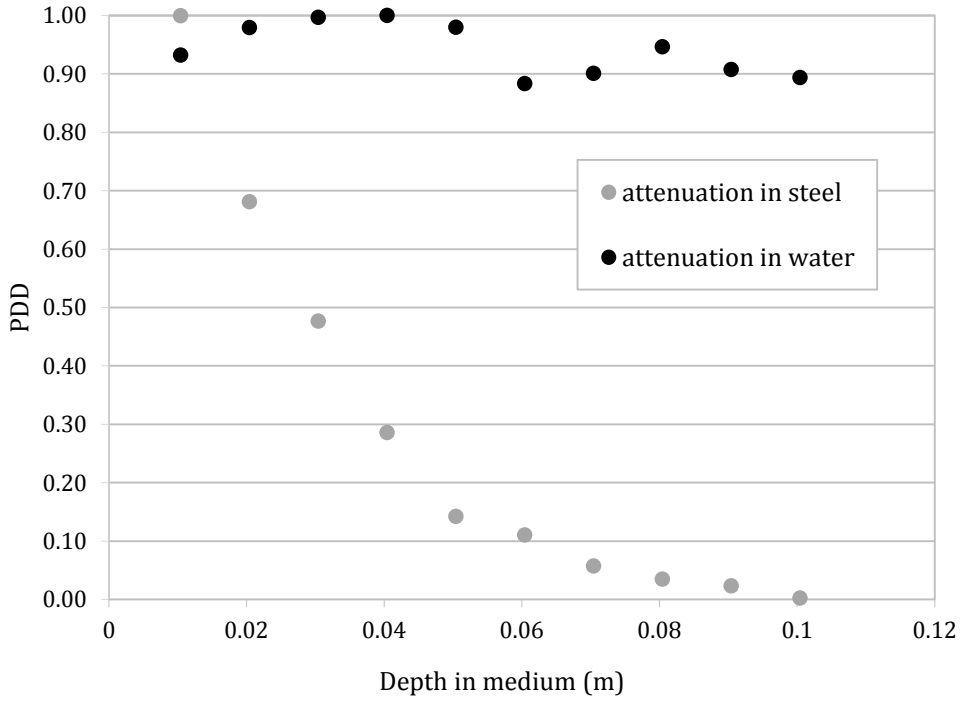

Figure 16. Effect of attenuation in water and steel (inverse square law normalised).

It was initially thought that GEANT4 was not simulating attenuation through water correctly when the results for the ISL normalised PDDs in water showed a relatively uniform dose deposition with the dose only dropping to 90% at a 100 mm depth in water. As expected, the attenuation in steel showed a trend similar to an exponential curve (Beer-Lambert law). From the steel attenuation plot, it was concluded that the GEANT4 program did indeed simulate attenuation to a high level of accuracy and that secondary scattered radiation contributed significantly to the dose at depth in water.

This supports the gamma spectra shown in Figure 15, where the scattered low energy photons dominate at depth. Further, the plot showing the effect of attenuation in water (Figure 13) matched the trends of the radial dose function plot given by AAPM Report TG43 for an ^{192}Ir source (Nath et al. 1995). The radial dose

function describes the dose fall off away from the source, normalised for the effect of the inverse square law. As shown in Figure 17, the radial dose function for ^{192}Ir is unique because of its flatness compared to other sources, as was observed through the Monte Carlo simulations in this study.

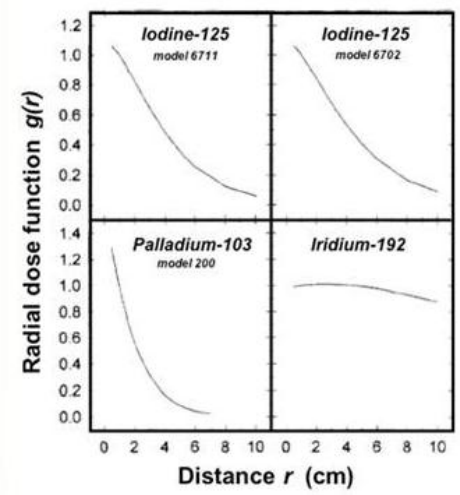

Figure 17. Radial dose functions (Nath R, et al., 1995).

Because of the large spectral changes in water, it may be expected that there is a depth dependent TLD energy response for ^{192}Ir in water because the mean energy of the radiation meeting the TLDs is different at different depths. This project has shown energy dependent responses for linac and SXR photon energies, so it is suggested that there would also be a depth dependent response for ^{192}Ir. Certainly, this notion of a depth dependent response for ^{192}Ir has already been proposed for TLD100 but results have been conflicting (Pradhan & Quast 2000) (Thomason & Higgins 1989).

Finally, a more detailed PDD, taken from 10^6 primary particles, is shown in Figure 18. The plot is not scaled to the reference conditions but rather normalised to the maximum dose point. The dose voxels are water, not LiF. Error bars are absent because each depth point was only simulated once.

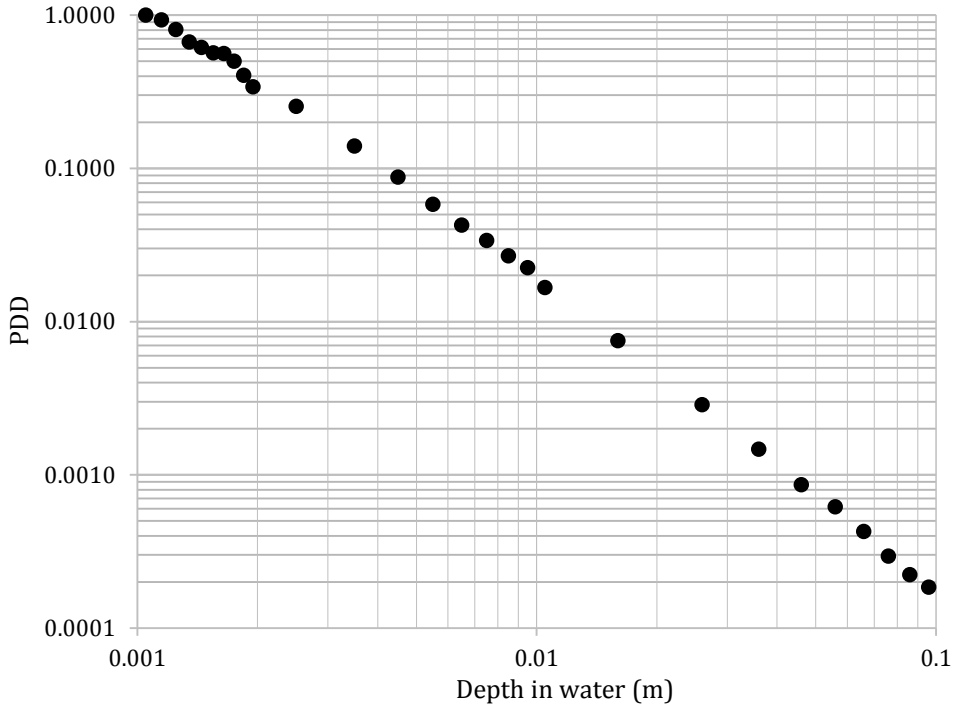

Figure 18. ^{192}Ir HDR source normalised percentage depth dose curve in water.

Once the dose to water was calculated for the reference activity and time at set distances, doses from any subsequent exposures at different activities and exposure times could be readily calculated.

In addition, exposure times could be appropriately calculated based on the apparent activity of the source at the time of experimentation, such that the dose to the TLD always fell in the linear dose response range of 1 – 10 Gy.

The dose D_r at a distance r from the centre of the source dwell position to the TLD was calculated as per Equation 4.9, where A_{app} is the apparent activity of the source at the time of the live experiment, t is the exposure time and $D_{r,MC}$ is the dose at distance r simulated through the Monte Carlo simulation scaled to 224 GBq and 300 s ($D_{r,MC} = D_{water}$ from Equation 4.6).

$$D_r = \frac{A_{app}}{224\ \text{GBq}} \frac{t}{300\ \text{s}}\ D_{r,MC} \tag{4.9}$$

5. TLD Energy Dependence for Iridium-192 Spectra

Once all Monte Carlo simulations were complete and a formalism had been established to accurately calculate the dose in water and air media, the energy dependence of TLD700:LiF could be determined for exposure to ^{192}Ir. In these sets of experiments, the energy dependence was first determined in air then at different depths in water.

5.1 Methods for In-Air Calibration

A PMMA jig was created to allow remote after-loading of the source from the TCS through a nylon catheter and dwell at a known location (Figure 19). The PMMA jig consisted of a rectangular frame measuring 50 cm × 60 cm with four cylindrical PMMA legs at each corner measuring 30 cm tall. Two nylon catheters threaded through and spanned the inside of the frame and were held under tension through the use of springs. The catheter could be fed straight into the after-loading unit, which houses and delivers the source.

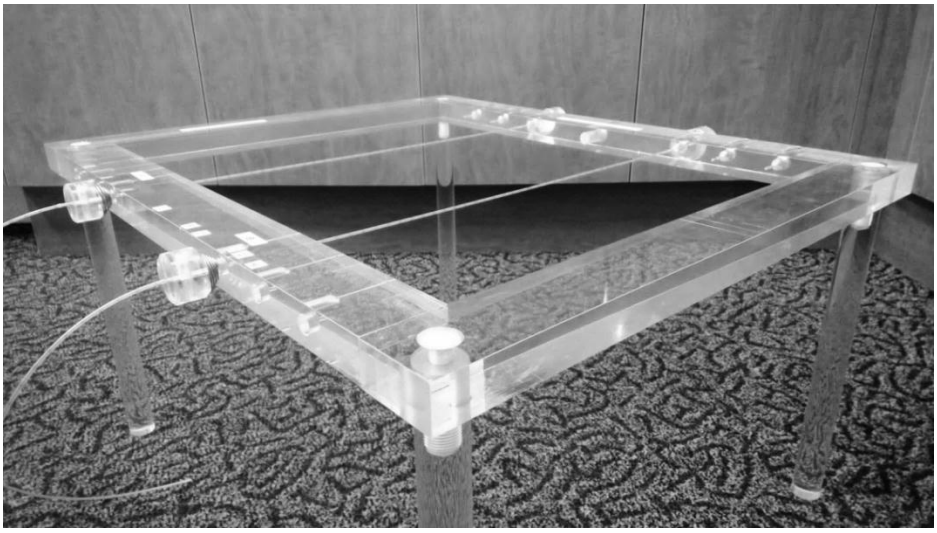

Figure 19. PMMA jig used for ^{192}Ir gamma exposure of TLDs.

Sets of four TLDs were sealed in plastic sleeve sachets, which were threaded with two thin fishing lines (Figure 20) and suspended at a distance of 50 mm away from the centre of the source dwell location inside one of the nylon catheters (perpendicular to the long axis of the source). The distance between the TLDs and

the centre of the source dwell location was measured using a dummy source and digital callipers to within 1.0 mm.

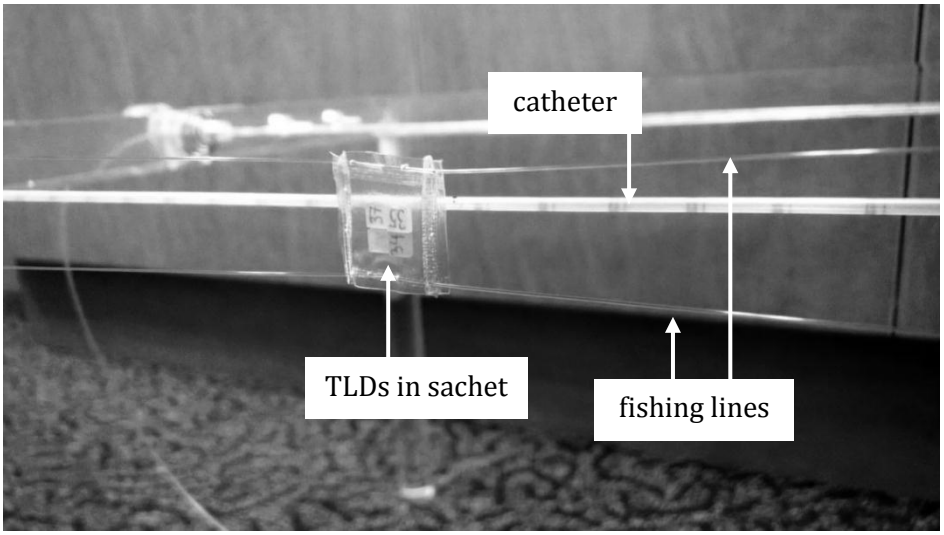

Figure 20. TLD700:LiF chips in their sachet (nylon catheter behind).

The apparent activity of the source on the day of the experiment was 89.39 GBq. The TLDs were exposed to the ^{192}Ir source for 1800 s at 50 mm, giving a dose of approximately 2 Gy (Equation 4.9). They were left for 24 hours to settle before being read with the TLD reader. The readings were compared with normalised readings from TLDs exposed to a calibrated 6 MV linac beam.

5.2 Results and Discussion for In-Air Calibration

The TLD chip readings from the in-air exposures at 50 mm distances from the centre of the source dwell position were referenced to the Monte Carlo dose simulation to determine the energy response relative to a 6 MV beam. The average chip reading normalised to 2 Gy was 12.44±0.12 μC and the average chip reading from the 6 MV beam normalised to 2 Gy was 11.18±0.18 μC which gave a ratio 1.113±0.021.

The error in the response was the absolute error, derived from the relative errors of the combined TLD readings for the batch irradiated added in quadrature. This was not the full uncertainty for TLD700:LiF energy response because experimental error was not yet taken into account. The distance between the centre of the TLD sachet and the centre of the source dwell position was measured with callipers and a conservative uncertainty estimate of 1 mm was adopted. The uncertainty from a shift in positions of 1.0 mm and 2.0 mm was calculated by

Equation 4.6, which characterises the dose drop-off from the source. The uncertainty in dose for positions of 10, 20, …, 100 mm are given in Table 9.

Table 9. Errors in dose due to positional uncertainty.

TLD position (m)	1 mm uncertainty error %	2 mm uncertainty error %
0.01	20.7	44.1
0.02	10.2	20.7
0.03	6.78	13.7
0.04	5.08	10.2
0.05	4.06	8.15
0.06	3.39	6.78
0.07	2.90	5.81
0.08	2.54	5.08
0.09	2.26	4.52
0.10	2.03	4.06

The dose uncertainty, due to positional uncertainty for the live experiment with TLDs at 50 mm, was therefore 4.06%. The positional error was added manually and was not inherent in the results because only one set of data was taken at each distance.

The error in calculated dose, caused by the uncertainty in the TLD sachet positioning found using Equation 4.6, had a very strong dependence on distance between the source and the TLD. The error in dose for a 2 mm uncertainty at 10 mm from the centre of the source dwell location was 44.13% compared with 8.15% at 50 mm. This effect was due to the very large dose gradient at small distances from the source. Brachytherapy often deals with dose calculations close to the source so such uncertainties are unavoidable. This means that, for brachytherapy dosimetry, large dose uncertainties of around 10% to 20% are often tolerable (as in clinical practice at the RAH), whereas for EBRT such errors are unacceptable. The error assigned to the energy response in air was therefore the standard deviation from the TLD readings combined with the spatial uncertainty, the uncertainty in the source activity and MC dose prediction (Table 10), by the addition of relative errors, and came to a total relative error of 6.28%.

Other uncertainties are given in Table 10, where the total uncertainty was calculated by adding all the individual uncertainties in quadrature. The source certificate (Appendix 8.10) gives an uncertainty in the source strength of ±5% at confidence level 99.7% - this corresponds to ±1.70% for 1 standard deviation. The

air kerma strength is independently verified trimonthly by the RAH at source exchange using the methods defined by Butler et al. (2008). Therefore, the energy response of TLD700:LiF in air from exposure to ^{192}Ir gamma rays is 1.113±0.070.

Table 10. Energy response uncertainties at 50 mm for in-air exposure from ^{192}Ir.

Description	Uncertainty (%)
SD in experiment results	1.87
Source Activity	1.70
MC Prediction of dose (Table 6)	4.08
Position estimate (Table 9)	4.06
Total	6.28

The results for the in-air experiments (average gamma ray energy of 359 keV, Table 8) showed a TLD over-response of 11.3% compared to 6 MV linac x rays. The response is consistent with the greater over-response from the SXR x rays and the slight under response from high-energy linac photons and electrons. However, it is different to the response calculated by Haworth et al. (2012) for TLD100 of 1%.

5.3 Methods for In-Water Calibration

The live in-air experiments were then repeated in a large water tank that measured 70 × 70 × 70 cm^3 and was filled with deionised water (Figure 21).

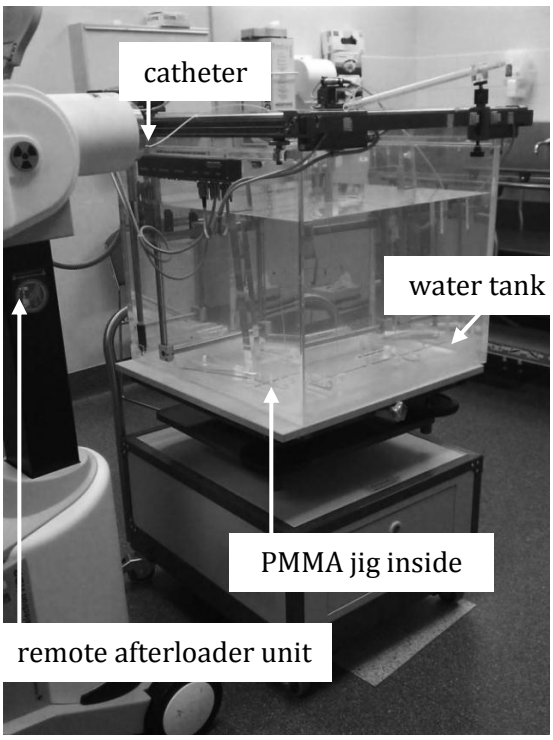

Figure 21. Jig and TLDs in the large water tank.

TLDs were again sealed in sets of four inside plastic sleeve sachets. These were suspended at distances of 20, 30, 40 and 50 mm from the middle of the source dwell location as measured with callipers. Only two sachets were used at a time, one on either side of a nylon catheter, so that a closer TLD would not affect the radiation meeting a TLD sachet behind it. The PMMA jig was lowered into the water until completely submersed. This experiment was performed on four separate occasions, so different exposure times were used depending on the activity of the source and the positions of TLDs (Table 11).

Table 11. Exposure times and doses for TLD exposure to ^{192}Ir.

Experiment number	Source apparent activity (GBq)	TLD sachet position (mm)	Exposure time (s)	Approximate dose (Gy)
1	282.2	20	100	2.00
		30	200	2.00
		40	400	2.00
		50	600	2.00
2	214.7	20	500	7.85
		30	500	3.60
		40	500	2.05
		50	500	1.29
3	204.7	20	405	6.06
		30	405	2.78
		40	1004	3.92
		50	1004	2.47
4	201	20	301	4.43
		30	301	2.03
		40	804	3.08
		50	804	1.94

After each water experiment, the TLD chips were read using the TLD reader and the results were compared with normalised readings from TLDs exposed to 6 MV photons. The batch of TLDs was annealed after each experiment and recalibrated by exposing a number of chips to 2 Gy of 6 MV photons.

5.4 Results and Discussion for In-Water Calibration

The TLD readings produced the energy response values given by Table 12 and Figure 22.

Table 12. Energy response to ^{192}Ir gamma rays.

Distance from source (mm)	Medium	Energy Response
20	water	1.170±0.125
30	water	1.125±0.074
40	water	1.064±0.089
50	water	0.976±0.043

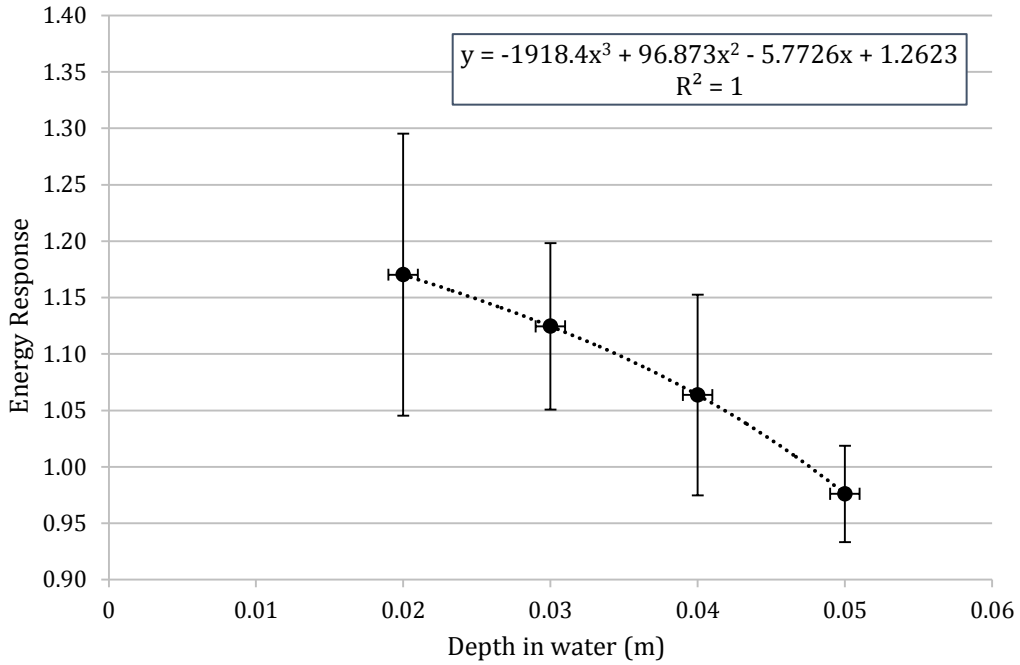

Figure 22. Energy response of TLDs in water to ^{192}Ir γ rays.

The dose to each TLD was calculated from Equation 4.6. Each data point represents the average response from the five experiments in water at the particular distance concerned. The vertical error bars represent the sample standard deviation in the results for each distance concerned, with the response uncertainty consistent with the positional errors given by Table 9. The horizontal error bars represent the conservative positional uncertainty estimate of 1 mm in the position of the TLD sachets. The trend line in Figure 22 is given by Equation 5.1 and gives the depth dependent response R_{depth} of the TLDs for depths r of 0.02 to 0.05 m in water relative to the response from 6 MV photons.

$$R_{depth} = -1920r^3 + 96.9r^2 - 5.77r + 1.31 \ (\pm 10\%) \qquad (5.1)$$

The uncertainty of 10% in the energy response factor for ^{192}Ir irradiation in water was derived by adding all the relative errors in quadrature (Table 13). The uncertainty in position is inherent in the spread of results because multiple experiments were made on separate occasions. Multiple TLDs were also read, which meant that the error in TLD reading was also inherent in the spread of results. However, factors like the uncertainty in dose calculations given by the Monte Carlo simulations (6.31%, Table 7) and the source activity (1.70% 1 SD, derived from the source data sheet) had to be considered. The standard deviation component of the

total uncertainty in Equation 5.1 was taken to be the average standard deviation for the results shown in Table 12 for the energy response to ^{192}Ir gamma rays.

Table 13. Energy response uncertainties for in-water exposure from ^{192}Ir.

Description	Uncertainty (%)
SD in experiment results	7.48
Source activity	1.70
MC prediction of dose (Table 7)	6.31
Total	10

The five in-water experiments had a standard deviation in each set of results that was consistent with the dose uncertainty trends given by Table 9. For example, taken as a relative error for the exposures at 20 mm, the sample standard deviation in the results for energy response was 12.5% about the sample mean. This was close to the predicted value of 10.2% for a 1 mm uncertainty in position (Table 9). The relative errors for all responses conformed well to the relative errors for a 1 mm spatial uncertainty given in Table 9, so the conservative estimate of a 1 mm uncertainty for the in air experiment was deemed appropriate.

Despite the considerable beam softening, the TLD over-responses in water at depths up to 30 mm were greater than those in air. A definite trend in depth dependent TLD response has been shown (Figure 22, Equation 5.1) with a decreasing over-response with increasing depth. This phenomenon was already predicted by the changing ratio of dose to water and TLD in a water medium (Figure 12). The considerable beam softening at depth (Figure 15, Table 8) also predicted a depth dependent response, but in the opposite manner if the relationship between the SXR and linac responses was considered. The lower energies of the SXR unit produce an over-response in the TLDs and this trend would imply that beam softening would produce a greater response at depth. Unexpectedly, the over-response declines at depth but is consistent with predictions derived from Figure 12.

There are few studies concerning the energy response of TLDs exposed to ^{192}Ir in water, compared with the response from exposure to 6 MV linac photons. The literature does detail several studies that mention the depth dependent responses or lack thereof, of TLD100 exposed to ^{192}Ir in a water medium. Pradhan et al. (2000) performed experiments in water equivalent phantoms and did not attempt an liquid water experiment as conducted in this project. Pradhan et al. measured an over-response of 8.5% at 100 mm in Solid Water and Haworth et al. (2012) interpolated an over-response of 3% for TLD100 at a depth of 50 mm in

water. The evidence in this project supports the predictions by Haworth et al. (2012), with TLD response approaching unity at greater depths. However, it should be noted that these studies concerned TLD100 and did not use Monte Carlo modelling for dose determination, so this group may have expected different results.

The very large uncertainty in the energy response of TLD700 for ^{192}Ir irradiation stems from the large standard deviation in the experimental results (despite a large sample) and the uncertainty in the Monte Carlo dose predictions (despite multiple runs with a large number of particles). Certainly, the standard deviation in the results could be attributed to the effects of positional uncertainty of the TLD sachets. This could have been reduced if Solid Water was utilised. The positional uncertainty for TLDs held in a solid phantom have the potential to be much less compared with suspending TLDs in water; and this reduction in systematic errors may have enabled other research groups to determine a more precise trend in depth dependent energy responses.

For this project, conducting the TLD700:LiF calibration for ^{192}Ir gamma rays in real water was important because OCP assumes a real liquid water medium. Even if the project were to conduct most exposures in a solid phantom to improve TLD positioning accuracy and have a reference water calibration measurement, the error from the water measurement would be transferred to the solid phantom results and, hence, would be unavoidable.

6. VERIFICATION OF A BRACHYTHERAPY TREATMENT PLANNING SYSTEM

Following dose calibration and energy response determination of the TLD700:LiF chips for the gamma spectrum of an ^{192}Ir brachytherapy source in a water medium, the TLD chips were used to independently verify the treatment planning system, Oncentra Prostate.

6.1 Treatment Planning, Setup and Materials

Oncentra Prostate (OCP) is supplied by Nucletron (an Elekta Company) and the version 3.2.3 was verified in this project. OCP is installed on a standalone computer that interfaces with an ultrasound (US) unit, a mechanical stepper unit that houses the rectal US probe (BK FlexFocus, BK Medical, Herlev, Denmark) and the TCS, which sends the source dwell information to the MicroSelectron afterloader unit from the control room of the Brachytherapy suite.

A purpose-made phantom for underwater use was constructed out of PMMA (Figure 23). The phantom could house the TLD chips in a dry environment (water-tight PMMA rods) at known locations. A HDR prostate brachytherapy treatment was mimicked by using the same grid template alignment that is used to insert hollow plastic catheters into the perineum during real procedures.

TLDs were placed inside the rods that were inserted into the phantom either inside or outside the catheter matrix. The phantom was attached to the US stepper unit, which mimicked the US probe travelling along the rectum to image the organs above (prostate, bladder, urethra etc.). The phantom could be fully submersed in water such that there was a water medium between all source dwell positions and TLDs to mimic the assumptions of the TPS.

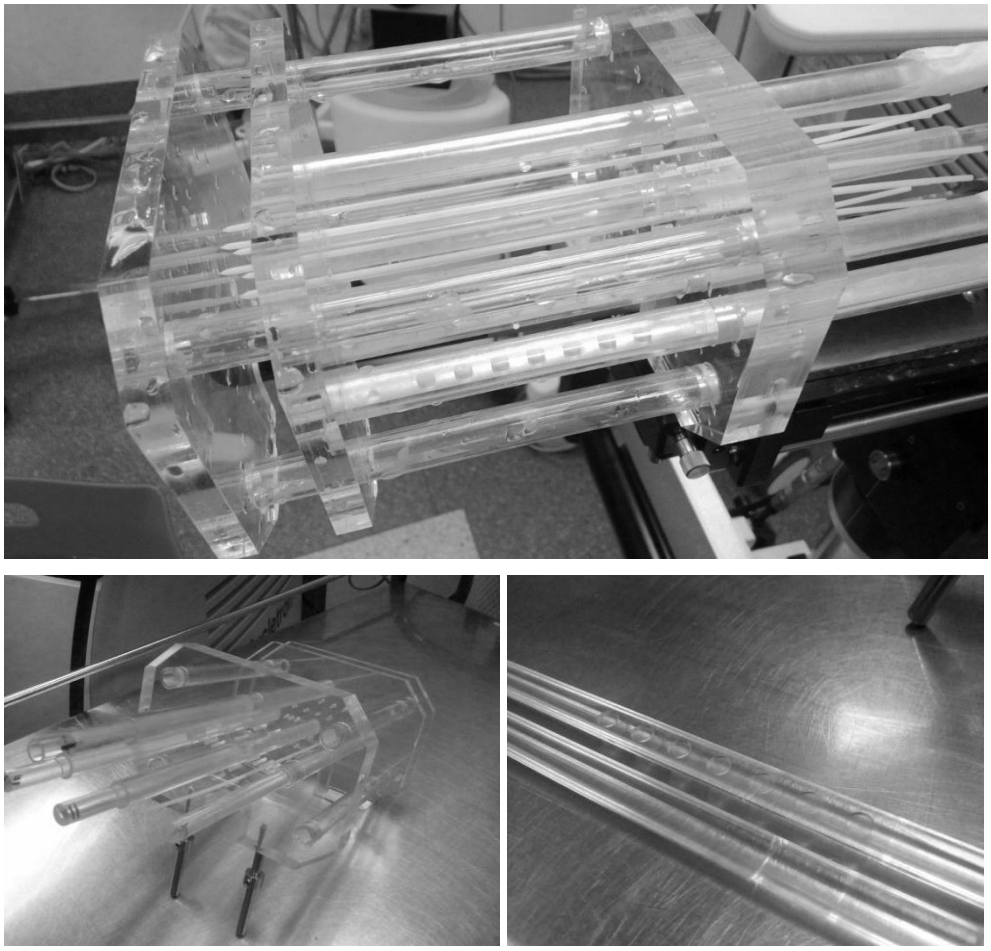

Figure 23. The HDR prostate phantom.
The top image shows the phantom with catheters inserted into the template matrix, the rectal ultrasound (US) stepper unit attached beneath and TLD holding rods inserted. The bottom left image shows the phantom without the US stepper attached. The bottom right image shows the TLD rods and the locations where TLDs chips can be inserted.

Firstly, the phantom had transverse images captured through use of the rectal US and stepper unit, which were reconstructed by the OCP software to obtain a three dimensional image set. The equipment used for imaging was the BK FlexFocus ultrasound unit (BK Medical, Herlev, Denmark). The US transducer probe was connected into the stepper unit where the phantom was also attached. The probe and phantom were then submersed in water. Catheters were inserted into the grid at set locations typical for a normal sized prostate – these catheters would appear in the ultrasound image as white lines. Figure 24 shows most of the grid that serves as the XY coordinates for the treatment planning system, OCP.

The phantom used in the project allowed insertion of catheters at grid locations shown as unfilled circles or filled circles on Figure 24.

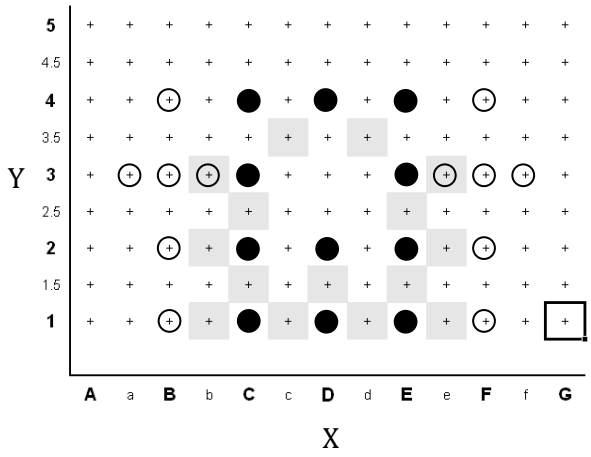

Figure 24. The HDR prostate grid template.

The grey marked coordinates denote the catheter locations typical for a medium sized prostate. The filled circles denote the location of catheter insertions chosen for this project and unfilled denote other locations available but not used.

Each grid position, shown in Figure 24 and denoted by a "+", has a spacing of 5 mm in the X and Y directions. The PMMA rods containing the TLDs could be inserted at the D3 position, the D5.5 and another position 5 mm left of A3, not part of the grid.

The US unit was connected to the planning computer where the captured images were saved and used for catheter reconstruction and treatment planning. The probe was moved in the $\hat{z}$ direction (perpendicular to the XY plane shown in Figure 24) to check that the z value on the stepper agreed with Oncentra Prostate. The probe was then moved to its deepest position in the water phantom corresponding to where the tips of the catheters were implied on the US image. This position was defined as the base plane in OCP and the stepper was set to zero. In a live procedure, the base plane would be set to the prostate base or slightly more superior if the seminal vesicles were to be treated. The US probe was then retracted smoothly and slowly through the water phantom and the images were captured (1 mm slice width) using the transverse crystal.

An arbitrary, average sized prostate and urethra were drawn into OCP using the inbuilt contouring tools. The shape and size of both structures mimicked that observed in actual procedures. On the OCP XY grid, the prostate occupied space between b1 and e1 in the X direction and between b1 and b3.5 in the Y direction. This meant that the anterior catheters at positions C4, D4 and E4 were not used because they would exist outside the planned target volume (PTV) and hence any

source dwell along those catheters gave an unwanted dose to normal tissue for a real procedure. The volume of the PTV was 36.08 cm^3 and the volume of the urethra was 0.93 cm^3.

The catheters, which appeared as white lines against a black background in the ultrasound image, were reconstructed in OCP. The catheter free lengths (length of catheter inferior to the grid insertion point) were measured with a ruler (90 mm for all catheters). This was entered into OCP in order to accurately set the catheter end positions (catheter ends points could not be accurately resolved on the image).

Once the virtual prostate and urethra had been contoured, a treatment plan was created. Three different experiments were to be performed, one with TLDs on the inside of the virtual prostate (PTV contour) and the other two with TLDs on the outside (in normal tissue regions where the dose is much lower). For the former, a dose of 7 Gy to the prostate was prescribed and for the latter, 15 Gy. OCP was then used to optimise the source dwell times along each point of the catheters inside the PTV (using inverse optimisation and the usual clinical PTV and OAR optimisation limits and weightings used at the RAH).

The dose distribution is calculated by OCP using the dosimetry formalism of AAPM Report TG43 for a line source (Nath et al. 1995) and the data of Daskalov et al. (1998). The source dwell times provided were adjusted slightly so that the dose to the PTV and urethra met the requirements used in a typical HDR prostate brachytherapy treatment at the Royal Adelaide Hospital (Table 14).

Table 14. DVH criteria used clinically at the RAH (primary dosimetry values in red).
The D10 and D90 are the maximum doses to 10% and 90% of the PTV volume respectively, while the V100 is volume that receives 100% of the prescribed dose, V150 and V200 receive 150% and 200%.

Prostate Target (PTV):	
	D90 = 100% to 110%,
	V100 ≥ 95% ideal, > 90% good, > 85% is acceptable.
	V150 ≤ 40 %,
	V200 ≤ 10%.
Urethra:	Vcrit = 0% (critical dose = 115%), D10 < 115%

The plan was saved in OCP and was unchanged for each experiment apart from the dose prescription. Changing the dose prescription changed the dwell times by the same relative amount so did not change the dose distribution in the treatment planning system. In addition, the dwell times were also automatically

changed by OCP to maintain the prescribed dose according to the ^{192}Ir source strength at the time of the plan delivery.

OCP is able to calculate the dose at any point in the treatment plan within the captured ultrasound image set. This tool was used to provide the predicted values of dose to the TLD chip coordinates. The TLD chips, in the PMMA rods, were at known locations and their positions could be translated into OCP coordinates to yield predicted dose points.

Figure 25 to Figure 27 are screenshots from the treatment planning system after the treatment plan was finished and saved. Figure 25 shows the three dimensional view of the contoured prostate and catheters. The ultrasound images can be seen in three planes and each plane can be moved through its set of coordinates. The dark vertical band in the ultrasound image is one of the ends of the phantom seen in Figure 23 where the TLD rods end but the catheters are able to pass through. The prostate is the green mesh object and the catheters are drawn in pink – several catheters can be seen in the ultrasound image also. The dwell positions of the source are denoted by the red circles in the catheters, where the size of the sphere is related to the dwell time. The blue objects denote points of interest where the TLDs were located. These points provide dose as calculated by the treatment planning system.

Several “points of interest” (user set points where OCP reports dose) can be seen in the Figure 25 to Figure 27, e.g. the D6 position and 5 mm left of A3 where the TLDs are located in their rods. Again, in Figure 27, the dark band is indicative of one of the PMMA ends of the phantom - catheters can be seen passing through this. Figure 27 also shows the location of the TLD chips in a straight line in their PMMA rod with points P2 through to P8. Point P1 served as a reference origin point for calculating the coordinates of the TLD positions and translating them into the coordinate system of the treatment planning system.

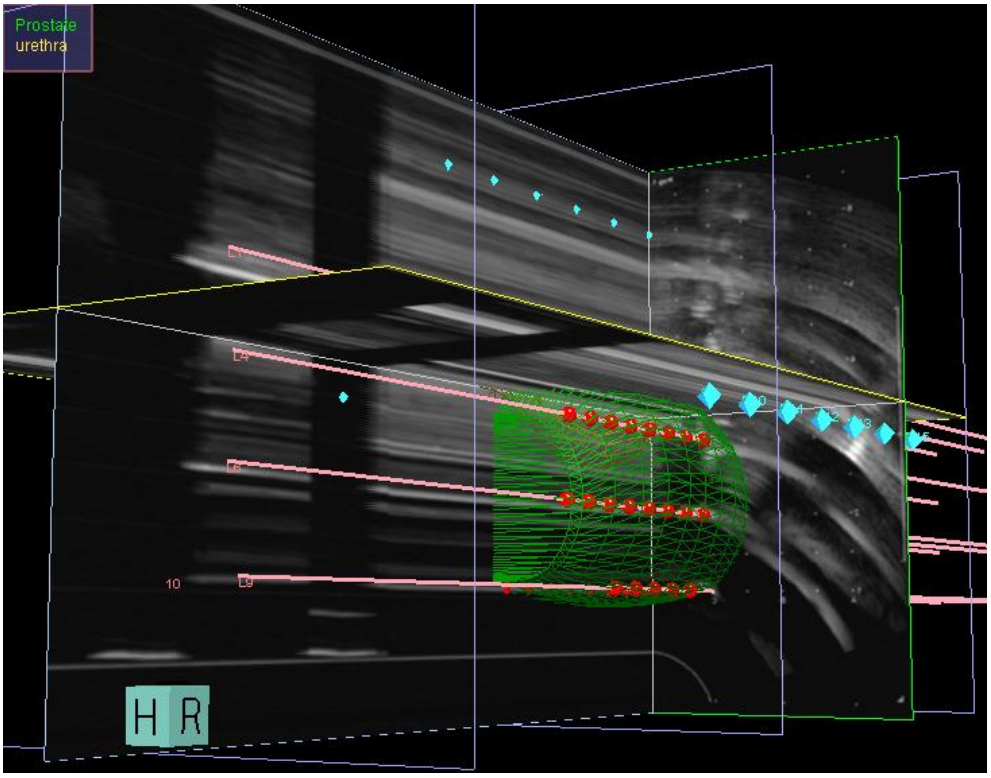

Figure 25. Three-dimensional view of the treatment plan in OCP.

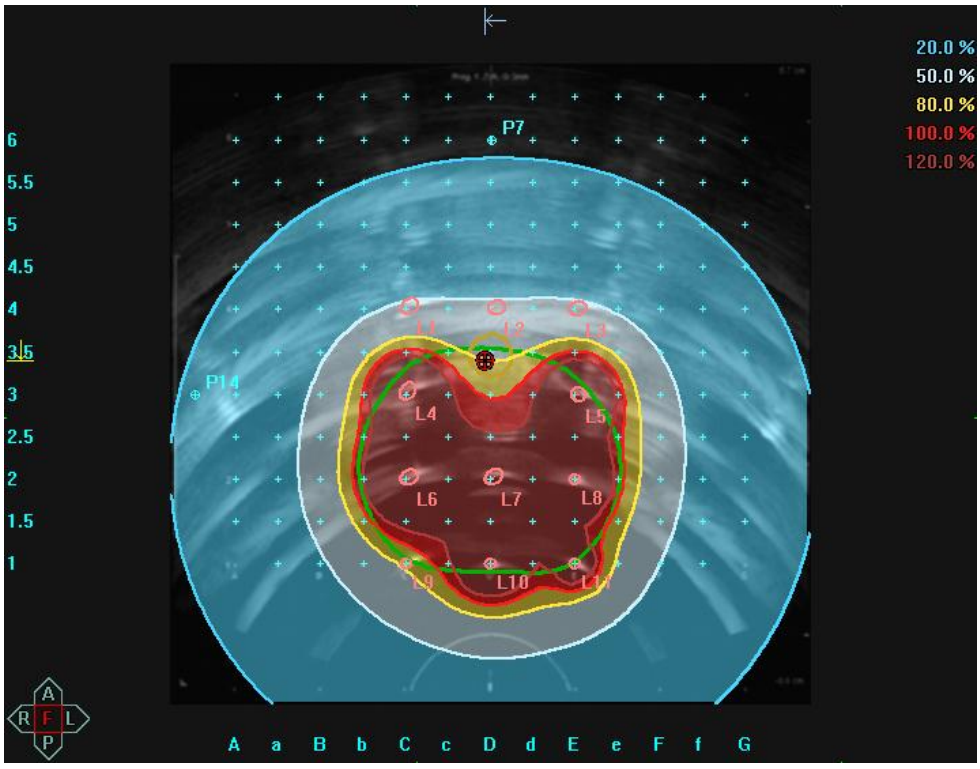

Figure 26. Two-dimensional transverse slice of the treatment plan in OCP.

The colour wash shows the dose distribution calculated by the TPS based on the source dwell locations and times. Dark red shows regions of the prostate that received 120% of the dose prescription, red denotes 100%, yellow 80%, white 50% and blue denotes 20 % of the dose prescription.

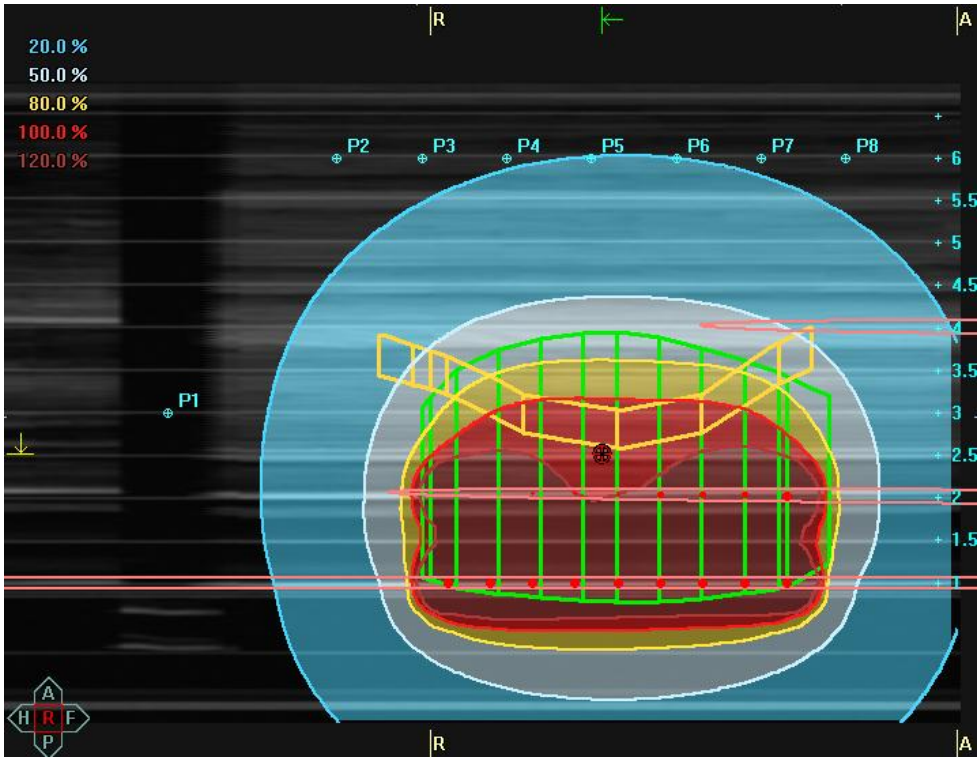

Figure 27. Two-dimensional sagittal slice of the treatment plan in OCP.

The treatment plan created in Oncentra Prostate for experiments #1, #2 and #3 had the cumulative dose volume histogram (DVH) shown in Figure 28 and the corresponding differential DVH shown in Figure 29. These plots show the fraction of the prescribed dose that is deposited in each fraction of contoured volumes.

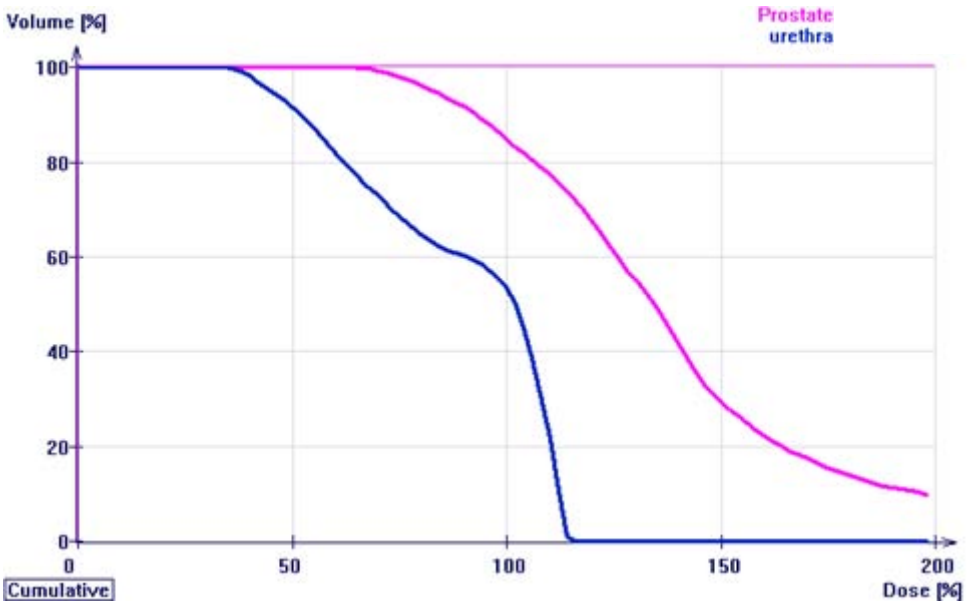

Figure 28. Cumulative DVH data for the PTV (prostate) and OAR (urethra).

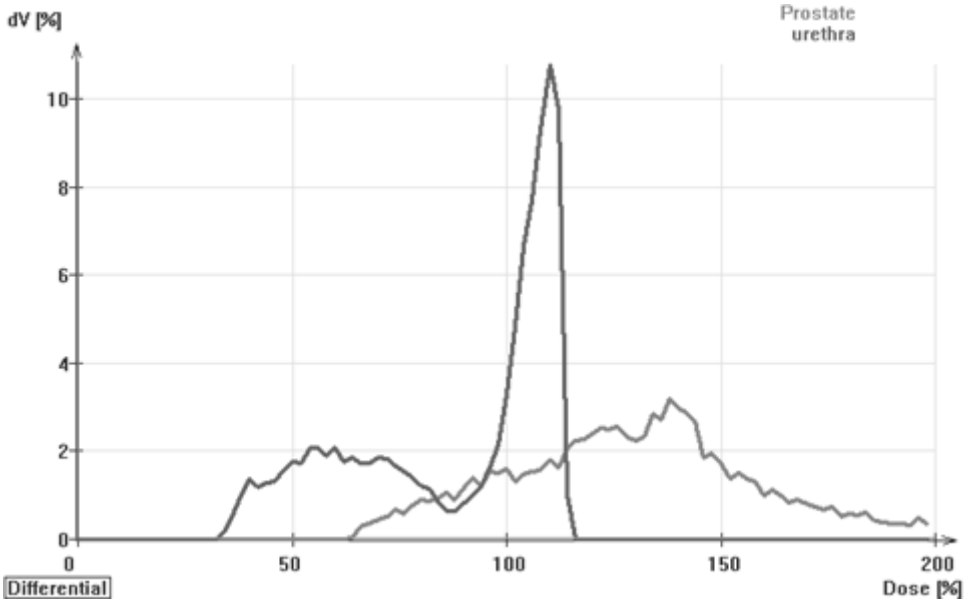

Figure 29. Differential DVH data for the PTV (prostate) and OAR (urethra).

A more detailed breakdown of the DVH details are listed in Table 15 for a 100% dose prescription of 7 Gy.

Table 15. DVH data for the PTV (prostate) and OAR (urethra).

Prostate (PTV)		
V:	35.66 cm^3	
Dmin:	62.99%	4.41 Gy
Dmax		
global:	694.87%	48.64 Gy
DVH:	Value out of DVH range	
Dmean:	142.41%	9.97 Gy
D90:	92.78%	6.49 Gy
D100:	62.99%	4.40 Gy
V100:	84.88%	30.27 cm^3
V150:	29.44%	10.50 cm^3
V200:	9.50%	3.39 cm^3
V90:	91.73%	32.71 cm^3

Urethra (OAR)		
V:	0.85 cm^3	
Dmin:	34.79%	2.44 Gy
Dmax		
global:	115.01%	8.05 Gy
DVH:	116.00%	8.12 Gy
D crit.:	115.00%	8.05 Gy
V crit.:	0.51%	0.00 cm^3
D10:	112.16%	7.85 Gy
V100:	53.38%	0.45 cm^3
V125:	0.00%	0.00 cm^3

The prostate treatment plan created in OCP conformed to the requirements for dose to OAR (urethra) and PTV (prostate), used in clinical HDR brachytherapy treatments for high risk prostate cancer. The plan created in this project had 100% of the prostate volume receiving 85% of the prescribed dose, which was within tolerance and as good as could be achieved with limited catheter positions available in the PMMA phantom.

For the urethra, the V125 = 0 and D10 = 112.16%. These statistics, shown in Figure 28, Figure 29 and Table 15, indicate adequate conformity between the requirements of standard treatments and the plan created for the OCP verification.

Since the TPS dose calculations were computed using well-defined parameters found in AAPM Report TG43 (Nath et al. 1995), verifying a treatment plan in OCP where there was only one source dwell position was also deemed a valid exercise, i.e. having TLDs surround a single dwell position and having OCP compute the doses to these positions would equally verify the dosimetric accuracy of the TPS for the simplest case.

Including contours of the PTV and OAR was not absolutely necessary, as these had no influence on the dose calculations. However, a full plan was created, in order to verify the TPS for the most complicated scenario where multiple dwell positions are used and dwell times vary between positions. It also verified OCP for the full subset of simpler scenarios where fewer source dwells are used. The simpler experiment of one source dwell position was still performed in this work for completeness and to compare with MC outcomes where a single source was modelled.

6.2 Experimentation

6.2.1 Full Prostate Treatment Plan

The first experiment involved a treatment plan with a 15 Gy dose prescription to the PTV. TLDs were placed in two rod locations outside of the PTV and were oriented to face the origin point defined at D3 (Table 16). The phantom was submerged in water and transfer tubes were connected between catheters and the remote afterloader unit. The treatment plan had dwell times updated for the source strength at the time of delivery and was sent to the TCS, which controls the source through the remote afterloader unit.

Table 16. Outline of TPS verification experiments.

Experiment	Description	Rod positions
#1	Full prostate treatment plan, TLDs outside PTV	D5.5 & 5 mm left of A3
#2	Full prostate treatment plan, TLDs inside PTV	D3 (facing $\hat{x}$)
#3	Full prostate treatment plan, TLDs inside PTV	D3 (facing $\hat{y}$)
#4	Single dwell position	D5.5 & 5 mm left of A3

Figure 30 shows the phantom irradiation experimental setup. The US stepper unit with the probe attached can be seen, as well as the US unit in the background. The US unit was only present for the first experiment, as subsequent experiments did not require additional ultrasound scans because the water phantom and catheter locations remained unchanged. The straw-coloured transfer tubes can be seen connecting the white catheters in the phantom to the remote afterloader unit. TLD rods were taped in so that they did not move or rotate during the experiment.

Figure 30. OCP verification experimental setup using a PMMA phantom submersed in a water medium.

The treatment was then delivered to the TLD phantom. The TLD energy response factors derived from the MC calibration (Equation 5.1) as well as individual chip sensitivity factors (discussed in Section 3.1) were applied to the TLD readings. The response of the TLDs was shown to vary with distance from the source, so, for complete accuracy, multiple response factors would have needed to be calculated for each chip and for each dwell location of the source, i.e. many calculations per TLD. In the interest of time, a single energy response factor for each rod of seven TLDs was derived from the average of the distances between middle of

the PTV and the location of the TLDs. Thus for Experiment #1, TLDs irradiated in the rod at D5.5 were, on average, 3.10 cm from the centre of the PTV, so an energy response factor of 1/1.167 = 0.857 was applied. Similarly, TLDs irradiated in the rod at the position 5 mm left of A3 in experiment #1 were at a mean distance of 4.07 cm, so a factor of 1/1.106 = 0.904 was applied. The corrected readings were then compared to the readings from chips irradiated with a known dose from 6 MV linac x rays to obtain the final absolute dose to the TLD chips. These doses were then compared with the doses predicted by OCP (Table 17). Experiment #1 was then repeated.

Experiment #2 was similar to #1, with two changes: the prescribed dose to the PTV was 7 Gy and the TLDs were placed in a rod located in the D3 "in prostate volume" position, facing the X plane. Experiment #3 was the same as #2, except that the TLDs faced the Y plane. For both experiments #2 and #3, a mean distance of 1.95 cm was used to extrapolate an energy response factor of 1/1.220 = 0.820. The absolute dose was determined as for experiment #1 and compared to the predicted dose points from OCP (Table 18).

The TPS optimises the dose distribution to the PTV while also aiming to minimise the dose to the OAR such as the urethra and other normal tissue. It does this by varying the source dwell times in the catheters. Dwell times for the treatment plan used in this project with a 7 Gy prescription and a source activity of 399.64 GBq are given in Table 25 in Section 8.1.

A Student's *t* test was performed on the results from experiments #1 - #3 in order to determine their significance.

The total treatment time for the plan with a 7 Gy prescription and a source activity of 399.64 GBq was 501.07 s (8 min 21.07 sec). The dwell times increased and decreased automatically by the same factor depending on the prescription and the source activity at the time of delivery.

In order to enter dose points into OCP that matched the TLD's physical location, the TLD positions needed to be determined. An origin point was defined in OCP on the image of the phantom surface, shown as a cross on Figure 31. This point was chosen because it could be easily located on the US image (the side lateral view had an obvious dark band at the middle PMMA structure). In the top view, the origin lies at the D3 position.

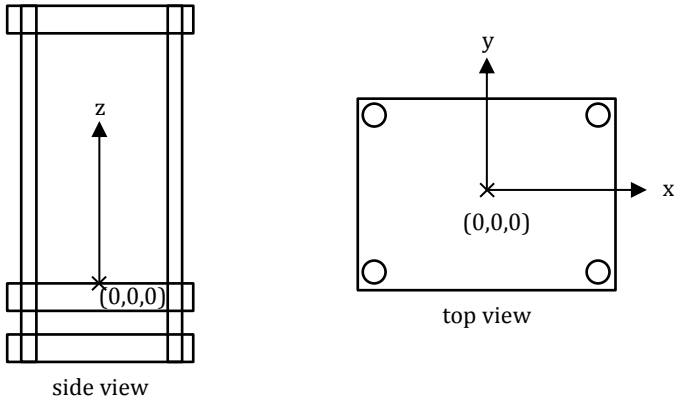

Figure 31. Schematic of the PMMA phantom, indicating the origin point (red X) used for the TLD coordinate calculation.

The rods that housed the TLD chips were inserted into grid position D3, D6 and 5 mm left of the A3 position. Using the coordinate system defined in Figure 31, these points translated to (0, 0), (0, 30 mm) and (–35 mm, 0) in the XOY plane. The base of the rods sat at z = –5 mm, and the TLD positions started at 25 mm from the base of the rod, with subsequent TLDs 10 mm apart (seven TLDs per rod). On the TPS, a point of interest placed at the origin gave an OCP coordinate of (3.79 cm, 3.90 cm, –3.00 cm). This meant the TLD coordinates translated to the coordinates given in columns 2 - 4 of Table 17 and Table 18. These points were entered into OCP, which gave the point doses shown in column 5 and the doses as a percentage of the PTV prescription shown in column 6 of the tables.

Table 17. Dose to TLD points outside PTV (Experiment #1).

point	x (cm)	y (cm)	z (cm)	Dose (Gy)	Dose (%)
P1	*3.79*	*3.90*	*-3.00*	*1.655*	*11.03*
P2	3.79	0.90	-5.00	1.913	12.76
P3	3.79	0.90	-6.00	2.404	16.03
P4	3.79	0.90	-7.00	2.818	18.79
P5	3.79	0.90	-8.00	3.028	20.19
P6	3.79	0.90	-9.00	2.989	19.93
P7	3.79	0.90	-10.00	2.717	18.11
P8	3.79	0.90	-11.00	2.274	15.16
P9	0.29	3.90	-5.00	2.190	14.60
P10	0.29	3.90	-6.00	2.848	18.98
P11	0.29	3.90	-7.00	3.392	22.62
P12	0.29	3.90	-8.00	3.662	24.41
P13	0.29	3.90	-9.00	6.635	24.23
P14	0.29	3.90	-10.00	6.290	21.94
P15	0.29	3.90	-11.00	2.678	17.85

Table 18. Dose to TLD points inside PTV (Experiment #2).

point	x (cm)	y (cm)	z (cm)	Dose (Gy)	Dose (%)
P1	*3.79*	*3.90*	*-3.00*	*0.772*	*11.03*
P2	3.79	3.90	-5.00	2.378	33.97
P3	3.79	3.90	-6.00	4.919	70.26
P4	3.79	3.90	-7.00	7.207	102.96
P5	3.79	3.90	-8.00	7.403	105.75
P6	3.79	3.90	-9.00	7.364	105.20
P7	3.79	3.90	-10.00	6.806	97.22
P8	3.79	3.90	-11.00	4.053	57.91

The dose delivered to the TLDs in all experiments was within the TLD700:LiF's linear dose response range of 1 – 10 Gy. A maximum dose of 6.64 Gy and minimum of 1.91 Gy was delivered for the experiments with TLDs outside the PTV. For the experiments with TLDs inside the PTV, the maximum dose delivered was 7.40 Gy, while the minimum was 2.38 Gy. It should be noted that OCP does not give an uncertainty in its dose calculation because it is determined by an analytic equation (Equation 2.1) for a set distance without any spatial uncertainty. However, there is an inherent uncertainty of 10% since the equation comes from AAPM report TG43 which does provide a systematic uncertainty estimate of about 10% for determining dose to a point (Nath et al. 1993).

6.2.1 Single Dwell Position Plan

A fourth and final experiment was performed for a single source dwell position. The purpose of the single dwell position plan was to improve upon the accuracy of the previous experiments by eliminating the assumptions in energy correction factors. It was also performed to provide data on the accuracy of the dosimetric calculations made by TPS for the simplest scenario and to compare results directly with MC modelling results.

The treatment plan in OCP was modified such that the dwell time was zero seconds at all but one source dwell position. The one dwell position that remained was dwell position number 16 of catheter 1, which was in the C4 position on the OCP grid. Two TLD holding rods were used, each with seven TLDs inside. These were placed in the two slots that existed outside the PTV. A dose prescription of 12 Gy was applied, which gave the source dwell position an appropriate dwell time in order for the TLDs to receive doses in their linear range of 1 – 10 Gy. Separate dose calculations (different to Table 17 and Table 18) were made because the treatment plan only featured a single source dwell position. This is shown in

Table 19 for a 12 Gy prescription to the PTV. The TLD rods both faced toward the origin as in the first TPS verification experiments

Table 19. The dose delivered to TLD points for a single dwell position plan (Experiment #4).

point	x (cm)	y (cm)	z (cm)	Dose (Gy)	Dose (%)
P1	*3.79*	*3.90*	*-3.00*	*1.1830*	*9.86*
P2	3.79	0.90	-5.00	2.542	21.18
P3	3.79	0.90	-6.00	4.149	34.58
P4	3.79	0.90	-7.00	6.663	55.53
P5	3.79	0.90	-8.00	9.013	75.11
P6	3.79	0.90	-9.00	8.308	69.23
P7	3.79	0.90	-10.00	5.604	46.70
P8	3.79	0.90	-11.00	3.445	28.71
P9	0.29	3.90	-5.00	2.215	18.46
P10	0.29	3.90	-6.00	3.257	27.14
P11	0.29	3.90	-7.00	4.601	38.34
P12	0.29	3.90	-8.00	5.608	46.73
P13	0.29	3.90	-9.00	5.331	44.42
P14	0.29	3.90	-10.00	4.055	33.73
P15	0.29	3.90	-11.00	2.806	23.38

A reference batch of TLD chips were irradiated with 2 Gy of 6 MV photons and the corrected TLD chip readings were compared with the 6 MV x ray exposed TLDs to give the absolute dose. Because there was only one source dwell location, only one calculation per TLD was made for an energy correction factor according to the distance between the source and the TLD (Equation 5.1). The TLD dose was then compared to the dose predicted by OCP, shown in Table 19, to give values of D_{TLD}/D_{OCP}. A Student's t test was performed on TLD measured doses, to determine their significance.

An attempt was made to further reduce the uncertainty in the results by comparing the results predicted by OCP directly with the formula for dose deposition in water derived from the Monte Carlo simulations in this work (Equation 4.6 and Equation 4.9).

The source dwell position was translated into the OCP coordinate system (81 mm from the tip of the catheter) and the catheter was inserted into the C4 position on the OCP grid, which was at X = 2.79 cm and Y = 2.90 cm in the TPS. The Z coordinate of the base of the rod was Z = 0.00 cm which meant that the coordinates of the source were (2.79, 2.90, –8.10). This provided a simple method to calculate the distances r between each of the TLDs and the source using Pythagoras' theorem. These values of r were used in Equation 4.6 for dose calculation. The

points of interest used in the MC comparison of experiment #4 were the TLD locations in the rods placed outside of the PTV (5.5D and 5 mm left of A3).

Such calculations would eliminate the uncertainties in the source strength and calibration of the TLDs and demonstrate any differences in results without the complication of TLD usage. However, time permitted only the simple, single dwell case to be calculated. Comparing the MC results in this way was a more accurate method of verifying the treatment planning system because both OCP and MC simulations assume a liquid water medium without the presence of a jig. A Student's t test was finally performed on results for the MC comparison, to determine their significance.

6.3 Results and Statistical Analysis

6.3.1 Full Prostate Treatment Plan

The results of the experiments provided values of the ratio D_{TLD}/D_{OCP} between the doses measured by the TLDs and those predicted by OCP. Values greater than 1.0 implied that the TLDs received greater dose than predicted by OCP. A mean dose ratio and corresponding sample standard deviation were calculated and used in a hypothesis test to determine if the results were significantly different to a dose ratio of 1.0 (see Appendix 8.2).

The results of the TPS verification experiments are shown in Table 20, where $\bar{x}$ is the mean value of D_{TLD}/D_{OCP} and s is the corresponding sample standard deviation.

Table 20. TPS verification experiment results (Experiments #1 - #3).

Experiment	No. of TLDs	$\bar{x}$	s
#1a	14	0.995	0.061
#1b	14	1.052	0.063
#2	14	0.998	0.114
#3	14	1.047	0.127

The average of the results from experiment #1 (#1a and #1b), with TLDs outside the PTV, show that there may be some slight overdosing, but such inference can only be supported through hypothesis testing. The difference in average results from experiment #1 and its repeat may have been a product of the accuracy of the coordinate system in the treatment planning system when choosing the TLD points

corresponding to the live experiment and the source not being driven out to the same exact position.

Compared to the results from experiments #2 and #3 with TLDs inside the PTV, the standard deviation in the sample of results from experiment #1 and its repeat were much smaller (approximately half). The greater uncertainty for experiments #2 & #3 is most likely due to the very steep dose gradient in the region of ~10 mm where the TLDs were exposed. In this region, a slight misplacement of the TLDs would have an amplified difference in dose (Table 9). In addition, because an average energy factor was assumed for calculation of doses, greater uncertainty had been introduced because the energy response factor changed the most when closer to the source (Equation 5.1). Further still, the mean dose ratios from experiments #2 and #3 were in agreement with the results from experiment #1, with mean values of D_{TLD}/D_{OCP} very close to unity (Table 20), deeming the use and extrapolation of Equation 5.1 for a depth dependent energy correction factor of 0.820 to be appropriate. The notion of over response pends the results of the hypothesis test.

A Student's t test was performed on the sample of 42 values of D_{TLD}/D_{OCP} from experiments #1 - #3 for a full prostate treatment plan in water, to determine if the sample mean was statistically different from the expected value of D_{TLD}/D_{OCP} = 1.0 (null hypothesis H_0). This formed the basis for the verification of the TPS.

With a significance level α of 0.05 (two-tailed test) and 41 degrees of freedom, the critical values c were ±2.02. The total uncertainty in the TLD results was used for the statistical test, where the relative uncertainty in the TPS verification experiments (sample standard deviation divided by the sample mean) was combined in quadrature with the uncertainty in the TLD calibration of 10% (Table 13). Equation 8.3 gave the test statistic t^* value to be 1.15 which was less than the upper critical value of 2.02, so the null hypothesis (that TLD and OCP doses equal) was retained. The p value assessment was also considered, where the corresponding p value for the test statistic of 1.15 and a Student's t distribution with 41 degrees of freedom was 0.256 which was greater than the value of 0.05 needed to reject the null hypothesis at the 5% significance level. Equation 8.4 gives that with confidence level 95%, the true value of D_{TLD}/D_{OCP} lies in the confidence interval 1.023±0.041.

Therefore, the work completed in experiments #1, #2 and #3 did not provided sufficient evidence to show that OCP does not correctly calculate dose for its prostate treatment plans. The statistical values are summarised in Table 21.

Table 21. Statistical parameters from the verification of a full OCP treatment plan.

$\bar{x}$	s	total uncertainty	degrees of freedom	t^*	c	p	95% CI
1.023	0.086	0.131	41	1.15	2.02	0.256	(0.982, 1.064)

The total uncertainty in the results may be improved in future work by running longer Monte Carlo simulations for better dose prediction when calibrating the TLDs and by also finding more accurate ways to determine the energy response.

One similar study by Schumer et al. (1991) showed that a non-concentric shift in source position of 0.25 mm caused a ±5% variation in dose at 10 mm. This large error in dose with spatial uncertainty was certainly observed in the current project; with a shift in source position of 0.25 mm causing a ±5.08% variation in dose at 10 mm. Schumer et al. stated that their group was able to verify their TPS within ±4%. Despite the uncertainty in the water calibration of TLD700:LiF for ^{192}Ir and the spread of results from the TPS verification experiments themselves, this project has still been able to reproduce the precision shown by Schumer et al with a 95% CI of ±4% about the sample mean.

6.3.2 Single Dwell Position Plan

The results of D_{TLD}/D_{OCP} and D_{MC}/D_{OCP} for the single source dwell plan are shown in Table 22, where $\bar{x}$ is the mean value of D_{TLD}/D_{OCP} or D_{MC}/D_{OCP} and s is the corresponding sample standard deviation.

Table 22. TPS verification experiment results (Experiments #4).

Experiment	No. of TLDs or points of interest	$\bar{x}$	s
#4 TLD	11	1.058	0.132
#4 MC	14	1.029	0.094

Both results for TLD and MC comparisons of OCP for the single source dwell plan show similar results to experiments #1 - #3, with the possible notion of a slight over response. This was an expected result for the TLD component of experiment #4 because the full treatment is made up of a superposition of single dwells. It was also a very important result for the MC portion of experiment #4 because it provides evidence that the TLDs were calibrated correctly.

The sample standard deviation for the TLDs was much greater than expected with a value greater than that of the previous experiments. This may have been due to the sample size or a slight difference in the position the source was driven out to in the phantom (±1 mm clinical tolerance). Such a difference in position would have a much greater effect on the TLD results for a single dwell position plan compared to the full array of dwell positions and times seen in a full prostate plan. These factors may have masked any improvements on the spread of results gained through individual calculations of energy response factors. The standard deviation in the MC sample of results was similar to that seen for the previous experiments for TLDs, showing that experimental error may not have contributed to the spread of results as much as previously thought.

A Student's *t* test was performed to determine if the sample means from the TLD and OCP comparisons was statistically different from the expected value of 1.0 (null hypothesis H_0). A Student's t distribution with 10 degrees of freedom was assumed and, like the statistical tests performed for the full prostate treatment plan, the total uncertainty was used, where the relative uncertainty in the TPS verification experiment was combined in quadrature with the uncertainty in the TLD calibration of 10% (Table 13). This produced a test statistic t^* of 1.20 (Equation 8.3) and a p value of 0.258. The p value was greater than 0.05, so supports that $D_{TLD}/D_{OCP} = 1$ at the 95% confidence level. Equation 8.4 gives that with confidence level 95%, the true value of D_{TLD}/D_{OCP} lies in the confidence interval 1.058±0.089.

Therefore, the TLD results from experiment #4 produced no significant finding or improvement upon the accuracy of the verification of the full prostate plan but are consistent with the previous results. The parameters used in the statistical test are summarised in Table 23, where c is the critical value for 10 degrees of freedom and a 5% significance level.

Table 23. Statistical parameters from the TLD verification of a single dwell plan.

$\bar{x}$	s	total uncertainty	degrees of freedom	t^*	c	p	95% CI
1.058	0.132	0.160	10	1.20	2.23	0.258	(0.969, 1.147)

A similar statistical test was performed on the results for the comparison of MC and OCP where a Student's t distribution with 13 degrees of freedom was assumed. The total uncertainty was again used, where the relative uncertainty in the TPS verification experiment was combined in quadrature with the uncertainty in the MC prediction of dose of 6.31% (Table 7). This produced a test statistic t^* of 1.04

(Equation 8.3) and a p value of 0.339. The p value was greater than 0.05, so supports that D_{MC}/D_{OCP} = 1 at the 95% confidence level. Equation 8.4 gives that with confidence level 95%, the true value of D_{MC}/D_{OCP} lies in the confidence interval 1.029±0.064.

Thus, the MC results from experiment #4 have provided more evidence that OCP correctly predicts the dosimetry of the ^{192}Ir source. The parameters used in the statistical test are summarised in Table 24, where c is the critical value for 13 degrees of freedom and a 5% significance level.

Table 24. Statistical parameters from the MC verification of a single dwell plan.

$\bar{x}$	s	total uncertainty	degrees of freedom	t^*	c	p	95% CI
1.029	0.094	0.111	13	1.04	2.16	0.339	(0.965, 1.093)

The reduction in uncertainty stems from the removal of experimental error. However, improvement could still be made by using longer MC simulations of dose deposition in water. Future work may also include direct MC dose calculation from Equation 4.6 for the full prostate treatment plan shown in Experiment's #1 - #3. Like the calculation of energy response factors, multiple calculations of dose would be needed for a single TLD for every dwell location of the ^{192}Ir source, thus a separate program would need to be written in MATLAB, for example. This could not be completed in the timeframe for this project but warrants further investigation in the future.

7. SUMMARY

7.1 Conclusion

The initial aim of this study was to determine the energy response of a set of 0.9 mm thick TLD700:LiF chips after exposure to a range of clinical radiation beams, including high-energy photon and electron beams from a Varian iX Linear Accelerator (Varian Medical Systems, Inc.,), superficial (kV) x ray beams from a Gulmay D3150 x ray machine (Gulmay Limited) and a Nucletron ^{192}Ir brachytherapy source (Nucletron, an Elekta Company), relative to 6 MV x rays. Having pre-determined TLD energy response factors for each clinical radiation beam is of value for a Radiation Oncology Department because of the simple method of TLD calibration when needed for patient dosimetry or for Medical Physics quality assurance procedures, through a single exposure of a small TLD chip subset to a known dose of 6 MV x rays.

With the TLD energy response determined for a wide energy range, the study continued with the aim of verifying the accuracy of a HDR brachytherapy treatment planning system, Oncentra Prostate v3.2.3 (Nucletron Pty. Ltd., an Elekta company), which is used clinically at the Royal Adelaide Hospital for intermediate to high-risk prostate cancer patients.

Previous research had not yet comprehensively characterised the energy response of TLD700:LiF for superficial x ray and linear accelerator beam energies. Some studies have focused on the more popular variant of TLD available, TLD100:LiF. TLD700 differs in its composition from TLD100 by their fractions of the isotopes ^{7}Li and ^{6}Li. TLD700 contains 99.99% ^{7}Li so has a smaller neutron interaction cross section. As such, TLD700 energy dependence was not expected to be identical to TLD100. Nonetheless, trends from past studies concerning TLD100 were used for comparison in the current study results to aid in validation of the results.

To fulfil the aims above, TLD700:LiF chips were first exposed to known doses of radiation from nominal 6 MV and 18 MV photon beams as well as 6 MeV, 9 MeV, 12 MeV, 16 MeV and 20 MeV electron beams from a linear accelerator. Results showed that, relative to the response from the 6 MV beam, TLDs under-responded by approximately 4% for all electron beams and by approximately 3% for the 18 MV photon beam. This trend fitted well with past and current research in the literature on the energy response of TLD100:LiF, in which multiple papers have

stated an approximately uniform response (±5%) for high-energy linear accelerator beams, using a ^{60}Co reference beam (having an average beam energy of 1.25 MeV).

The TLD700:LiF chips were then calibrated for exposure from superficial x ray beams with peak energies of 30, 40, 50, 80, 100, 120 and 150 kVp. An over-response of up to approximately 54% was observed for 40 to 150 kV beams. This trend also fitted well with results from other studies on TLD100:LiF material exposed using superficial x ray machines from various vendors. In most cases, a large over-response was measured, with a tapering off of response for higher kV energies, which is in accordance with the current results using TLD700:LiF.

The TLD700:LiF chips were then calibrated for exposure from an ^{192}Ir source. The methods used in this study build upon previous work by using Monte Carlo simulations (GEANT4) to model the dose deposited in TLD700:LiF chips from an ^{192}Ir source. This was used directly to calibrate dose to the chips for subsequent exposure from ^{192}Ir.

From the modelling process, a formula was derived for the percentage depth dose curve of ^{192}Ir in water, which could be scaled to the appropriate activity of the source at the time of exposure. The Monte Carlo simulations also provided useful data regarding the difference in dose deposition in water and LiF voxels, attenuation of the ^{192}Ir energy spectrum through water, as well as the total effect of attenuation of the beam through water, where plots of the percentage depth dose normalised for the inverse square law were compared for different media.

To experimentally determine their brachytherapy energy response, the TLD700:LiF chips were exposed to the ^{192}Ir source in air using a custom made jig, as well as at varying depths in water within water-tight rods within a plastic phantom, with responses for each scenario compared to the response from the 6 MV beam. The chips over-responded by approximately 11% in air and the response was dependent on the distance between the chip and source when irradiated in water. Determining the energy response of TLD700:LiF in this way was a novel and thorough approach.

Figure 32 shows a plot of the energy dependence of TLD700:LiF as determined through the different exposures in this study. Each response point could have been plotted against the corresponding peak energy, average energy or nominal energy. The choice was made to reflect the most relevant unit in clinical use.

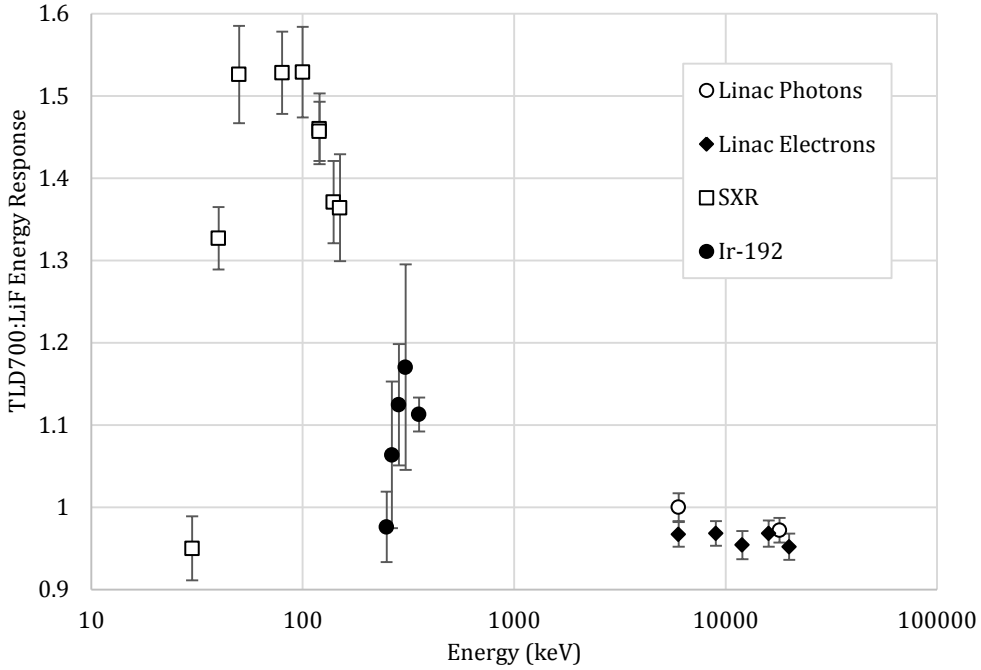

Figure 32. Plot of energy response of TLD700:LiF.
SXR beam responses are plotted against tube voltage, ^{192}Ir responses are plotted against the average γ ray energy according to the depth exposed in water (Table 8), linac beam responses are plotted against nominal energy.

Once calibrated for their energy response, the TLD700:LiF chips were finally used to verify the Oncentra Prostate brachytherapy treatment planning system, by exposing them to a set of treatment plans while within a PMMA water phantom. A clinically realistic prostate treatment plan was created on a reconstructed ultrasound image data set of the phantom. The treatment plan was delivered to the phantom with the TLD chips at known locations inside and outside of the planned target volume. The dose delivered to the TLDs was compared to the simulated doses at corresponding points in the phantom. A plan with a single dwell position was also delivered, where the dose to the TLDs was compared directly with Monte Carlo predictions of delivered dose.

Statistical tests (Student's t test) were conducted to determine the significance of the results of the ratios between the TLD measured doses and the Oncentra Prostate predicted values (D_{TLD}/D_{OCP}), and the Monte Carlo predicted dose values and the Oncentra Prostate predicted values (D_{MC}/D_{OCP}).

For the case of the full prostate treatment simulation, the mean ratio of D_{TLD}/D_{OCP} was not statistically different from 1.0, which meant that the TLDs measured the same dose as predicted by the TPS (p = 0.256, 5% significance level). With confidence level 95%, the true value of D_{TLD}/D_{OCP} was shown to lie in the

confidence interval 1.023±0.041. These statistics were based on the spread of the individual D_{TLD}/D_{OCP} values from the treatment plan verification experiment. OCP was therefore considered verified for the full prostate treatment plan.

For the case of the single dwell position plan, the mean ratio of D_{MC}/D_{OCP} was also not significantly different to 1.0, indicating the dosimetric accuracy of OCP and the correct calibration of the TLDs (p = 0.339, 5% significance level). With confidence level 95%, the true value of D_{MC}/D_{OCP} was shown to lie in the confidence interval 1.029±0.064. These statistics were based on the spread of the individual D_{MC}/D_{OCP} values combined with the uncertainty in the Monte Carlo simulation. Thus, OCP has been verified for a single dwell position plan through Monte Carlo methods.

This study has successfully completed all planned work and answered the initial study aims. It has also provided the Medical Physics field with novel TLD data, calibration techniques and brachytherapy treatment planning system verification results.

7.2 Future Development

The results produced in this project have raised further questions that may be answered by additional work in the future.

The first shortcoming that may be addressed is the uncertainty in the TLD700:LiF calibration factors for exposure to ^{192}Ir in water. The spatial uncertainty in TLD position, when exposed to the ^{192}Ir source, was shown to have a great effect on the dose uncertainty. This is partly owing to the fact that placement of the TLDs in liquid water is quite crude due to the methods used. A more accurate method of determining the distance between the source and TLD may be explored. Other possible options would be to irradiate in a gel (which is mostly H_2O) or to vacuum seal the TLDs in a thin plastic in order to measure the separation from the source more accurately. The Monte Carlo simulations used for dose determination also contributed to the uncertainty in the energy calibration factor due to their unexpectedly high uncertainties. Further studies with longer simulations may reduce the fluctuations between simulations. This improvement would produce more precise results for the MC verification of the single source dwell plan (experiment #4).

The other main limitation exposed through this project was the degree of accuracy to which OCP could be considered verified. This was partly because of the accuracy of the energy calibration factor explained above, but may also be attributed to the assumption of a mean energy calibration factor for all distances in the water

experiments involving a full prostate treatment plan. This assumption was made because of the time constraints of this project but leaves room for further work to be carried out. A depth dependent response was shown to be evident for TLD700:LiF exposed to ^{192}Ir gamma rays in water, which was most likely due to the beam softening of the ^{192}Ir spectra at depth. Therefore, the accuracy of the TPS verification experiments for the full prostate plan could have theoretically been improved if these factors were applied for individual chips, for the full array of source dwell locations and times.

This concept was applied to the simplified experiment with a single source dwell but resulted in unexpectedly poor results. A possible explanation for this was that the ^{192}Ir source was not driven to the correct point in its catheter. Such an occurrence is extremely unlikely due to the thorough quality assurance checks conducted at the RAH but would have a much greater effect on the dose distribution compared to its occurrence for one position in a complete prostate treatment with multiple dwells. Experiments using a small number of dwells could be conducted as well as a full prostate treatment if the smaller arrays produced more precise results. TLD dose calculations for the single dwell position were time consuming because each was calculated manually using the equations derived in this project through Monte Carlo simulation (Equation 4.6, Equation 4.9 and Equation 5.1). This process would become much longer if multiple dwells were used, so a program would need to be written to calculated the doses more efficiently.

8. APPENDIX

8.1 Tables

Table 25. Source dwell times (s) for experiments #1 - #3.
7 Gy prescription and 399.64 GBq source, discussed in Section 6.2.

		catheter dwell positions									
		12	13	14	15	16	17	18	19	20	21
live catheter numbers	1	0	0	0	0	0	0	0	0	0	0
	2	0	0	0	0	0	0	0	0	0	0
	3	0	0	0	0	0	0	0	0	0	0
	4	10.78	9.39	6.93	6.85	6.46	5.9	7.02	9.44	12.24	0
	5	0	17.57	15.14	13.44	12.47	11.51	10.66	10	10.9	0
	6	16.53	13.07	8.45	4.35	5.24	7.51	10.27	13.96	18.21	0
	7	6.61	2.09	0.24	0.01	0.03	0.03	0.4	3.07	6.49	0
	8	11.52	8.51	5.73	0.57	0.12	4.4	6.46	8.42	9.08	8.97
	9	0	0	6.67	7.25	6.95	5.93	5.77	0	0	0
	10	11.04	8.35	6.77	5.78	5.55	5.53	5.6	7.42	9.57	0
	11	0	8.65	7.31	5.71	5.76	6.27	6	6.12	0	0

8.2 Statistical Equations and Theory

The arithmetic mean $\bar{x}$ of a sample is given by Equation 8.1, where n is the number of data values and x_i are the data values.

$$\bar{x} = \frac{1}{n}\sum_{i=1}^{n} x_i \tag{8.1}$$

The sample standard deviation s_{N-1} for N data values and a sample mean of $\bar{x}$ is given by Equation 8.2.

$$s_{N-1} = \sqrt{\frac{1}{N-1}\sum_{i=1}^{N}(x_i - \bar{x})^2} \tag{8.2}$$

If the amount of data collected is insufficient to approximate a normal distribution, a z test cannot be used to determine the statistical significance of results. A Student's t distribution is a more appropriate choice, which depends on the number of data points in the sample. The corresponding t test can used to determine the significance of the results, where the test statistic t^* is given be Equation 8.3

$$t^* = \frac{\bar{x} - \mu_0}{s/\sqrt{n}} \tag{8.3}$$

where $\bar{x}$ is the sample mean, s is the sample standard deviation, n is the number of data points in the sample and μ_0 is the value of the null hypothesis ($s/\sqrt{n}$ is the standard error in the sample mean). The null hypothesis used in this project is that the ratio of doses between the TLD and OCP (D_{TLD}/D_{OCP}) is unity i.e. H_0: μ_0 = 1 and H_A: $\mu_0 \neq 1$. The null hypothesis is rejected, within a certain confidence interval (CI), if the test statistic lies outside of the critical value c for the t distribution with $n - 1$ degrees of freedom. Statistical tables provide the critical values for different significance levels α, one tailed or two tailed tests and different degrees of freedom. In this project, a 95% confidence interval was used with a two tailed test and 41 degrees of freedom. For a 95% confidence interval and a two tailed test, the significance level α is 0.05. For 41 degrees of freedom, the critical values are ±2.02. If the test statistic t^* falls outside of (–2.02, 2.02) then the null hypothesis is rejected and if it falls inside then the null hypothesis is retained. With confidence level 95%, the true value of D_{TLD}/D_{OCP} (μ) lies in the confidence interval given by Equation 8.4.

$$\mu \in \left(\bar{x} - c\frac{s}{\sqrt{n}}, \bar{x} + c\frac{s}{\sqrt{n}}\right) \tag{8.4}$$

Alternatively, one could consider the corresponding p value to the test statistic which represents the probability of measuring the sample mean given that the null hypothesis is true. If the p value lies inside of the significance level of choice then the null hypothesis is retained. The 95% confidence interval for the true value of μ (D_{TLD}/D_{OCP}) is given by Equation 8.4. For example, if the significance level was 95% then a p value less than 0.05 would imply that the null hypothesis should be rejected.

8.3 Detector Construction GEANT4 Code

```
//
// DetectorConstruction
//
// Build the geometry and sensitive elements of our model
//

#include "DetectorConstruction.hh"

#include "G4NistManager.hh"
#include "G4Material.hh"

#include "G4Box.hh"
#include "G4LogicalVolume.hh"
#include "G4PVPlacement.hh"
```

```
#include "G4VisAttributes.hh"

#include "G4SDManager.hh"
#include "VoxelScoring.hh"

#include "G4Box.hh"
#include "G4Tubs.hh"

//
// Constructor
//
DetectorConstruction::DetectorConstruction()
{;}

//
// Construct
//
// Do the actual work
//
G4VPhysicalVolume *DetectorConstruction::Construct()
{

  //
  // Define materials from the GEANT4 database
  //
  /* Defining Materials */

  //Air
  G4NistManager* man = G4NistManager::Instance();
  G4Material* air = man->FindOrBuildMaterial("G4_AIR");
  //G4Material* water = man->FindOrBuildMaterial("G4_WATER");

  //List of Elements used
  G4Element *Ir = new G4Element("Iridium", "Ir", 77, 192.217*g/mole);
  G4Element *Mn = new G4Element("Manganese", "Mn", 25, 54.938*g/mole);
  G4Element *Si = new G4Element("Silicon", "Si", 14, 28.085*g/mole);
  G4Element *Cr = new G4Element("Chromium", "Cr", 24, 51.996*g/mole);
  G4Element *Ni = new G4Element("Nickel", "Ni", 28, 58.6934*g/mole);
  G4Element *Fe = new G4Element("Iron", "Fe", 26, 55.845*g/mole);
  G4Element *Li = new G4Element("Lithium", "Li", 3, 6.94*g/mole);
  G4Element *F = new G4Element("Flourine", "F", 9, 18.9984*g/mole);
  G4Element *C = new G4Element("Carbon", "C", 6, 12.011*g/mole);
  G4Element *H = new G4Element("Hydrogen", "H", 1, 1.008*g/mole);
  G4Element *N = new G4Element("Nitrogen", "N", 7, 14.007*g/mole);
  G4Element *O = new G4Element("Oxygen", "O", 8, 15.999*g/mole);

  //*Water
  G4double water_density = 1.0*g/cm3;
  G4Material* water = new G4Material("water", water_density, 2);
  water->AddElement(O, 0.888);
  water->AddElement(H, 0.112);


  //Steel
  G4double steel_density = 8.02*g/cm3;
  G4Material* steel = new G4Material("steel", steel_density, 5);
  steel->AddElement(Mn, 0.02);
  steel->AddElement(Si, 0.01);
  steel->AddElement(Cr, 0.19);
  steel->AddElement(Ni, 0.10);
  steel->AddElement(Fe, 0.68);

  //LiF
  G4double LiF_density = 2.635*g/cm3;
  G4Material* LiF = new G4Material("LiF", LiF_density, 2);
  LiF->AddElement(Li, 0.27);
  LiF->AddElement(F, 0.73);
```

```
  //Nylon
  G4double nylon_density = 1.10*g/cm3;
  G4Material* nylon = new G4Material("nylon", nylon_density, 4);
  nylon->AddElement(C, 0.637);
  nylon->AddElement(H, 0.097);
  nylon->AddElement(N, 0.124);
  nylon->AddElement(O, 0.142);

  //Source
  G4double source_density = 22.56*g/cm3;
  G4Material* source = new G4Material("source", source_density, 1);
  source->AddElement(Ir, 1.0);

  //PMMA
  G4double PMMA_density = 1.18*g/cm3;
  G4Material* PMMA = new G4Material("PMMA", PMMA_density, 3);
  PMMA->AddElement(C, 0.6);
  PMMA->AddElement(H, 0.08);
  PMMA->AddElement(O, 0.32);



//*****************************************************************
*//
//*********************Begin
Geometry***********************************//
//*****************************************************************
*//

  //
  // Build our mother volume, the "lab", the object that holds
  // the lab apparatus.
  //
  // (We don't want a lab that is too big, since this determines how
  // far particle travel and effects visualization).
  //
  G4double lab_half_x = 250*m;
  G4double lab_half_y = 250*m;
  G4double lab_half_z = 250*m;

  G4Box* labSolid = new G4Box( "labSolid",
                           lab_half_x,
                           lab_half_y,
                           lab_half_z );

  G4LogicalVolume *labLogical = new G4LogicalVolume( labSolid,
                                          water,
                                          "labLog",
                                          0,
                                          0,
                                          0 );

  G4VPhysicalVolume *lab = new G4PVPlacement( 0,
                                      G4ThreeVector(0,0,0),
                                      labLogical,
                                      "labPhys",
                                      0,
                                      false,
                                      0 );

  //
  // We generally don't want to include the lab in any pictures
  //
  labLogical->SetVisAttributes( G4VisAttributes::Invisible );

  //
  //Build air Tube
```

```
  //
  G4double  airRMin = 0*mm;
  G4double  airRMax = 1*mm;
  G4double  airDz = 250*mm;
  G4double  airSPhi = 0;
  G4double  airDPhi = 2*M_PI;

  G4Tubs* airTubeSolid = new G4Tubs( "airTubeSolid",
                                  airRMin,
                                  airRMax,
                                  airDz,
                                  airSPhi,
                                  airDPhi);

  G4LogicalVolume *airTubeLogical = new G4LogicalVolume( airTubeSolid,
                                                  air,
                                                  "airTubeLogical",
                                                  0,
                                                  0,
                                                  0 );

  G4VPhysicalVolume *airTubePhysical = new G4PVPlacement( 0,
                                                   G4ThreeVector(0,0,0),
                                                   airTubeLogical,
                                                   "airTubePhys",
                                                   labLogical,
                                                   false,
                                                   0 );
  //
  //Build Nylon Tube
  //
  G4double  NylonRMin = 0.75*mm;
  G4double  NylonRMax = 1*mm;
  G4double  NylonDz = 250*mm;
  G4double  NylonSPhi = 0;
  G4double  NylonDPhi = 2*M_PI;

  G4Tubs* NylonTubeSolid = new G4Tubs( "NylonTubeSolid",
                                  NylonRMin,
                                  NylonRMax,
                                  NylonDz,
                                  NylonSPhi,
                                  NylonDPhi);

  G4LogicalVolume *NylonTubeLogical = new G4LogicalVolume(
NylonTubeSolid,
                                                   nylon,
                                                   "NylonTubeLogical",
                                                   0,
                                                   0,
                                                   0 );

  G4VPhysicalVolume *NylonTubePhysical = new G4PVPlacement( 0,
                                                    G4ThreeVector(0,0,0),
                                                    NylonTubeLogical,
                                                    "NylonTubePhys",
                                                    airTubeLogical,
                                                    false,
                                                    0 );


  //
  //Build Steel Cylinder
  //
  G4double  SteelRMin = 0;
  G4double  SteelRMax = 0.45*mm;
  G4double  SteelDz = 101*mm;
  G4double  SteelSPhi = 0;
```

```
  G4double  SteelDPhi = 2*M_PI;

  G4Tubs* SteelCableSolid = new G4Tubs( "SteelCableSolid",
                                SteelRMin,
                                SteelRMax,
                                SteelDz,
                                SteelSPhi,
                                SteelDPhi);

  G4LogicalVolume *SteelCableLogical = new G4LogicalVolume(
SteelCableSolid,
                                                    steel,
                                                    "SteelCableLogical",
                                                    0,
                                                    0,
                                                    0 );

  G4VPhysicalVolume *SteelCablePhysical = new G4PVPlacement( 0,
                                          G4ThreeVector(0,0,99*mm),
                                          SteelCableLogical,
                                          "SteelCablePhys",
                                          airTubeLogical,
                                          false,
                                          0 );


  //
  //Build Source inside of steelcablephysical
  //
  G4double  SourceRMin = 0;
  G4double  SourceRMax = 0.35*mm;
  G4double  SourceDz = 1.8*mm;
  G4double  SourceSPhi = 0;
  G4double  SourceDPhi = 2*M_PI;

  G4Tubs* SourceSolid = new G4Tubs( "SourceSolid",
                              SourceRMin,
                              SourceRMax,
                              SourceDz,
                              SourceSPhi,
                              SourceDPhi);

  G4LogicalVolume *SourceLogical = new G4LogicalVolume( SourceSolid,
                                                source,
                                                "SourceLogical",
                                                0,
                                                0,
                                                0 );

  G4VPhysicalVolume *SourcePhysical = new G4PVPlacement( 0,
                                        G4ThreeVector(0,0,-99*mm),
                                        SourceLogical,
                                        "SourcePhys",
                                        SteelCableLogical,
                                        false,
                                        0 );



  //
  // Add the sensitive elements
  //
  G4double vStart = 10.0;
  G4double vDepth = 0.9;
  G4double vSpace = 10.0;
  G4double vWidth = 1.0;
```

```
  G4Tubs *voxel1Solid = new
G4Tubs("voxel1Solid",vStart*mm,(vStart+vDepth)*mm,vWidth*mm,0.*deg,36.*de
g);
  G4LogicalVolume *voxel1Logical = new
G4LogicalVolume(voxel1Solid,LiF,"voxel1Logical",0,0,0 );
  G4VPhysicalVolume *voxel1Physical = new
G4PVPlacement(0,G4ThreeVector(0,0,0),voxel1Logical,"voxel1Phys",labLogica
l,false,0);

  G4Tubs *voxel2Solid = new
G4Tubs("voxel2Solid",(vStart+vSpace)*mm,(vStart+vSpace+vDepth)*mm,vWidth*
mm,36.*deg,36.*deg);
  G4LogicalVolume *voxel2Logical = new
G4LogicalVolume(voxel2Solid,LiF,"voxel2Logical",0,0,0 );
  G4VPhysicalVolume *voxel2Physical = new
G4PVPlacement(0,G4ThreeVector(0,0,0),voxel2Logical,"voxel2Phys",labLogica
l,false,1);

  G4Tubs *voxel3Solid = new
G4Tubs("voxel3Solid",(vStart+2.0*vSpace)*mm,(vStart+2.0*vSpace+vDepth)*mm
,vWidth*mm,72.*deg,36.*deg);
  G4LogicalVolume *voxel3Logical = new
G4LogicalVolume(voxel3Solid,LiF,"voxel3Logical",0,0,0);
  G4VPhysicalVolume *voxel3Physical = new
G4PVPlacement(0,G4ThreeVector(0,0,0),voxel3Logical,"voxel3Phys",labLogica
l,false,2);

G4Tubs *voxel4Solid = new
G4Tubs("voxel1Solid",(vStart+3.0*vSpace)*mm,(vStart+3.0*vSpace+vDepth)*mm
,vWidth*mm,108.*deg,36.*deg);
  G4LogicalVolume *voxel4Logical = new
G4LogicalVolume(voxel4Solid,LiF,"voxel4Logical",0,0,0);
  G4VPhysicalVolume *voxel4Physical = new
G4PVPlacement(0,G4ThreeVector(0,0,0),voxel4Logical,"voxel4Phys",labLogica
l,false,3);

G4Tubs *voxel5Solid = new
G4Tubs("voxel5Solid",(vStart+4.0*vSpace)*mm,(vStart+4.0*vSpace+vDepth)*mm
,vWidth*mm,144.*deg,36.*deg);
  G4LogicalVolume *voxel5Logical = new
G4LogicalVolume(voxel5Solid,LiF,"voxel5Logical",0,0,0);
  G4VPhysicalVolume *voxel5Physical = new
G4PVPlacement(0,G4ThreeVector(0,0,0),voxel5Logical,"voxel5Phys",labLogica
l,false,4);

G4Tubs *voxel6Solid = new
G4Tubs("voxel6Solid",(vStart+5.0*vSpace)*mm,(vStart+5.0*vSpace+vDepth)*mm
,vWidth*mm,180.*deg,36.*deg);
  G4LogicalVolume *voxel6Logical = new
G4LogicalVolume(voxel6Solid,LiF,"voxel6Logical",0,0,0);
  G4VPhysicalVolume *voxel6Physical = new
G4PVPlacement(0,G4ThreeVector(0,0,0),voxel6Logical,"voxel6Phys",labLogica
l,false,5);

  G4Tubs *voxel7Solid = new
G4Tubs("voxel7Solid",(vStart+6.0*vSpace)*mm,(vStart+6.0*vSpace+vDepth)*mm
,vWidth*mm,216.*deg,36.*deg);
  G4LogicalVolume *voxel7Logical = new
G4LogicalVolume(voxel7Solid,LiF,"voxel7Logical",0,0,0);
  G4VPhysicalVolume *voxel7Physical = new
G4PVPlacement(0,G4ThreeVector(0,0,0),voxel7Logical,"voxel7Phys",labLogica
l,false,6);

G4Tubs *voxel8Solid = new
G4Tubs("voxel8Solid",(vStart+7.0*vSpace)*mm,(vStart+7.0*vSpace+vDepth)*mm
,vWidth*mm,252.*deg,36.*deg);
  G4LogicalVolume *voxel8Logical = new
G4LogicalVolume(voxel8Solid,LiF,"voxel8Logical",0,0,0);
```

```
  G4VPhysicalVolume *voxel8Physical = new
G4PVPlacement(0,G4ThreeVector(0,0,0),voxel8Logical,"voxel8Phys",labLogica
l,false,7);

G4Tubs *voxel9Solid = new
G4Tubs("voxel9Solid",(vStart+8.0*vSpace)*mm,(vStart+8.0*vSpace+vDepth)*mm
,vWidth*mm,288.*deg,36.*deg);
  G4LogicalVolume *voxel9Logical = new
G4LogicalVolume(voxel9Solid,LiF,"voxel9Logical",0,0,0);
  G4VPhysicalVolume *voxel9Physical = new
G4PVPlacement(0,G4ThreeVector(0,0,0),voxel9Logical,"voxel9Phys",labLogica
l,false,8);

G4Tubs *voxel10Solid = new
G4Tubs("voxel1Solid",(vStart+9.0*vSpace)*mm,(vStart+9.0*vSpace+vDepth)*mm
,1*vWidth,324.*deg,36.*deg);
  G4LogicalVolume *voxel10Logical = new
G4LogicalVolume(voxel10Solid,LiF,"voxel10Logical",0,0,0);
  G4VPhysicalVolume *voxel10Physical = new
G4PVPlacement(0,G4ThreeVector(0,0,0),voxel10Logical,"voxel10Phys",labLogi
cal,false,9);

  //
  // Pass the voxel to the sensitive manager
  //
  G4SDManager *sensitiveManager = G4SDManager::GetSDMpointer();

  VoxelScoring *voxelScoring = new VoxelScoring( "voxelScoring" );
  sensitiveManager->AddNewDetector( voxelScoring );
  voxel1Logical->SetSensitiveDetector( voxelScoring );
  voxel2Logical->SetSensitiveDetector( voxelScoring );
  voxel3Logical->SetSensitiveDetector( voxelScoring );
  voxel4Logical->SetSensitiveDetector( voxelScoring );
  voxel5Logical->SetSensitiveDetector( voxelScoring );
  voxel6Logical->SetSensitiveDetector( voxelScoring );
  voxel7Logical->SetSensitiveDetector( voxelScoring );
  voxel8Logical->SetSensitiveDetector( voxelScoring );
  voxel9Logical->SetSensitiveDetector( voxelScoring );
  voxel10Logical->SetSensitiveDetector( voxelScoring );

  //
  // This method returns the mother volume
  //
  return lab;
}
```

8.4 Voxel Scoring GEANT4 Code

```
//
// VoxelScoring.cc
//

#include "VoxelScoring.hh"

#include "G4TouchableHistory.hh"
#include "G4Step.hh"
#include "G4ParticleDefinition.hh"
#include "G4VPhysicalVolume.hh"
#include "RunAction.hh"
#include "G4RunManager.hh"

//initialize counter

//
// Constructor
//
```

```
VoxelScoring::VoxelScoring(G4String name)
  :G4VSensitiveDetector( name )
{
       // Initialize the dose scoring array
       num_voxels = 10 ;
       total_energy_dep = new G4double[num_voxels];
       counter = new G4double[num_voxels];
       for(G4int i = 0;i<num_voxels;i++){
         counter[i]=0;
       }
       num_bins = 100;
       spectrum = new G4double[num_bins];
       for(G4int i=0;i<num_bins;i++){
         spectrum[i]=0;
       }
}

VoxelScoring::~VoxelScoring()
{
       delete total_energy_dep;
}

//
// Initialize
//
void VoxelScoring::Initialize( G4HCofThisEvent* )
{
  //reset index
  tIndex = -1;
  vIndex = -1;
  //G4cout << "index reset" << G4endl;

  // Zero the arrays at the beginning of each primary
  for(G4int i=0;i<num_voxels;i++){
    total_energy_dep[i]=0;
  }

}

//
// Process hits
//
G4bool VoxelScoring::ProcessHits( G4Step *step, G4TouchableHistory
*ROhist )
{
  //track information
  trackID = step->GetTrack()->GetTrackID();
  voxelID = step->GetPreStepPoint()->GetTouchable()->GetCopyNumber();
  KE = step->GetPreStepPoint()->GetKineticEnergy() /MeV;

  if (step->GetTrack()->GetParticleDefinition()->GetParticleName() ==
"gamma"){

    //voxel-by-voxel track counter
    if (vIndex != voxelID){
      vIndex = voxelID;
      if (KE > 0.25){
       counter[voxelID] += 1;
      }
    }

    if (tIndex != trackID){
      tIndex = trackID;

      //spectrum information
      if (voxelID == 0){

       for (G4int k=0;k<num_bins;k++){
```

```
          G4double k_d = (G4double)(k);
          G4double num_bins_d = (G4double)(num_bins);
          G4double Emin = k_d/num_bins_d;
          G4double Emax = (k_d+1.0)/num_bins_d;

          if((KE > Emin) && (KE <= Emax)){
            spectrum[k] += 1;
            break;
          }

        }

       }

     }
   }
   //
   // Find which voxel we are in
   //
   G4int voxel = step->GetPreStepPoint()->GetTouchable()->GetCopyNumber();

   //
   // Tally total energy deposited in MeV
   //
   total_energy_dep[voxel] += step->GetTotalEnergyDeposit()/MeV;
   /*E += step->GetTotalEnergyDeposit()/keV;
     if (step->GetTotalEnergyDeposit()/keV > 0){
     counter2 += 1;
     G4cout << step->GetTotalEnergyDeposit()/keV<< " keV deposited,
counter: "<<counter2<<", total(keV): "<<E<<G4endl;
     }*/

   return true;
}

//
// EndOfEvent
//
  void VoxelScoring::EndOfEvent( G4HCofThisEvent* )
  {
    // Pass the measured energy and binned counts to RunAction
    RunAction* myRunAction = (RunAction*)(G4RunManager::GetRunManager()-
>GetUserRunAction());
    myRunAction -> doseEvent(total_energy_dep);
    myRunAction -> spectrumEvent(spectrum);
    myRunAction -> counterEvent(counter);
  }
```

8.5 Run Action GEANT4 Code

```
//
// RunAction
// Controls what is done at the end of entire run and at end of each
event
//

#include "RunAction.hh"
#include "G4Run.hh"
#include "G4RunManager.hh"

#include <fstream>
#include <math.h>

using namespace std;

RunAction::RunAction()
```

```
{;}

RunAction::~RunAction()
{
       delete total_dose;
}

void RunAction::BeginOfRunAction(const G4Run*)
{

  num_bins = 100;
  num_voxels = 10;
  total_dose = new G4double[num_voxels];
  total_counter = new G4double[num_voxels];
  total_spectrum = new G4double[num_bins];
  for(G4int i=0;i<num_voxels;i++){
    total_dose[i]=0;
  }
  for(G4int i=0;i<num_voxels;i++){
    total_counter[i]=0;
  }
  for(G4int i=0;i<num_bins;i++){
    total_spectrum[i]=0;
  }
}


void RunAction::doseEvent(G4double total_energy_dep[])
{
  for(G4int i=0;i<num_voxels;i++){
    total_dose[i]+=(total_energy_dep[i]/joule) ;// /gray;
  }
}

void RunAction::spectrumEvent(G4double spectrum[])
{
  for(G4int i=0;i<num_bins;i++){
    total_spectrum[i]=spectrum[i];
  }
}

void RunAction::counterEvent(G4double counter[])
{
  for(G4int i=0;i<num_voxels;i++){
    total_counter[i]=counter[i];
  }
}

void RunAction::EndOfRunAction(const G4Run* )
{
       //
       // Print the arrays to file
       //
       ofstream outFile("Results.dat");
       // Print the data to a 2D for external visualization
       for(G4int i=0;i<num_voxels;i++){
         outFile << total_dose[i]<< " ";
              outFile << endl;
       }
       outFile.close();

       //print spectrum data
       ofstream outFile2("Spectrum.dat");
       for(G4int i=0;i<num_bins;i++){
         outFile2 << total_spectrum[i] << endl;
       }
       outFile2.close();
```

```
        //print voxel track counts
        ofstream outFile3("Counter.dat");
        for(G4int i=0;i<num_voxels;i++){
          outFile3 << total_counter[i]<<endl;
        }
        outFile3.close();
}
```

8.6 Physics List GEANT4 Code

```
//
// Build the physics processes
//

#include "PhysicsList.hh"

#include "G4EmLivermorePhysics.hh"
#include "G4LossTableManager.hh"
#include "G4ProcessManager.hh"
#include "G4EmProcessOptions.hh"
#include "G4RadioactiveDecayPhysics.hh"
#include "G4HadronQElasticPhysics.hh"
#include "G4IonBinaryCascadePhysics.hh"
#include "G4HadronInelasticQBBC.hh"

#include "G4BosonConstructor.hh"
#include "G4LeptonConstructor.hh"
#include "G4MesonConstructor.hh"
#include "G4BaryonConstructor.hh"
#include "G4IonConstructor.hh"
#include "G4ShortLivedConstructor.hh"

////////////////////////////////////////////////////////////////////////
///
PhysicsList::PhysicsList() : G4VModularPhysicsList()
{
  G4LossTableManager::Instance();
  defaultCutValue = 0.045*mm;
  cutForGamma     = defaultCutValue;
  cutForElectron  = defaultCutValue;
  cutForPositron  = defaultCutValue;

  SetVerboseLevel(1);

  // EM physics
  emPhysicsList = new G4EmLivermorePhysics();

  // The next two will not be needed in this simulation, but for future
reference...

  // Radioactive Decay
  decPhysicsList = new G4RadioactiveDecayPhysics();

  // Hadron physics
  hadElasPhysics = new G4HadronQElasticPhysics();
  ionInelasPhysics = new G4IonBinaryCascadePhysics();
  hadInelasPhysics = new G4HadronInelasticQBBC();

}

////////////////////////////////////////////////////////////////////////
///
PhysicsList::~PhysicsList()
{
  delete emPhysicsList;
  delete decPhysicsList;
```

```
  delete hadElasPhysics;
  delete ionInelasPhysics;
  delete hadInelasPhysics;
}

////////////////////////////////////////////////////////////////////////
///
void PhysicsList::ConstructParticle()
{
    // Construct all particles

    G4LeptonConstructor lepton;
    lepton.ConstructParticle();

    G4BosonConstructor boson;
    boson.ConstructParticle();

    G4MesonConstructor meson;
    meson.ConstructParticle();

    G4BaryonConstructor baryon;
    baryon.ConstructParticle();

    G4ShortLivedConstructor shortLived;
    shortLived.ConstructParticle();

    G4IonConstructor ion;
    ion.ConstructParticle();
}

////////////////////////////////////////////////////////////////////////
///
void PhysicsList::ConstructProcess()
{
  // transportation
  AddTransportation();

  // electromagnetic physics list
  emPhysicsList->ConstructProcess();
  em_config.AddModels();

  // decay physics list
  decPhysicsList->ConstructProcess();

  // hadronic physics
  hadElasPhysics->ConstructProcess();
  ionInelasPhysics->ConstructProcess();
  hadInelasPhysics->ConstructProcess();
}


////////////////////////////////////////////////////////////////////////
///
void PhysicsList::SetCuts()
{

  if (verboseLevel >0){
    G4cout << "PhysicsList::SetCuts:";
    G4cout << "CutLength : " << G4BestUnit(defaultCutValue,"Length") <<
G4endl;
  }

  // Need to set production cuts for these three particles
  SetCutValue(cutForGamma, "gamma");
  SetCutValue(cutForElectron, "e-");
  SetCutValue(cutForPositron, "e+");

  if (verboseLevel>0) DumpCutValuesTable();
```

```
}
```

8.7 Primary Generator Action GEANT4 Code

```
//
// This class defines the source of radiation
//
#include "PrimaryGeneratorAction.hh"

#include "G4Event.hh"
#include "G4ParticleGun.hh"
#include "G4Gamma.hh"
#include "Randomize.hh"


PrimaryGeneratorAction::PrimaryGeneratorAction()
{
       particleGun = new G4GeneralParticleSource();
}

PrimaryGeneratorAction::~PrimaryGeneratorAction()
{
       delete particleGun;
}

void PrimaryGeneratorAction::GeneratePrimaries(G4Event* anEvent)
{
       particleGun->GeneratePrimaryVertex( anEvent );
}
```

8.8 Main GEANT4 Code

```
using namespace std;

#include "G4RunManager.hh"

#include "DetectorConstruction.hh"
#include "PrimaryGeneratorAction.hh"
#include "RunAction.hh"
#include "PhysicsList.hh"

#include "G4UImanager.hh"
#include "G4UIterminal.hh"
#include "G4VisExecutive.hh"
#include "G4UIExecutive.hh"

#include <Randomize.hh>
#include <math.h>


int main( int argc, char** argv )
{

  //
  // Create a GEANT4 run manager. This controls GEANT4.
  //
  G4RunManager runManager;

  //
  // We need to give the run manager a detector and a list
  // of physics processes.
  //
  runManager.SetUserInitialization(new DetectorConstruction());

  runManager.SetUserInitialization( new PhysicsList() );
```

```
  //
  // We also need to supply a source of particles
  //
  runManager.SetUserAction( new PrimaryGeneratorAction() );

  //
  // Set the random number seed (makes sure two simulations don't give
same result
  //
  CLHEP::HepRandom::setTheEngine(new CLHEP::RanecuEngine);
  G4long seed=time(0);
  CLHEP::HepRandom::setTheSeed(seed);

  //
  // Initialize GEANT4
  //
  runManager.Initialize();

  //
  // Optional user Action Classes
  //
  runManager.SetUserAction( new RunAction() );

  //
  // Create a visualization manager if requested and enter into a session
  //
  if(argc>1){
    G4VisManager* myVisManager = new G4VisExecutive();
    myVisManager -> Initialize();
    G4UImanager *UI = G4UImanager::GetUIpointer();
    G4String command = "/control/execute ";
    G4String fileName = argv[1];
    UI->ApplyCommand(command+fileName);
       G4UIExecutive *ui = new G4UIExecutive(argc,argv);
    ui->SessionStart();
    delete ui;
  }
  else{
    //
    // Run the simulation without entering a session
    //
    runManager.BeamOn(10000);
  }
}
```

8.9 Macro File GEANT4 Code

```
# Macro file for PDD
#
# Can be run in batch, without graphic
# or interactively: Idle> /control/execute run1.mac
#
/control/verbose 0
#
/run/verbose 0
/tracking/verbose 0
/event/verbose 0
#
# Set General Particle Source Volume and Radioactive Isotope

/gps/pos/type Volume
/gps/pos/shape Cylinder
/gps/pos/radius 0.35 mm
/gps/pos/halfz 1.8 mm
/gps/pos/centre 0 0 0
/gps/particle ion
```

```
/gps/ion 77 192 0 0
/gps/energy 0 keV
#
/run/beamOn 5000000
```

8.10 Example Certificate for HDR Source

Certificate For sealed Sources

G2-00025U

ID:

Customer name and address: ROYAL ADELAIDE HOSPITAL SN31234
ATTN. T. DOORN VAN
NORTH TERRACE
SA500 ADELAIDE
AUSTRALIA

Issue Date: 2011-07-21 (1)

Product Code:	REF	105.002 (DRN 07736)
Serial number:	SN	NLF 01 D36C9071
Production Code:	LOT	87725/04

Serial no. Transport Container; 1010C6
Serial no. Check Cable: n.a.
Certificate number: AyLH5 rNcg# To1bW #eShP B0

SOURCE SPECIFICATIONS

Reference Air Kerma Rate: 48.46 mGy h^{-1} +/- 5% at 1 m (2)
Measured at: 2011-07-19 14:53 CET (1)
Apparent Activity: 440.51 GBq (11.90 Ci) at date of measurement (3,4)

Source Type: MICROSELECTRON V2
Capsule dimensions: 0.90 mm diameter, 4.50 mm length
Source pellet dimensions: 0.65 mm diameter, 3.60 mm length
Source pellet form: solid Iridium
Radionuclide: Ir192
Encapsulation: single
Capsule material: stainless steel, AISI 316L
ISO Classification: ISO/80/C63211
Special form certificate number: D/0070/S-96(REV.3)

QUALITY CONTROL

Cable Visual Inspection: passed
Source Visual Inspection: passed
Laser Weld Visual Check: passed
Source Capsule Integrity (15N pull test): passed
Leakage test: leakfree (5)
Surface contamination test: < 185 Bq (5nCi) (6)

The undersigned, authorized officer of Mallinckrodt Medical B.V., certifies that this source complies with the requirements of ISO2919 and that all of the information given in this certificate is true and correct.

QUALITY CONTROL SUPERVISOR ....

(1) Date format yyyy-mm-dd
(2) At Confidence level of 99.7%
(3) The apparent Activity is determined by applying a conversion factor (0.110 mGy m^2 h^{-1} GBq^{-1}) to the measured gamma radiation output of the sealed source determined with a calibration instrument. The instrument is calibrated against the standard of the Physikalisch-Technische Bundesanstalt (PTB), Braunschweig, Germany.
(4) The Apparent Activity is the Iridium-192 activity; other radionuclides not detectable
(5) Leakage test method according to ISO9978 method Liquid nitrogen bubble test (6.2.4)
(6) Surface contamination test according to ISO9978 method Wet wipe test (5.3.1)

Manufactured by Mallinckrodt Medical B.V. * Westerduinweg 3 * NL-1755 LE Petten * Telephone +31 224 567890
Manufacturer's code in accordance with Council Directive 2003/122/EURATOM: NLF 01
On behalf of Nucletron B.V.* Waardgelder 1 * NL-3900AX Veenendaal

9. REFERENCES

Almond, P & McCray, K 1970, 'The energy response of LiF, CaF_2, and $Li_2B_4O_7$:Mn to high energy radiations', *Phys. Med. Biol.*, vol 15, pp. 335-342.

Almond, P, Wright, A & Lontz , J 1966, 'The use of LiF thermoluminescent dosimeters to measure the dose distribution of high energy electron beams', *Phys. Med. Biol.*, vol 11, p. 622.

Almond, P, Wright, A & Lontz, J 1967, 'The use of Lithium Fluoride Thermoluminescent Dosemeters to measure the Dose Distribution of a 15 MeV Electron Beam', *Phys. Med. Biol.*, vol 12, pp. 389-391.

Anderson, L, Nath, R & Weaver, K 1990, 'Interstitial brachytherapy: physical, biological and clinical considerations', *Raven Press*.

Aukett, RJ, Burns, JE, Greener, AG, Harrison, RM, Moretti, C, Nahum, AE & Rosser, KE 2005, 'Addendum to the IPEMB code of practice for the determination of absorbed dose for x-rays below 300 kV generating potential (0.035 mm Al–4 mm Cu HVL)', *Phys. Med. Biol.*, vol 50, no. 12, p. 2739.

Aukett, RJ, Harrison, RM, Morettie, C, Nahum, AE & Rosser, KE 1996, 'The IPEMB code of practice for the determination of absorbed dose for x rays below 300 kV generating potential (0.035 mm Al-4 mm Cu HVL; 10-300 kV generating potential)', *Phys. Med. Biol.*, vol 41, no. 12, pp. 2605-25.

Bilski, P 2002, 'Lithium Fluoride: from LiF:Mg,Ti to LiF:Mg,Cu,P', *Radiaiton protection dosimetry*, vol 100, pp. 199-206.

Borg, J & Rogers, D 1991, 'Monte Carlo Calculations of Photon Spectra in Air from ^{192}Ir Sources', National Research Council Report PIRS-629r, Ontario, Canada.

Butler, D, Haworth, A, Sander, T & Todd, S 2008, 'Comparison of ^{192}Ir air kerma calibration coeffiicients derived at ARPANSA using the interpolation method and at the National Physical Laboratory using a direct measurement', *Australas. Phys. Eng. Sci. Med.*, vol 31, no. 4, pp. 332-338.

Cameron, JR, Suntharalingham, N & Kenney, GN 1968, *Thermoluminescent Dosimetry*, University of Wisconsin Press, Madison.

Cameron, JR, Zimmerman, DW & Bland, RW 1967, 'Thermoluminescence vs. Roentgens in Lithium Fluoride: a Proposed Mathematical Model', *USAEC*, pp. COO-1105-102.

Chang, J 2013, 'Table of Nuclides', *KAERI (Korea Atomic Energy Research Institute)*, viewed 31 October 2013, <http://atom.kaeri.re.kr/ton/>.

Chiu-Tsao, ST & Anderson, LL 1991, 'Thermoluminescent dosimetry for 103Pd seeds (model 200) in solid water phantom', *Medical Physics*, vol 18, pp. 449-52.

Cluchet, J & Joffre, H 1967, 'Applications of Thermoluminescence Dosimetry in Health Physics', *NRL Luminescence Dosimetry*, vol 68, pp. 349-58.

Crosby, EH, Almond, PR & Shalek, RJ 1966, 'Energy dependence of lithium fluoride dosemeters at high energies', *Phys Med Biol*, vol 11, pp. 131-2.

Das, RK, Perera , H & Williamson, JR 1996, 'Accuracy of Monte Carlo photon transport simulation in characterizing brachytherapy dosimeter energy-response artefacts', *Phys Med Biol*, vol 41, pp. 995-1006.

Das, R, Toye, W, Kron, T, Williams, S & Duchesne, G 2007, 'Thermoluminescence dosimetry for in-vivo verification of high dose rate brachytherapy for prostate cancer', *Australas. Phys. Eng. Sci. Med.*, vol 30, pp. 178-84.

Daskalov, GM, Löfller, E & Williamson, JF 1998, 'Monte Carlo-aided dosimetry of a new high dose-rate brachytherapy source', *Med. Phys.*,vol 25, pp. 2200–8

Davis, SD, Ross, CK, Mobit, PN & Van der Zwan, L 2003, 'The response of LiF thermoluminescence dosimeters to photon beams in the energy range from 30 kV x rays to ^{60}Co gamma rays', *Radiation protection dosimetry*, vol 106, pp. 33-43.

Duggan , L, Hood, C, Warren-Forward, H, Haque , M & Kron , T 2004, 'Variations in dose response with x-ray energy of LiF: Mg, Cu, P thermoluminescence dosimeters: implications for clinical dosimetry.', *Phys. Med. Biol.*, vol 49, no. 17, pp. 3831-3845.

Edwards, CR, Mountford, PJ, Green , S & Palethorpe, JE 2005, 'The low energy x ray response of the LiF:Mg,Cu,P thermoluminescent dosemeter: a comparison with LiF:Mg,Ti', *The British Journal of Radiology*, vol 78, pp. 543-7.

GEANT4 Collaboration 2013, *Geant4*, viewed 31 October 2013, <http://www.geant4.org/geant4/support/about.shtml>.

Glasgow, GP & Dillman, LT 1979, 'Specific γ-ray constant and exposure rate constant of ^{192}Ir', *Medical Physics*, vol 6, p. 49.

Haworth, A, Butler, DJ, Wilfert, L, Ebert, MA, Todd, SP, Hayton, J & Kron, T 2012, 'Comparison of TLD calibration methods for ^{192}Ir dosimetry', *Journal of applied clinical medical physics/American College of Medical Physics*, vol 14, no. 1, pp. 4037-4037.

Haworth, A, Wilfert, L, Butler, D, Ebert, MA, Todd, S, Bucci , J, Duchesne, GM, Joseph, D & Kron , T 2013, 'Australian brachytherapy audit: Results of the 'end-to-end' dosimetry pilot study', *Journal of Medical Imaging and Radiation Oncology*, vol 57, pp. 490-498.

Holt, JG, Edelstein, GR & Clark, TE 1975, 'Energy dependence of the response of lithium flouride TLD rods in high energy electron fields', *Phys Med Biol*, vol 20, pp. 559-70.

International Atomic Energy Agency 2000, 'Absorbed dose determination in external beam radiotherapy. An international code of practice for dosimetry based on standards of absorbed dose to water, Technical Report Series No. 398', IAEA, Vienna.

Johns, HE & Cunningham, JR 1983, *The Physics of Radiology*, 4th edn, Charles C. Thomas, Springfield IL.

Karaiskos, P, Angelopoulos, A, Skalliou, L, Antypas, C, Vlachos, L & Koutsouveli, E 1998, 'Monte Carlo and TLD dosimetry of an Ir-192 high dose-rate brachytherapy source', *Medical Physics*, vol 25, pp. 1975-1984.

Klein, E, Hanley, J, Baymouth, J, Yin, F, Simon, W, Dresser , S, Serago, C, Aguirre, F, Ma, L, Arjomandy, B & Liu, C 2009, 'Task Group 142 report: Quality assurance of medical accelerators', *Medical Physics*, vol 36, no. 9, pp. 4197-212.

Kron, T 1994, 'Thermoluminescence dosimetry and its applications in medicine: Part 1. Physics, materials and equipment', *Australas. Phys. Eng. Sci. Med.*, vol 17, pp. 175-99.

Kron, T, Duggan, L, Smith, T, Rozenfeld, A, Butson, M, Kaplan, G, Howlett, S & Hyodo, K 1998, 'Dose response of various radiation detectors to synchrotron radiation', *Phys. Med. Biol.*, vol 43, pp. 3235-59.

Kron, T, Smith, A & Hyodo, K 1996, 'Synchrotron radiation in the study of the variation of dose response in thermoluminescent dosimeters with radiation energy', *Australas. Phys. Eng. Sci. Med.*, vol 19, pp. 225-36.

Meigooni, A, Sabnis S & Nath, R 1990, 'Dosimetry of ^{103}Pd brachytherapy sources for permanent implant', *Endocurietherapy Hypertherm. Oncol.*, vol 6, pp. 107-17.

Mobit, PN, Nahum, AE & Mayles, P 1998, 'A Monte Carlo study of the quality dependence factors of common TLD materials in photon and electron beams', *Phys Med Biol*, vol 43, pp. 2015-2032.

Muhogora , WE, Ngoye, WN, Lema, US & Mwalongo, D 2002, 'Energy response of LiF:Mg,Ti dosemeters to ISO 4037 and typical diagnostic x ray beams in Tanzania', *Journal of radiological protection - Official journal of the Society for Radiological Protection*, vol 22, pp. 175-84.

Nath, R, Anderson, L, Luxton, G & Weaver, K 1995, 'Dosimetry of interstitial brachytherapy sources: Recommendations of the AAPM Radiation Therapy Committee Task Group No. 43', *Medical Physics*, vol 22, p. 209.

Nath, R, Meigooni , AS, Muench, P & Melilo, A 1993, 'Anisotropy functions for ^{103}Pd, ^{125}I and ^{192}Ir interstitual brachytherapy sources', *Medical Physics*, vol 20, pp. 1465-73.

Palmer, RJ 2001, *Polyamides, Plastics. Encyclopaedia Of Polymer Science and Technology.*

Pradhan, AS & Quast, U 2000, 'In-phantom response of LiF TLD-100 for dosimetry of ^{192}Ir HDR source', *Medical Physics*, vol 27, pp. 1025-9.

Schumer, W, Fernando, W, Carolan, M & Wong, T 1991, 'Verification of brachytherapy dosimetry with radiochromatic film', *Medical Dosimetry*, vol 24, pp. 1025-9.

Suntharalingham, N & Cameron, JR 1969, 'Thermoluminescent response of lithium fluoride to high-energy electrons', *Ann NY Acad Sci*, vol 161, pp. 77-85.

Thomason, C & Higgins, P 1989, 'Radial dose distribution of ^{192}Ir and ^{137}Sc seed sources', *Medical Physics*, vol 16, pp. 254-7.

Toye, W, Das, R, Kron, T, Franich, R, Johnston, P & Duchesne, G 2009, 'An in vivo investigative protocol for HDR prostate brachytherapy using urethral and rectal thermoluminescence dosimetry', *Radiotherapy and Oncology*, vol 91, pp. 243-248.

Williamson, JF 1991, 'Comparison of measured and calculated dose rates in water near I-125 and Ir-192 seeds', *Medical Physics*, vol 18, pp. 776-89.